

On the Application of Fluid Power Transmission in Offshore Wind Turbines

PROEFSCHRIFT

ter verkrijging van de graad van doctor
aan de Technische Universiteit Delft,
op gezag van de Rector Magnificus Prof. ir. K.C.A.M. Luyben,
voorzitter van het College voor Promoties,
in het openbaar te verdedigen
op donderdag, 29 augustus 2013 om 12.30 uur
door

Niels Frederik Boudewijn DIEPEVEEN

Ingenieur Luchtvaart- en Ruimtevaarttechniek,

geboren te Leiden.

Dit proefschrift is goedgekeurd door de promotor:

Prof. dr. ir. G.A.M. van Kuik

Samenstelling promotiecommissie:

Rector Magnificus	voorzitter
Prof. dr. ir. G.A.M. van Kuik	Technische Universiteit Delft, promotor
Dr. ir. J. van der Tempel	Technische Universiteit Delft/Ampelmann
ir. P.S. Albers	Albers Hydrauliek
Dr.ir. H. Polinder	Technische Universiteit Delft
Univ.-Prof. Dr.-Ing. H. Murrenhoff	RWTH Aachen University
Prof.dr.ir. C. van Rhee	Technische Universiteit Delft
Prof.dr.ir. W.S.J. Uijttewaai	Technische Universiteit Delft
Prof.dr.ir. J.G. Rots	Technische Universiteit Delft, reservelid

Copyright © 2013 by Niels Diepeveen

All rights reserved. No part of the material protected by this copyright notice may be reproduced or utilized in any form or by any means, electronic or mechanical, including photocopying, recording or by any information storage and retrieval system, without the prior permission of the author.

ISBN 978-94-6186-180-1

This research was supported by WE@Sea.

Typeset by the author with the L^AT_EX Documentation System.

Printed by: Vandenberg Concept & Design Printmedia

Author email: nielsdiepeveen@gmail.com

Abstract

Offshore wind energy is currently characterized by the high costs associated with installation and maintenance. To a large extent these costs are down to the way in which energy in the wind is converted to electricity. A wind turbine rotor converts power in the wind to rotating kinetic energy in the form of torque and rotation speed. Practically every turbine placed offshore so far contains a gearbox which lowers the torque and increases the rotation speed. The gearbox is coupled to a generator. In order to feed the electricity into the grid the voltage and frequency are regulated using power electronics.

Gearboxes in particular have been singled out as a key source of the high maintenance costs of offshore wind farms. For a given wind speed the rotor torque increases cubically with the diameter of the swept area. As the maximum size of offshore wind turbines continues to increase, mass reduction and reliability are of growing importance for the system's economy.

In any industry where robust machinery is required to handle large torques, the hydraulic drive systems are applied. It is therefore almost the obvious solution for wind turbines. The functionality is explained as follows. Using a hydraulic pump, the torque and speed of the rotor are transformed to pressure and fluid flow. A hydraulic motor converts the pressure and flow back into torque and rotation speed. Although the solution is not new, it has renewed potential thanks to developments in hydraulic machinery.

The research presented in this thesis is centered around the questions of whether and how the application of fluid power technology is feasible as an alternative to current (gearbox and generator) and upcoming (permanent magnet direct drive generators) drive train technologies for offshore wind turbines.

The approach is to define several possible configurations of the fluid power trans-

mission system. From these, a concept for centralized electricity production within an offshore wind farm is subjected to further analysis. Through research, modeling and experiments, the feasibility of this concept is analyzed. Due to its wide use in relevant literature, the NREL 5MW Offshore Baseline turbine is selected as reference technology. In the conceptual and preliminary designs as well as the majority of the computational models, the properties of the rotor of this reference turbine are used.

The modularity of hydraulic components gives rise to many options for the architecture of a power transmission system for offshore wind turbines. Three configurations presented in this thesis are:

1. The nacelle solution, where the entire fluid power transmission system is located in the nacelle.
2. The tower-base solution, with a pump in the nacelle and the motor and generator located at the foot of the turbine tower.
3. The hydraulic wind farm solution, where the idea is to employ seawater as power transmission medium and use one hydro-power-like generator station to convert the pressurized flow from multiple turbines into electricity.

The most unique of these configurations is number 3, the Delft Offshore Turbine (DOT) concept. This concept for centralized electricity production within an offshore wind farm is selected for further analysis through research, modeling and experiments.

The main challenge in coupling a hydraulic drive train to a wind turbine rotor is matching the speed and torque ranges of the aerodynamic rotor and the pump to which it is coupled. The modeling of hydraulic pumps, motors, valves and piping is to a large extent based on empirical relations. The power performance of a wind turbine rotor is essentially a function of the tip speed ratio λ and the pitch angle θ of the wind turbine blades. In particular the presence of the turbine tower and the stochastic nature of wind introduce noise in the torque it produces. A fluid power circuit, such as may be applied in the transmission of a wind turbine, essentially behaves as a second order system. To be able to describe a system in this way is beneficial for the simplicity of the analysis of its dynamic behavior. The amount and the compressibility of the fluid in the system have a significant influence on the stiffness of the transmission system and hence pressure transients. On the other hand, the rotor mass moment of inertia has an important influence in the time response of pressure and rotational speed, leading to a slower but smoother response of the system. From experiments with a 1MW-class single circuit oil-hydraulic transmission system for wind turbines, it was observed that high and low frequent variations in the torque applied to the drive train are quickly damped, leading to a smoothed electrical power output. Apart from

mapping the dynamic response characteristics, the measurements were also used to validate simulation models of the test bench.

It was found that in theory it is possible to configure the fluid power transmission system in such a way that no form of active control is required for the drive train. Experiments with a 600W setup in a wind tunnel showed that the passive torque control solution works as expected. This control method has enormous potential for the DOT wind farm. It significantly simplifies the design and regulation of the wind turbine drive train without sacrificing the aerodynamic performance of the rotor.

On the basis of the afore mentioned research and experiments a preliminary design of the DOT transmission system is defined. This system runs from the shaft of the NREL rotor to the hydro turbine at the generator station. The estimated DOT nacelle mass is approximately one third of the nacelle mass of the reference turbine. The nominal power output is limited due to the design constraint for the maximum speed of the blade tip and the optimal tip speed ratio. Using properties derived from current state-of-the-art off-the-shelf components, the transmission efficiency from rotor to hydro turbine is calculated to be around 80%. The main source of efficiency loss is the seawater pump. The relatively large bulk modulus of seawater makes that the stiffness of the simulated response of the system to dynamic wind loads on the rotor is still satisfactory for a seawater pipeline more than 10km long. The phenomenon of pipeline flow dynamics requires further research.

To make offshore wind a competitive source of electricity requires more than incrementally improving and scaling-up onshore turbines. The DOT concept for power transmission is technically feasible. Pumps suitable for direct coupling to multi-MW wind turbines rotors do not exist at the time of this writing. Current developments in the fluid power industry suggest that such pumps will be commercially available within the next few years. The design as presented in this thesis will significantly reduce the complexity of offshore wind energy technology. With currently available off-the-shelf components, it is possible to construct a DOT drive train prototype with up to around 1MW of nominal power output. A way to further prove the functionality and demonstrate the possible use of such a drive train is by building and testing it, preferably in a real turbine, offshore.

Samenvatting

Offshore windenergie wordt momenteel gekenmerkt door de hoge kosten voor installatie en onderhoud. Veel van deze kosten zijn te herleiden naar de manier waarop de energie in de wind wordt omgezet naar elektriciteit. De rotor van een wind turbine zet het vermogen in de wind om in roterende kinetische energie in de vorm van een draaimoment (koppel) en de rotatie snelheid. In vrijwel iedere op zee geplaatste turbine zit een tandwielkast die het koppel verlaagt en het toerental verhoogt. Dit component in het bijzonder wordt geassocieerd met hoge onderhoudskosten. De tandwielkast is gekoppeld aan een generator. Om de opgewekte stroom aan het net te kunnen voeden moeten de spanning en de frequentie geregeld worden door diverse vermogenslektronica. Voor een gegeven windsnelheid neemt het draaimoment van de rotor kubisch toe met de diameter van het bestreken oppervlak.

De maximale grootte van offshore windturbines blijft almaar toenemen. Massavermindering en betrouwbaarheid worden hierdoor in toenemende mate van economisch belang.

In iedere industrie waar robuuste machines nodig zijn om grote draaimomenten over te brengen wordt met hydrauliek gewerkt. Het is dan ook een bijna voor-de-hand liggende uitkomst voor windturbines. Het functionele principe is als volgt. Een hydraulische pomp, gekoppeld aan de rotor, zet het draaimoment en de draaisnelheid om in druk en de stroming van vloeistof. Een hydraulische motor zet deze stroming en druk weer terug om in koppel en draaisnelheid. Hoewel deze oplossing niet nieuw is, heeft hij hernieuwde potentie gekregen dankzij actuele ontwikkelingen van hydraulische aandrijfcomponenten.

Het onderzoek dat in dit proefschrift wordt gepresenteerd gaat over de vraag of en hoe de toepassing van hydraulische technologie haalbaar is als alternatief voor huidige (tandwielkast & direct aangedreven generatoren)

overbrengingstechnologieën in offshore windturbines.

De modulariteit van hydraulische componenten leidt tot vele mogelijkheden voor de architectuur van het systeem voor de vermogensoverbrenging. In dit proefschrift zijn drie configuraties voor hydraulische transmissie in offshore wind turbines gedefinieerd:

1. Het gehele transmissiesysteem is in de gondel ondergebracht.
2. Er is enkel een pomp in de gondel. De motor en de generator bevinden zich aan de voet van de turbinetoren.
3. Dit is een uitbreiding van configuratie 2. De motor aan de voet van de toren is gekoppeld aan een tweede circuit, waarin zeewater wordt gebruikt als hydraulische vloeistof. Er is slechts één generator voor meerdere turbines. In een soort waterkrachtcentrale worden de inkomende hoge druk vloeistofstromen omgezet naar elektriciteit door enkele waterturbines.

De meest unieke van deze configuraties is nummer 3, beter bekend als het Delft Offshore Turbine (DOT) concept. Dit concept voor gecentraliseerde elektriciteitsproductie in een offshore windpark is geselecteerd voor verdere analyse middels onderzoek, modellering en experimenten. Vanwege het ruime gebruik ervan in relevante literatuur, wordt de NREL 5MW Offshore Baseline turbine gebruikt als referentietechnologie.

De belangrijkste uitdaging in het ontwerpen van een hydraulische aandrijftrein voor een windturbine is het afstemmen van de karakteristieken voor het toerental en draaimoment van de aerodynamische rotor en de pomp waaraan die is gekoppeld. Het modelleren van hydraulische pompen, motoren, kleppen en leidingen is in grote mate gebaseerd op empirische relaties. De vermogensprestatie van de rotor van een windturbine is voornamelijk een functie van de tipsnelheidsverhouding en de standhoek van de windturbine bladen. In het bijzonder de aanwezigheid van de turbinetoren en de stochastische aard van wind leiden tot ruis in het draaimoment van de rotor. Een hydraulisch circuit, zoals kan worden toegepast in de transmissie van een windturbine gedraagt zich in wezen als een tweede orde systeem. Het beschrijven van een systeem op deze manier is gunstig voor de eenvoud van de analyse van het dynamisch gedrag. De hoeveelheid en de samendrukbaarheid van de vloeistof in het hydraulisch systeem heeft een aanzienlijke invloed op de stijfheid van de transmissie. Anderzijds heeft het massastraagheidsmoment van de rotor een belangrijke invloed op de respons van druk en rotatiesnelheid. Uit experimenten met een 1 MW-klasse olie-hydraulische overbrenging voor windturbines is waargenomen dat hoog en laag frequente variaties in het draaimoment op de aandrijving snel gedempt worden. Naast het in kaart brengen van dynamische responskarakteristieken zijn de metingen ook gebruikt om simulatiemodellen te valideren.

In theorie is het mogelijk om het hydraulische overbrengingssysteem zodanig te configureren dat geen enkele vorm van actieve regeling vereist is. Uit experimenten met een 600W opstelling in een windtunnel is gebleken dat deze passieve vorm van regeling werkt zoals verwacht. Deze regelmethode biedt veel potentie voor het DOT windparkconcept. Het ontwerp en de regulering van de aandrijving worden er aanzienlijk mee vereenvoudigd zonder dat de aerodynamische prestatie van de rotor vermindert.

Op basis van het genoemde onderzoek en experimenten is een voorontwerp van het DOT transmissiesysteem gedefinieerd. De grenzen van dit ontwerp zijn enerzijds de as van de rotor en anderzijds de waterturbine van het generator station. De geschatte massa van de DOT gondel is ongeveer een derde van de gondel massa van de referentieturbine. Het nominale vermogen wordt beperkt door de maximaal toelaatbare snelheid van de uiteindes van de bladen en de optimale tipsnelheidsverhouding. Met behulp van eigenschappen die zijn afgeleid van de meest geavanceerde huidig verkrijgbare componenten, is het rendement van de transmissie tussen rotor en waterturbine berekend op ongeveer 80%. De belangrijkste bron van rendementsverlies is de zeewaterpomp. Uit simulaties met dynamische windbelasting blijkt dat de relatief hoge stijfheid van zeewater ervoor zorgt dat een zeewaterpijplijn meer dan 10km lang haalbaar is. De dynamiek van de stroming in de hydraulische leidingen vereist verder onderzoek.

Om offshore wind een concurrerende bron van elektriciteit te maken is er meer nodig dan het stapsgewijs verbeteren en opschalen van de soort turbines die op land staan. Het DOT concept voor de energieoverbrenging in offshore windturbines en parken is technisch haalbaar. Hoge druk pompen die geschikt zijn voor directe koppeling met multi-MW windturbinerotoren bestaan niet ten tijde van dit schrijven. De huidige ontwikkelingen in de hydraulische industrie suggereren dat dergelijke pompen in de komende jaren op de markt komen. Het ontwerp van de aandrijving zoals het is gepresenteerd in dit proefschrift zal leiden tot een aanzienlijke vermindering van de complexiteit van de offshore windenergie technologie. Met de huidig beschikbare componenten is het mogelijk om een prototype te bouwen van de DOT aandrijving met een nominaal vermogen van ongeveer 1 MW. Een manier om van een dergelijke aandrijftrein de functionaliteit verder te bewijzen en de mogelijke bruikbaarheid te tonen is middels bouwen en testen, bij voorkeur in een echte windturbine, offshore.

Acknowledgements

Many people and institutions have contributed directly and indirectly to this thesis. I am grateful to the following people in particular:

- My supervisors Jan van der Tempel for creating a PhD position combining an academic environment with an industrially orientated research focus, Gijs van Kuik and Peter Albers, for their dedication and their wisdom.
- My TU Delft colleagues Antonio Jarquin Laguna for the very pleasant and fruitful cooperation over the years, David Cerda Salzmänn, Wybren de Vries, Michiel Zaayer, Maxim Segeren for their assistance, feedback and support.
- My colleagues from IFAS: Johannes Schmitz and Nils Vatheuer for the use of their experimental facilities and the pleasant cooperation.
- Sander de Vree & Tonny Schuit for allowing us to contaminate the Waterlab at Civil Engineering with oil hydraulics.
- Nico van Beek, Nando Timmer and Ruud van Rooij for the use of the Open Jet Facility and the assistance with the experiments.
- Sylvia Willems, Joke Baan, Otti Kievits and Ayaita Oemraw for their service and support.
- My former students Anton, Koen, Dennis, Dimitris, Emiel, Birgit, Karen, Titi-aan, Jacques, Tom, Robert, Mathijs, Francesco.

Contents

Abstract	i
Samenvatting	v
Acknowledgements	ix
1 Introduction	1
1.1 Motivation	1
1.1.1 Background: Challenges of Exploiting Wind Offshore	1
1.1.2 Wind Turbine Power Conversion and Transmission Technology	2
1.1.3 The Proposed Idea: Fluid Power Transmission	3
1.2 Research Objective	4
1.3 Approach and Structure	4
2 Fluid Power Technology and the Application in Wind Turbines	7
2.1 Introduction	7
2.2 A Brief History of Fluid Power Technology	8
2.3 State-of-the-Art Hydraulic Pumps	10
2.3.1 The Positive Displacement Pump	10
2.3.2 The Radial Piston Pump	11
2.3.3 (Sea)Water Hydraulic Pumps	13
2.4 Common Components of Hydraulic Circuits	14

2.5	Fluid Power Transmission Applications in Wind Turbines	15
2.5.1	Ideas Born from the Oil Crises	15
2.5.2	The Big Push for Renewable Energy	17
2.6	The Delft Offshore Turbine (DOT) Project	21
2.7	Advantages and Disadvantages of Applying Fluid Power Transmis- sion in Large Offshore Wind Turbines	23
2.7.1	Advantages	23
2.7.2	Disadvantages	24
2.7.3	Arbitrary Issues	25
2.8	Concluding Remarks	25
3	Conceptual Designs of Fluid Power Transmission Systems for Offshore Wind Turbines	27
3.1	Introduction	27
3.1.1	Background	27
3.1.2	Objective	28
3.1.3	Approach	28
3.1.4	Self-Imposed Constraints	29
3.1.5	The NREL 5MW Offshore Reference Turbine	30
3.2	Offshore Wind Farm Design Considerations	31
3.2.1	Offshore Wind Farm Economics	31
3.2.2	The Competition for Space	32
3.2.3	Water Depth: Fixed versus Floating Turbines	33
3.2.4	Distance to Port & Onshore Grid	33
3.3	Design Considerations for the Fluid Power Transmission System . . .	34
3.3.1	Resonant Frequencies	34
3.3.2	Flow Ripple	34
3.3.3	Heat Management	36
3.3.4	Choice of Fluid	36
3.3.5	Seawater as Hydraulic Fluid	37
3.3.6	Sources of Charge Pressure for a Pump at Hub-Height	38
3.4	Design Requirements for the Fluid Power Transmission System . . .	40
3.4.1	Functional Requirements	40
3.4.2	General Requirements	40
3.5	Hydraulic Circuit Configuration Options	41
3.5.1	Variable Speed Operation	41
3.5.2	Options for Closed-Circuit Hydraulics	42
3.5.3	Options for Open-Circuit Hydraulics for Centralized Elec- tricity Production	43
3.6	Control Options	45

3.6.1	Control of Hydrostatics	45
3.6.2	Option 1: Maximum Power Point Tracking	45
3.6.3	Option 2: Model-Based Control	46
3.7	Design Concept Selection	46
3.7.1	Overview of Feasible Concepts	46
3.7.2	Selection of the DOT Concept for Further Development	47
3.8	Selection of main component types	49
3.8.1	PD Pump	49
3.8.2	Hydraulic Motor	50
3.8.3	Hydro Turbine	52
4	Coupling Rotor Aerodynamics and Fluid Power Transmission	55
4.1	Introduction	55
4.1.1	Torque Balance	55
4.1.2	Objective & Approach	57
4.1.3	Macroscopic vs. Microscopic Approach to System Modeling	57
4.1.4	Three Governing Equations	58
4.1.5	Assumptions & Conditions	59
4.2	Modeling Rotor Aerodynamics	59
4.2.1	Blade Element Momentum (BEM) Theory	59
4.2.2	Model Extensions for Dynamic Simulation	62
4.2.3	C_P - C_T - λ Relation	63
4.2.4	The Power Curve	67
4.3	Modeling Fluid Power Transmission Components	68
4.3.1	Important Fluid Properties	68
4.3.2	The Effective Bulk Modulus	71
4.3.3	Modeling a Hydraulic Pump	72
4.3.4	Modeling a Hydraulic Motor	74
4.3.5	Efficiencies of Hydraulic Pumps	74
4.3.6	Efficiencies of Hydraulic Motors	75
4.3.7	Modeling Nozzle Flow	78
4.4	Modeling Fluid Power Transmission Dynamics	79
4.4.1	Inertia & Hydraulic Induction	79
4.4.2	Compressibility & Hydraulic Capacitance	81
4.4.3	Hydraulic Resistance: Pressure & Flow Losses	82
4.4.4	Derivation of the Characteristic System Equations	84
4.4.5	Conversion to State Space	86
4.4.6	Calculation of Natural Frequencies	87
4.4.7	Calculation of Damping Ratios	87
4.4.8	Acquiring Realistic Values of L_H , C_H , R_H	88

4.5	Matching Rotor and Hydraulic Pump Characteristics	88
4.5.1	Pump-Rotor Matching	88
4.6	Conclusion	92
5	Dynamic Response Analysis of Fluid Power Drive Trains	93
5.1	Introduction	93
5.1.1	Background & Objective	93
5.1.2	Approach	94
5.1.3	Assumptions & Conditions	95
5.2	Stability Analysis of the Linear Second Order System Model	95
5.2.1	Linearized model of Rotor & Transmission	95
5.2.2	Conditions for (In)stability	98
5.3	Parameter Sensitivity Analysis for a 5MW Wind Turbine Drive Train	101
5.3.1	Simulation Setup	101
5.3.2	PI Control strategy for variable speed	103
5.3.3	Reference Properties and Steady-state Operation	103
5.3.4	Results for Variations from Default Properties	105
5.4	Experiments with a 1MW Hydrostatic Transmission System	108
5.4.1	Experimental Setup	108
5.4.2	Transmission Input: Fixed-Speed Rotor Simulation	109
5.4.3	Drive Train Control Configurations	112
5.4.4	Overview of Consulted Loads Cases	114
5.4.5	Response to Torque Step on Rotor Shaft including Rotor Inertia	115
5.4.6	Effect of Torque Control	115
5.5	Conclusion	119
6	Passive Torque Control for Variable Speed Wind Turbines using Fluid Power Technology	121
6.1	Introduction	121
6.2	Passive Operation	123
6.2.1	Description of Principle	123
6.2.2	Dimensioning of the Constant Area Nozzle	125
6.2.3	Performance evaluation	128
6.3	Validation through Wind Tunnel Experiments	129
6.3.1	Overview of the Experimental Setup	129
6.3.2	Experimental Results	130
6.3.3	Simulation versus Measured Results	135
6.4	Conclusion	137
6.4.1	Concept of Passive Torque Control	137
6.4.2	Passive Control for $U_{\infty} > U_{rated}$	137

6.4.3	Forced Shutdown Control Options	137
6.4.4	Proof of Concept: Wind Tunnel Experiments	138
6.4.5	Design Point	138
6.4.6	Drawback of Passive Torque Control: No “Frequency Skip- ping”	138
7	Preliminary Design of the DOT Fluid Power Transmission System Using the NREL 5MW Rotor	141
7.1	Introduction	141
7.1.1	Background, Objective & Approach	141
7.1.2	Functional Requirements of the Power Transmission System of a Single DOT	142
7.2	Design Considerations for the DOT Fluid Power Transmission System	143
7.2.1	Cooling of the Oil Circuit	143
7.2.2	Boosting, Filtering and Cooling of the Seawater Circuit	143
7.2.3	Startup Torque	143
7.2.4	Control System Properties	145
7.2.5	Local Electric Power Source	146
7.3	Dimensioning of the Main Transmission System Components	146
7.3.1	Method for Dimensioning	146
7.3.2	Oil Circuit Components Properties	147
7.3.3	Seawater Circuit Components Properties	148
7.3.4	Reduction of Mass	150
7.4	Power Performance Simulation of a Single DOT	151
7.4.1	Steady State Response: The Power and Torque Curves	151
7.4.2	Setup of Dynamic Response Simulation	153
7.4.3	Response to Step Input and Turbulent Wind Loads	154
7.5	Conclusion	157
8	Conclusion	159
8.1	Main Conclusions	159
8.2	Answers to Main & Key Research Questions	159
8.3	Recommendations for Future Research	163
	Bibliography	167
A	Reduction of Nacelle Mass	175
A.1	Introduction	175
A.2	Reference Turbine Characteristics	177
A.3	Inventory of Data and Established Relations	177

A.3.1	Offshore Wind Turbines Currently Installed	177
A.3.2	Scaling Studies	178
A.4	Rotor Mass Modeling	179
A.5	Nacelle Mass Modeling	180
A.5.1	Introduction	180
A.5.2	Conventional Drive Train	181
A.5.3	Fluid Power Drive Train	182
A.5.4	Other Components	184
A.5.5	The Complete Nacelle	186
B	MicroDOT 10kW Demonstrator	187
C	Description of IFAS Experimental Setup	193
C.1	Description of the Main Components of the IFAS 1MW Test Bench	193
C.1.1	Hydraulic Drives	193
C.1.2	Hydraulic Fluid	194
C.2	Requirements & Limitations	195
C.3	Control Strategy for Optimal Power Production	196
C.4	Hardware in the Loop	198
C.5	Rotor Simulation	199
C.5.1	Rotor Properties	199
C.5.2	Pitch Control Settings	199
C.5.3	Matching the Rotor Size to the Drive Train	200
D	Experimental Setup for Passive Control Validation	203
D.1	The Open Jet Facility	203
D.2	The Aerodynamic Rotor	204
D.3	The Water-Hydraulic Circuit	205
D.4	Nozzles	205
D.5	Sensors & Data Processing	206
	Curriculum Vitae	209

Introduction

1.1 Motivation

1.1.1 Background: Challenges of Exploiting Wind Offshore

As a source of renewable energy, offshore wind has enormous potential. Its utilization is not yet cost effective without subsidies. The engineering challenge is to find technical solutions which are compatible with free market economics: i.e. making offshore wind an economically competitive source of energy.

The offshore environment is notoriously harsh, in particular for any object at or just above the sea surface. An offshore wind turbine should sustain the continuous attack by forces from wind and waves, corrosion, erosion, solar radiation and marine growth throughout its design lifetime.

Currently installed offshore wind turbines are enormously complex machines. Each consists of a multitude of subsystems. The sheer number of electric and mechanical components results in a need for frequent maintenance and contributes to high cost of operation and maintenance (O&M). Other points of concern in modern wind turbine technology are the use of vast amounts of copper and the amount of software and switch gear required to run all systems.

With increasing competition for offshore sites to place wind turbines, there is a gradual move to more remote and deeper locations. Mass, reliability and complexity will therefore have an even bigger impact on the wind farm economics.

In 2008 DUWIND, the Delft University wind energy research institute, launched the Delft Offshore Turbine (DOT) project. The goal of the project is to find technical solutions which will make offshore wind energy an cost-competitive source of energy

without subsidies. The approach is to re-evaluate the way in which wind energy offshore is converted to electricity onshore. The project's defining research line is the re-assessment of the power conversion and transmission technology applied in offshore wind turbines.

1.1.2 Wind Turbine Power Conversion and Transmission Technology

Primary Function

The primary function of a wind turbine is to convert power from the flow of air into electricity. Air has a relatively low density, hence a relatively large aerodynamic rotor is required to extract energy. The rotational speed of the rotor is limited by the airspeed experienced by the blade tips. A typical limit for the blade tip speed (in-plane) is 80m/s, though the move to higher design tip-speeds is being advocated [1]. The great length of the blade thus means that large wind turbine rotors are designed to convert the kinetic power in the wind to mechanical power in the form of high torque and low rotation speed.

State of the Art

So far, two techniques have been commercially applied to convert high torque, low speed mechanical power into electricity.

1. The drive train of each wind turbine installed offshore so far has a mechanical gearbox coupled to a high speed generator. Wind (and wave) loads are highly dynamic and stochastic. Vibrations and asymmetric loading have caused components, which have been designed to last 20 years, to break down too soon, sometimes after only one year [2, 3, 4, 5]. Gearboxes in particular have been singled out as a key source of the high O&M costs of offshore wind farms.
2. Direct drive technology, wherein the rotor is directly coupled to a low speed/high torque generator, reduces the number of mechanical drive train components. Drive technology using electromagnets, as commonly seen onshore (Enercon), is considered too bulky to install offshore. New direct drive technology using permanent magnets (Siemens, Alstom) is more compact, but requires the use of expensive rare earths, which is widely considered as unsustainable.

The conventional model for wind turbines both onshore and offshore is to install a generator in the nacelle. Supplying each turbine with its own generator, frequency converter and voltage transformer has several disadvantages:

- It demands large amounts of copper, making wind farms expensive.
- The nacelle is heavy and thus requires a strong support structure.
- Continuous efficient conversion from kinetic to electric energy requires many high-tech and intelligent control systems.

There Must Be a Better Way

The power transmission system of a wind turbine offshore should be safe, simple, robust, reliable and energy efficient. It should not break down due to software problems. It should be easy to install. It should be easy to maintain. Offshore wind turbines should not require a lot of attention, yet produce a lot of power.

1.1.3 The Proposed Idea: Fluid Power Transmission

In industries such as mining, building, demolition, agriculture and shipping, fluid power technology is a well-established solution for operations involving high torques. The option to use oil hydraulics for the conversion to low torque high speed in wind turbines was first tested in the early 1980s [6]. Low efficiency at partial load and the lack of required components rendered the application unsuccessful. Recently, hydraulic transmission has been given a second chance. The maturing of the industry has led to fluid power technology having the reputation of being reliable and robust. Other reasons are the high torque to weight ratio (compactness), the option for variable transmission and improvements in energy efficiency due to precision engineering. As the size of wind turbines continues to increase, mass reduction and reliability have become of paramount importance to the system's economy. Several parties around the world are now developing fluid power drive trains for wind turbines. The lack of suitable multi-MW drives has led these parties to develop their own hydraulic drive systems.

The modular nature of hydraulic equipment makes it possible to manipulate the architecture of a transmission system. For instance, it is possible to place the entire hydraulic circuit in the nacelle or only a pump. It is also possible to have high pressure flows from several sources come together and be converted into electricity by one generator. This presents an interesting option for an offshore wind farm. The distance between the turbines means using vast amounts of hydraulic oil is out the question. So what about just using seawater as hydraulic fluid? Despite some seemingly obvious objections, such the corrosive and non-lubricating nature of seawater, this form of power transmission has several benefits.

1.2 Research Objective

The central theme of this dissertation is the application of fluid power technology as an alternative to current drive train technologies in offshore wind turbines. What we essentially want to know is whether fluid power is a feasible alternative to what is used currently (geared transmission) and in the near future (direct drive permanent magnet generators). The main research question of this thesis is therefore:

How can fluid power transmission be applied for large offshore wind turbine drive trains?

1.3 Approach and Structure

In figure 1.1, an overview is given of the structure and essential approach to answer the main research question and the key questions.

To motivate the application of fluid power transmission in offshore wind turbines, the approach in chapter 2 is to investigate the history and state-of-the-art of fluid power technology. In chapter 3 an analysis is made of several possible fluid power drive train configurations. The one which is selected for further development is known as the Delft Offshore Turbine (DOT) concept. The DOT concept is to have centralized electricity production using high pressure seawater hydraulics between each turbine and the generator station. To work out the conceptual design requires knowledge of the modeling of the power performance of both wind turbine rotors and fluid power circuits. The necessary equations for dimensioning hydraulic power transmission system and matching it to an aerodynamic rotor are given in chapter 4. In chapter 5, the dynamic interaction between the aerodynamic rotor and a simplified fluid power drive train is analyzed. The results are obtained through:

1. a co-simulation between a self-derived model of the hydraulic drive train and commercial software for the rest of the wind turbine.
2. experiments with a 1MW fluid power drive train on a test bench.

In chapter 6 a novel control method for fluid power drive trains and its validation through experiments are described. The assembled knowledge of the previous chapters is combined in chapter 7 to yield the preliminary design of the DOT fluid power transmission system, coupled to the aerodynamic rotor of a 5MW reference turbine. The overall conclusion of the presented work and recommendations for further research are given in chapter 8.

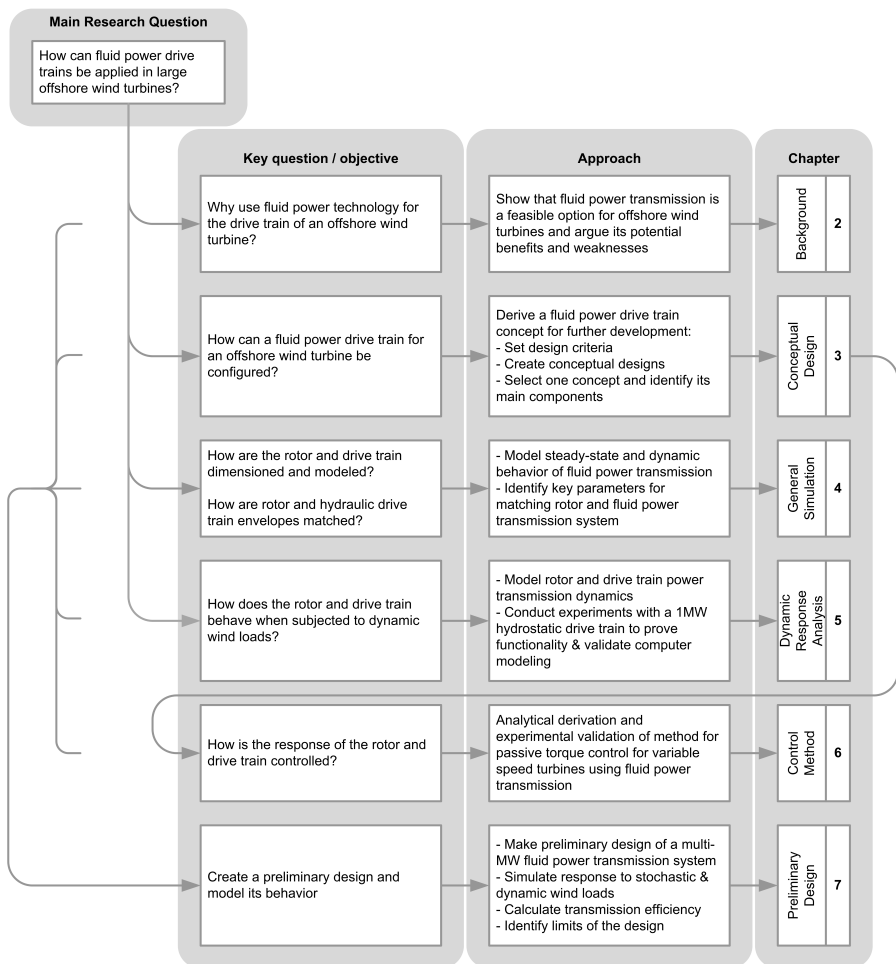


Figure 1.1: Flow chart of the structure of this thesis

Fluid Power Technology and the Application in Wind Turbines

2.1 Introduction

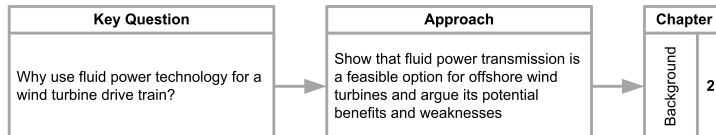


Figure 2.1: Flowchart of the objective and approach of this chapter

The idea of using hydraulic transmissions in wind energy systems is not a novelty. However, modern production technology has given rise to the commercial development of highly compact and efficient drives that make this option more attractive than before.

Already several institutions and companies all over the world are developing oil hydraulic circuits for wind turbine application. Their common vision is solely the replacement of the gearbox and frequency converter. The working principle behind this concept as presented in figure 2.2 is that rotating mechanical power from the prime mover is converted into a fluid flow at high pressure, i.e. fluid power, by a positive displacement pump. At the other end of the hydraulic circuit, the fluid power is converted back to mechanical power by a hydraulic motor.

The development of fluid power technology has until recently been focused on the application of force or torque. For the application as power transmission, the focus

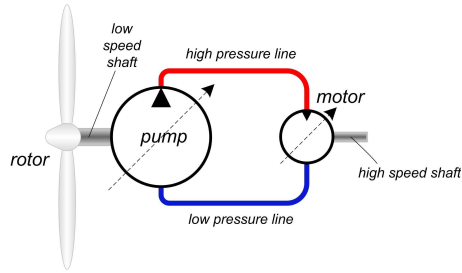


Figure 2.2: The functioning principle of fluid power transmission for wind turbine application

is shifting towards energy efficiency. Due to a lack of suitable components for multi-MW drive trains, several parties are currently developing their own hydraulic drives as is described in section 2.5.

This chapter adds background and motivation to the research question posed in section 1.2. The objective and approach are stated in the flowchart in figure 2.1.

2.2 A Brief History of Fluid Power Technology

Early Developments

Evidence of the use of water power dates back to 250 BC. The most common application up to well into the 20th century was in the form of watermills, which were used to grind grains. The Romans were responsible for large scale watermill development. Evidence surviving today is the Barbegal aqueduct and watermill, near Arles, France and a similar mining site at Janiculum, Italy.

Pascal's Principle

Blaise Pascal (1623 - 1662) noted that pressure applied to a confined fluid is transmitted undiminished in all directions and acts with equal force on equal areas and at right angles to them. The possibility to apply this principle to multiply force or torque is what makes fluid power technology so attractive.

Victorian-Age Water Power

The use of high pressure in hydraulics was introduced on a large scale in the second half of the 19th century. In major cities such London, Liverpool and Melbourne, hy-

	rating		
property	high	middle	low
power to weight	H	P	E,EM,M
torque to inertia	H	P	E,EM,M
speed of response	H	E,EM	P,M
controllability	EM,H	E,EM,P	M
load stiffness	H	M	E,EM,P
velocity range	EM,H	E,EM	P,M

Table 2.1: Comparison of drive properties for various systems [8]: E = Electronic, EM = Electromechanical, H = Hydraulic, M = Mechanical, P = Pneumatic

draulic mains (first cast-iron, later steel) were installed beneath the streets. Pressure was maintained by hydraulic power stations, originally driven by coal-fired steam engines. Short-term energy storage was provided by hydraulic accumulators, which were large vertical pistons loaded with heavy weights and tanks in high towers. Applications included cranes, elevators, presses, extruding machines and theater curtains.

At its peak in 1939, pumping stations at the city-edge of London were supplying an average flow of around 14,000 liters of water per min at nearly 60 bar pressure. This translates to an average power production of around 1.35MW. Around 1900 electricity took over as the primary source of power. Wartime bomb damage, the departure of manufacturing firms from the city center and the rise of power electronics gradually led to the shut down of the last pumping station in 1977.

Developments in Hydraulic Oils

In 1906, the first documented application of oil hydraulics was for the control of the barrel direction of British warship guns. The advantages of using oil over water are that it is more lubricant, more viscous (leading to less leakage, though slightly more friction), less corrosive and has a wider temperature range wherein the fluid is in liquid state [7]. Hence forth, oil (petroleum base and synthetic) became the dominant hydraulic medium. Nowadays, oil-based hydraulic equipment is omnipresent in countless types of industrial equipment. Modern industrial applications of oil hydraulics include heavy lifting machines such as cranes, bulldozers, digging machinery, rock crushing machinery, ship propellers, jack-up systems, bridges as well as water-lock doors. Table 2.1 gives an indication of why hydraulic systems are so popular. In commercial wind turbines hydraulic equipment is used for motion control: for blade pitching and turbine azimuth (yaw) systems.

Hydraulic oils are tailored to suit specific hydraulic applications. Important con-

siderations for the choice of a hydraulic fluid are:

- Compatibility with the other hydraulic components. Usually the manufacturers of hydraulic equipment have clearly listed which type of fluids may be used. Failure to comply will likely lead to damage to the equipment.
- The application environment. Consider potential fire hazards, or risk of leakage or damage and subsequent pollution to a sensitive ecosystem. Comply with regulation.
- The encountered temperature range. The properties (density, viscosity, etc.) may change significantly over a range of temperatures.
- The handling characteristics of the oil. If frequent handling is likely, for instance due to spillage from parts replacement, contact with human skin is also likely.

Other considerations include cost and lubricity. The viscosity, density and bulk modulus may also be considered, but these are usually available in the required ranges.

Environmental awareness has led to the development of hydraulic oil with high biodegradability. The term “biodegradability” essentially refers to the speed at which a fluid is broken down by micro-organisms in the environment, ultimately yielding carbon dioxide and water as end products. Throughout literature a distinction is made between *readily* or *ultimate* (fast) biodegradability, where a fluid breaks down over 90% in 28 days and *inherently* (slow) biodegradability. An overview of the biodegradation test methods employed by and other standardization organizations such as ISO and ASTM is listed in [9].

2.3 State-of-the-Art Hydraulic Pumps

2.3.1 The Positive Displacement Pump

The invention of the hydraulic or positive displacement (PD) pump is accredited to Ctesibius, a Greek inventor and Mathematician around 200 B.C. The term “positive displacement” refers to the phenomenon where fluid is moved by confining a fixed amount of it and then forcing (displacing) that trapped volume out of the confining. Today this is still the only method to create high pressure difference ($>50\text{bar}$) over a single pump in hydraulic systems.

Pumps can be divided in two general categories: kinetic (or hydrodynamic) and PD pumps. In hydrodynamic pumps such as centrifugal pumps, the flow is continuous from inlet to outlet and results from kinetic impulse given to the fluid stream.

The output is characterized by low pressure and high volume. Inefficiency and easy stalling as a result of back-pressure make these pumps unsuitable for control. In PD pumps, fluid flows through an inlet into a chamber. As the pump shaft rotates, the (positive or definite) volume of fluid is sealed from the inlet and transported to the outlet where it is subsequently discharged. The essential difference between these two main categories is that kinetic pumps are for fluid transport systems and PD drive systems are for fluid power systems. By far the most widely used type of pump is the

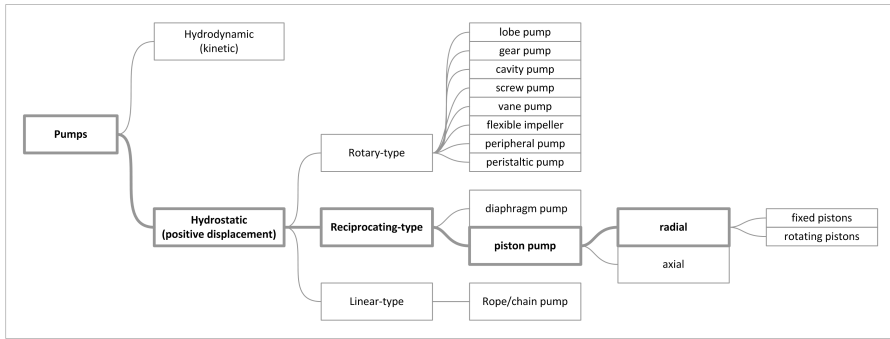


Figure 2.3: Classification of positive displacement pumps

centrifugal pump (kinetic). Positive displacement pumps only account for about 10% of pumps in existence [10].

The PD pump exists in several configurations, see figure 2.3. It converts mechanical power ($\text{torque} \times \text{rotation speed}$) to a pressurized fluid flow ($\text{pressure} \times \text{volumetric flow rate}$).

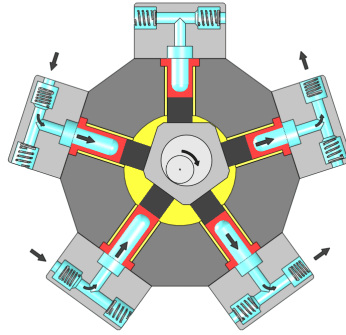
The choice of which type to apply depends predominantly on the rotation speed, the required pressure and on occasion the type of fluid. Another consideration is the need for fixed or variable volumetric displacement. Pumps with variable displacement allow the operator to vary the fluid displaced per revolution of the pump. For power transmission systems, energy efficiency is also a criterium.

2.3.2 The Radial Piston Pump

Large offshore wind turbines rotate with relatively low speed and high torque. Currently there is one clear market leader manufacturing efficient low speed/high torque hydraulic motors which are also applicable as pumps. Where a PD pump converts torque into pressure, a positive displacement (PD) motor converts pressure into torque. Swedish company Hägglunds Drives AS (since 2010 gradually integrated



(a) View of the cam ring, pistons and rollers inside a Häggglunds Compact hydraulic motor (also applicable as pump) [11]



(b) Animation a radial piston pump [12]

Figure 2.4: Examples of radial piston pump and motor configurations

into the Bosch Group) developed its first hydraulic motor for low speed/high torque applications in 1960. Since then, several types of radial piston motors were developed for different industrial applications. Recently the focus of the design of their drive systems has also moved to power transmission applications in renewable energy technology, such as wind and tidal turbines. The key to their technology is that the radial pistons roll along a cam ring. The number of cams determines how frequent each cylinder charges and discharges per revolution of the pump shaft. High volumetric efficiency is possible through a combination of small tolerances and effective seals between piston and cylinder wall and a sufficiently high cylinder cycle frequency.

If one considers the wind turbine rotor to be directly coupled to a single pump, the current product range offers solutions for wind turbines up to approximately 1MW installed capacity. The reason that a suitable drive for a 5MW rotor is not available is due to lack of demand, not technical feasibility.

Because Häggglunds pumps are the state-of-the-art of what is suitable for wind turbine application, their properties are used in several design calculations and simulation models throughout this thesis.

2.3.3 (Sea)Water Hydraulic Pumps

When the rotation shaft seal of a pump or motor wears out or a hose bursts, hydraulic fluid spills into the surrounding environment. Current measures to minimize the impact on this environment are to use fluids with high biodegradability and to contain and clear the spillage using absorbing materials. During the Dutch Fluid Power Conference in September 2012 the consensus was that in particular offshore hydraulic systems will gradually be forced to use (sea)water as hydraulic medium to minimize pollution. Using (sea)water as medium has some important benefits:

1. It is freely available and in abundance.
2. There is little or no risk of pollution.
3. No cooling is needed.
4. There is a reduced risk of fire.

A breakthrough in the development of seawater hydraulics was announced in an article in volume 82 of “New Scientist”, published on April 12th 1979. It mentions that, at the time, hydrostatic motors using seawater instead of oil were near to commercial production. These motors, developed by the British National Engineering Laboratory (NEL), were expected to have a short life and be relatively expensive. An article in the same journal from June 25th 1987, p.45 mentions the development by NEL of pumps sizing up to a stroke volume of 73.3cc (110 lit/min at 1500rpm).¹ However, the market for seawater hydraulics has remained a niche with only few specialist manufacturers.

In 1994 Danish hydraulic components manufacturer Danfoss introduced new water hydraulics technology called Nessie. Its systems are capable of matching the performance characteristics of oil hydraulic systems. Initially the technology was developed for filtered (10 μ m) tap water. Later, systems for technical water and seawater were developed. So far, the Nessie axial piston drives have been developed up to a volumetric displacement of 100cc/rev. The main types of application are:

- Jetting, i.e. creating either a high velocity jet (fire fighting, industrial cleaning) or mist (for cooling, dust suppression)
- Reverse osmosis (RO) for water desalination, including energy recovery from RO.

¹A subsidiary company “Scot Tech” was to be formed for commercial development of these pumps as part of what is now Fenner Power Transmission Group. What has eventually become of this technology is unknown to the author. Communications with Fenner proved unfruitful.

- Conventional hydraulics (forges, presses, food processing equipment)

Water hydraulics is widely used in the mining and steel/non-ferrous metals industries. Here, the high working temperatures and hazardous environments have oil hydraulics undesirable. Initially focused on mining, Hydrowatt from Schaffhausen [12], Switzerland developed radial pressure pumps (so far up to 250cc/rev), which are capable of using seawater as medium. The key technology in this pump is the sleeve inside the piston which is slightly stretched when the piston is charged. The use of this sleeve means there is no leakage across the piston. This is beneficial in terms of volumetric efficiency, however the heat created by the expansion and contraction of the piston sleeve will reduce mechanical efficiency. In 2009 IHC Hydrohammer developed a seawater hydraulic system for deep sea pile driving [13], incorporating the Hydrowatt drives (see figure 2.5). A key advantage of this system is the option to use an open circuit (i.e. the fluid is not circulating). Although this cancels the need for cooling equipment, a disadvantage is that it is likely that filters have to be cleaned more frequently.

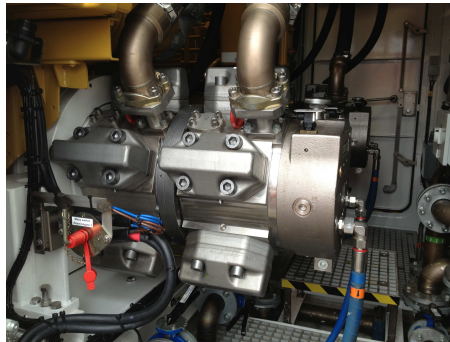


Figure 2.5: The R250/250S Hydrowatt radial piston pump in a seawater hydraulic power pack of IHC Hydrohammer

2.4 Common Components of Hydraulic Circuits

A common setup of a hydraulic transmission is to have a prime mover, usually a diesel engine or electric motor, directly coupled to a hydraulic pump. The pump charges the fluid to sufficient pressure to move a linear (cylinder) or rotary (motor) actuator.

The prime mover typically operates at constant speed (normally 1500 or 1800 rpm). Only the required torque (electric current) varies. Here, Pascal's principle is

exhibited again: low torque at high speed is converted into low speed and high torque or force. Common additional circuit components are:

- **Pressure relief valves** to avoid overpressure. One of the major advantages of a hydrostatic drive train over an electro-mechanical drive train is the safety relief valve. Once the pressure in the system reaches a predetermined threshold, the valve opens. The maximum pressure in the system is thus limited. A functional diagram of this component is given in figure 2.6.
- **Directional valves** to ensure the flow direction.
- **Control valves** to control flow to respective actuators.
- **Piping**, lines typically distinguished are:
 1. the work line (high pressure),
 2. the return line (low pressure),
 3. the supply or charge line (low pressure),
 4. the drain line (low pressure) which drains internally leaked fluid from a pump or motor.
- **Filters** - to reduce wear of components. The degree of filtration is given in micrometer (μm), also referred to as “micron” (not an SI-unit). A typical value for hydraulic systems is $10\mu\text{m}$.
- **A charge system** or “boost” system is required if the pump has no self priming ability. Failure to secure fluid supply to such pumps will cause cavitation. The charge system thus secures a feed flow to the pump.

2.5 Fluid Power Transmission Applications in Wind Turbines

2.5.1 Ideas Born from the Oil Crises

The global oil crises in the 1970s led to a push in the search for alternative energy sources. Major and minor programs were set up to develop wind energy technology. The oldest found patent application stating the idea of applying fluid power transmission dates from 1981 [14]. Like most of the major wind energy projects [15] of that time, both the experimental projects described here enjoyed limited success.

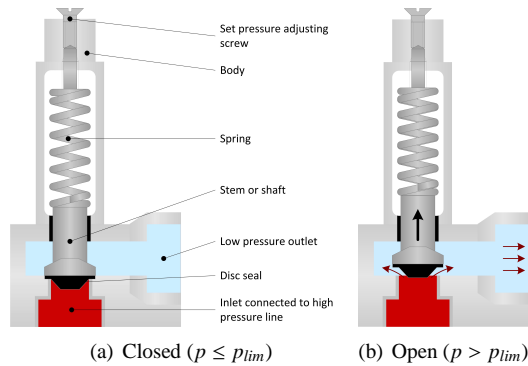


Figure 2.6: A pressure relief valve

The Bendix/Schackle 3MW Turbine

Around 1980, this variable speed turbine, designed by Charles Schackle and built by the Bendix Corporation, was erected at the Southern California Edison Wind Center, USA. The upwind 3-bladed turbine had an optimal tip speed ratio of 6 and a rotor manufactured of wood and fibreglass with a diameter of approximately 50m. The drive train was a hybrid system that included a one-stage gearbox coupled to a variable hydraulic transmission. The hydraulic circuit consisted of fourteen fixed displacement axial piston pumps operating in conjunction with eighteen variable displacement axial piston motors at ground level. The yaw system was located at the ground level, so that the triangular truss tower also rotated when the turbine was faced into the prevailing wind direction. The turbine had a relatively high rated wind velocity of 40mph (17.9m/s) and a cut-out wind velocity of 55mph (24.6m/s).

The conclusion of the project involving this prototype was that the application of hydraulic transmission was unsuited for wind turbine application. The main reason was the lack of components specifically designed for the needs of efficient wind power generation [16, 6]. The hydraulic components that were used yielded low energy efficiency (particularly at partial load) and often proved to be unreliable.

JERICO - 6.3kW

In 1981, The Jacobs Energy Research Inc. (JERICO) submitted a report to the US Department of Energy with the results of using a small wind turbine with hydraulic transmission (one step gearbox coupled to a gear pump) [17]. Testing the system was done by mounting a five meter diameter turbine on a trailer behind a pickup truck

and pulling it over the road. The results showed a maximum output of 6.3 kW at a wind speed of 11.1 m/s and a corresponding pressure of 82.7 bar. A lack of precision engineering resulted in an overall low efficient system, which required high start-up torques.

The general conclusion of this project is that for small scale applications, a hydraulic drive train is not a practical solution, but that for larger systems “these drawbacks may become less significant and the advantages may be more prominent”.

2.5.2 The Big Push for Renewable Energy

Between the early 1980s and late 2000s, research and development on wind energy technology continued, particularly in Europe. However, research on hydraulic transmission for wind turbines was only sporadically published.

Since the end of the 1990s, the rise in the global demand for fossil fuels has seen the cost of energy rapidly increase. This, in combination with the growing popular awareness of the effects of global warming, led to a second push for alternative energy sources. The last ten years have seen an exponential growth of the wind turbine industry.

Around 2007, the typical large (0.5 - 5MW) wind turbine onshore and offshore had an upwind rotor with three pitch-controlled blades. Two general configurations of the drive train were distinguishable:

1. a gearbox with between 1 and 3 stages of helical and/or planetary gears, coupled to a variable speed generator, which was connected to a frequency converter and a voltage converter.
2. a direct drive generator, also connected to a frequency converter and a voltage converter.

The increased competition for space on the European main land and the favorable wind climate and shallow waters of the North Sea, the Baltic Sea and the Irish Sea incited the movement offshore. However, since the commissioning of the first large (10MW+) offshore wind farm in 2002 at Horns Rev, concerns have arisen on reliability and maintainability and the subsequent drop in availability (i.e. revenue). These have led to wide-spread questioning of the way in which energy is being extracted from offshore wind.

The enormous growth of the wind energy market has also incited parties to look for new technical solutions or to reconsider older ones. Since 2007 a wide variety of drive train concepts have been presented, including the hydrodynamic gearbox [18] and superconducting generators [19]. Developments in hydraulic equipment and the possible advantages listed in section 2.7 have led several parties to research the application of fluid power drive trains for wind, wave and tidal turbines.

ChapDrive AS

The Norwegian company ChapDrive AS has developed a hydraulic transmission with a variable speed control system. The principal characteristic of their concept is the relocation of the major components from the nacelle at the top of the turbine tower to a power unit at the base of the tower using a hydrostatic transmission with a synchronous generator. They have refitted conventional wind turbines (onshore) into 225 and 900 kW functioning prototypes.

In 2010, Chapdrive diverted from their initial idea of having the generator at ground level. Hence, the main difference between the Chapdrive and the Artemis concept is the use of a fixed displacement versus a variable displacement pump. A variable displacement motor is directly coupled to a synchronous high voltage generator, eliminating the need for a frequency converter and a voltage transformer. Currently systems with a rated capacity of 3.3MW and 6.6MW are being developed [20].

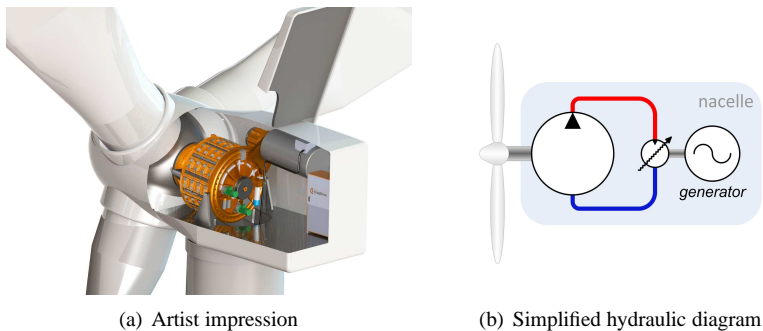


Figure 2.7: Chapdrive drive train solution for wind turbines [21]

Artemis Intelligent Power

Artemis is a spin-off company from a research group at the University of Edinburgh which initially focused on wave energy converters. It has developed a high efficient hydraulic pump/motor by means of computer controlled high speed solenoid valves.

The volumetric displacement of the radial piston pump is changed by controlling poppet valves with high speed actuators. Individual cylinders are thus reconfigured to either pump or idle on each stroke, resulting in high efficiencies over the complete range of operation, with a high level of controllability. These obtained efficiencies are comparable to that of a current wind turbine transmission and the technique is widely

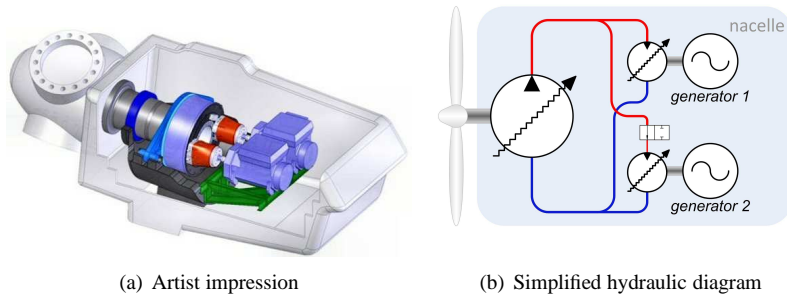


Figure 2.8: Artemis digital displacement concept [22]

regarded as potentially revolutionary for fluid power drives. This technology is also being developed for applications in different industries including hybrid vehicles, off-road vehicles and renewable energy generation.

In December 2010 Artemis Intelligent Power was acquired by Mitsubishi Heavy Industries, which also has a wind turbine manufacturing division. At the 2011 EWEA Offshore conference in Amsterdam, Mitsubishi announced their target of having their first hydraulic offshore wind turbine “Sea Angel”[23, 24], with an installed capacity of 7MW operational in 2015.

IFAS - 1MW Testbench

The Institute for Fluid Power Drives and Control at Aachen University in Germany (IFAS) is developing and testing a hydrostatic drive train for wind turbines in the 1MW-class. The 1MW test bench that was completed in 2010 allows measurements under realistic conditions as experienced by a wind turbine. This is so far the biggest test bench that allows real time simulation of the different components with promising results. Static and dynamic behavior is being explored with overall achieved efficiencies of 85% throughout a wide power range. A more detailed description of the IFAS hydrostatic transmission is given in section 5.4.1.

The Statoil/Häggglunds Two-Speed Concept

Statoil ASA and hydraulic motor company Häggglunds recently presented their idea for a two-speed hydraulic transmission with fixed displacement pumps and motors. The reasoning is that current state of the art variable displacement motors are less efficient at partial load. This concept employs four highly efficient Häggglunds motors

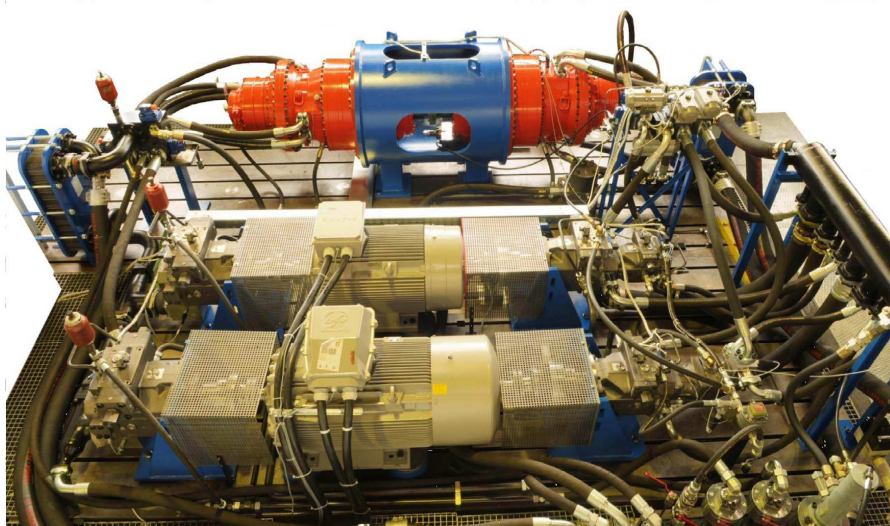


Figure 2.9: IFAS 1 MW test bench as described in section 5.4.1 and in [25]

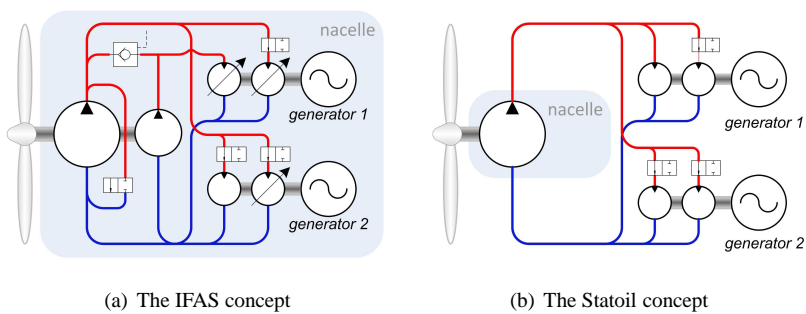


Figure 2.10: Simplified hydraulic diagrams of the IFAS and Statoil concepts

that can be switched on/off to allow the rotor to operate at or above the optimum tip speed ratio. The aerodynamic efficiency will be slightly reduced for the greater part of the envelope, but the transmission efficiency will significantly increase [26, 27]. The conversion from hydraulic to electric power happens at the base of the turbine tower. Statoil is also involved in the development of floating wind turbines [28]. The mass reduction that this hydraulic drive train concept introduces is thus particularly interesting.

2.6 The Delft Offshore Turbine (DOT) Project

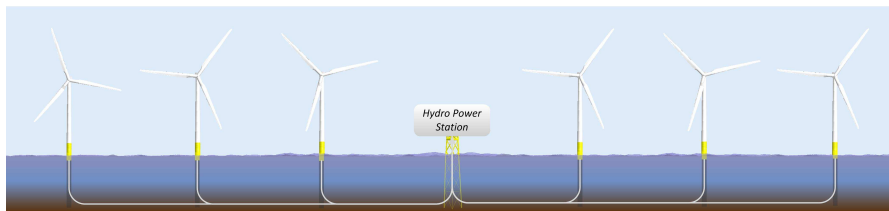
To stimulate the innovation in offshore wind energy technology, the Delft University wind energy research institute DUWIND launched the “Delft Offshore Turbine” (DOT) project in August 2008 [29]. This project is focused on the development of technical solutions to make offshore wind energy a commercially competitive source of energy. The approach is to step away from incremental improvements and reconsider how wind energy can be converted to useful electricity in the most technical-economic way. The physical scope of the project ranges from the horizontal axis rotor to the power grid connection onshore.

The DOT project was set up to re-examine every aspect of offshore wind turbine technology. However, in this dissertation, the focus is only on the power transmission system.

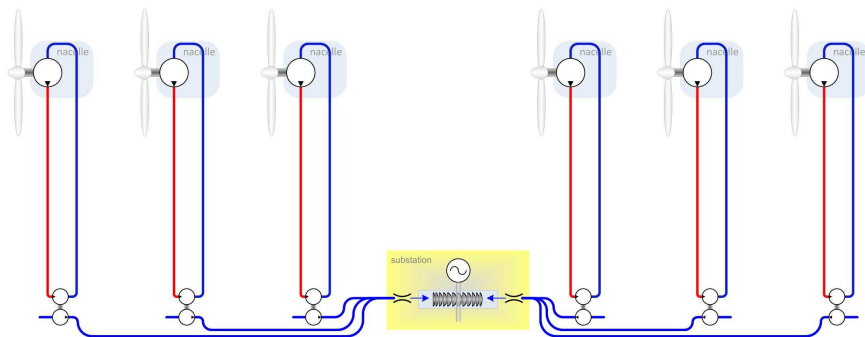
The energy conversion process from wind to electricity is radically different from conventional techniques. Recognizing the potential of fluid power transmission for wind turbines, the DOT pushes this idea one step further to fluid power transmission for offshore wind farms, with centralized electricity production and seawater as hydraulic fluid. The energy in the seawater from multiple turbines is thus relayed to one station where it is converted to electricity. This idea was invented and patented by Jan van der Tempel [30].

Centralized conversion to electricity should minimize the amount and total volume of electronic equipment. The only drive train component located in the nacelle is a directly driven positive displacement pump. The priming of the pump in the nacelle is an issue that is discussed in section 3.3.6. A single pipe will transport seawater from each turbine to the generator platform. This gives the wind farm an open-circuit seawater-based power transmission system. The goal is to use as few components and as little software as possible in order to simplify assembly and functionality, and reduce installation and maintenance requirements.

An overview of the DOT transmission concept is given in figure 2.11. The project objectives stated in this section form a platform from which to start the process of designing the fluid power transmission system. The development of the conceptual



(a) Artist impression



(b) Hydraulic diagram

Figure 2.11: The DOT transmission concept

design of the DOT transmission system is described in chapter 3. For the preliminary design in chapter 7 choices have to be made on the size or power rating of the rotor (see section 3.1.5) and which kind of pumps to use (see section 3.8.1).

Before the realization of the DOT, other decisions must be made, such as on:

- The design of the power/transformer station.
- If and how to include an option of long term or short term energy storage.
- How to deal with marine growth.
- How to minimize and ease maintenance requirements.
- How to maximize the ease of installation.

These issues are considered outside the scope of this thesis.

2.7 Advantages and Disadvantages of Applying Fluid Power Transmission in Large Offshore Wind Turbines

2.7.1 Advantages

1. The option of continuous variable transmission: this enables variable (optimal) rotor speed control with a constant output speed at the generator, thereby eliminating the need for a frequency converter.
2. The higher torque to weight ratio of the transmission in comparison with current commercial technology reduces the overall nacelle mass. This will influence the support structure dimensions [31].
3. The damping properties of hydraulic transmission systems mean that load peaks are smoothened, this is explained in more detail in section 4.4. It is one of the reasons why these systems have a reputation for tolerating highly dynamic and stochastic loads. An example of a common application where such loads are observed is in hydraulic excavators.
4. The low maintenance requirements: according to the product manual of the Hägglunds CBP motor, the only parts of the hydraulic circuit that require regular replacement are the filters. The condition of the hydraulic fluid must also be monitored. Controlling the oil contamination is essential for maintaining the reliability of the circuit components.

5. The presence of a non-rigid (i.e. soft or flexible) coupling: the connection between the pump and the rest of the circuit is usually not rigid. Hydraulic hoses allow for a degree of flexibility. For application in a wind turbine this is a significant advantage. One of the main sources of failure in offshore wind turbine is misalignment between the bearings of the low speed shaft and the gearbox connection [32, 33]. Although marginal, the misalignment causes eccentricity in the already highly dynamic loading of the gearbox. This leads to local peak loads which are higher and more frequent than was designed for.
6. Low risk of overload and subsequent overheating: every hydraulic circuit should contain one or more pressure relief valves. The pressure relief valve protects a line from excess pressure by opening at a predetermined threshold. Hence, damage to the system is prevented. As is demonstrated in section 6.3.2, this low cost solution to overloading is beneficial in wind turbine application.
7. Possibility of simple condition monitoring: on-line particle counters are widely used in the fluid power industry to monitor contamination of hydraulic fluids due to wear in the system.
8. Hydraulic components are modular. Hence different brands and sizes can be coupled.
9. The principle construction material of hydraulic components is steel. No rare earth metals are required.

2.7.2 Disadvantages

1. The energy efficiency is comparatively lower than a gearbox. When using state-of-the-art variable displacement motors this is even more so at partial load.
2. There might be external leakage. This is most frequently the case when components need to be disconnected. This means hydraulic fluid will spill into the surrounding environment. Depending on the type of hydraulic fluid, this may cause pollution or increase the risk of fire.
3. The availability of multi-MW components is limited, but growing. The research and developments mentioned in section 2.5 pushes this growth.
4. In preparation for the wind tunnel experiments described in section 6.3, it was found that water hydraulic pumps have a relatively high start-up torque due to internal friction. However, seeing how the torque at cut-in wind speed increases with wind turbine size, this is not expected to be an issue for large wind turbines.

2.7.3 Arbitrary Issues

1. Fluid power drives have a reputation for toughness/robustness, i.e. a high reliability of components.

The challenge with wind turbines is that continuous operation is required over a lifetime of at least 20 years. In comparison: a typical motorized road vehicle achieves no more than three years of continuous operation (based on 1,000,000km at an average speed of 40m/s).

According to the product manual, the design lifetime of a Hägglunds CB motor is 40,000 hours which corresponds to roughly four and a half years of continuous operation. The expected use is for 500 hours per 3 months, yielding a design lifetime of 20 years.

What is important to consider here is the effect that a component failure will have on the availability of a turbine. Availability can be increased by reducing the number of components, improved reliability of the components in place and reduced maintenance per component.

2. The presence of high frequency noise, caused by the switch of each piston between low and high pressure. How this compares to geared or direct drive transmission systems is not yet known for large wind turbines.

2.8 Concluding Remarks

The application of fluid power technology for the purpose of energy transmission was first applied in the later half of the 19th century. The idea of applying of fluid power transmission in wind turbines dates from before 1980, although developments around this time proved unsuccessful.

So what exactly has changed over approximately the last 30 years that have lead to a new attempt at fluid power drive trains? Two main developments hold the key:

1. the development of computer based precision engineering, which has allowed tolerances to become smaller, yielding drives with higher efficiency.
2. the development of the radial piston pump in combination with a cam ring. This enables energy efficient operation at low rotational speeds.

The efficiency of current variable displacement drives is still deemed unsatisfactory by developers of fluid power transmission and wind turbine manufacturers. This problem is mitigated by developing new drives, specifically designed for high efficiency and by coupling multiple fixed displacement via control valves to have a form of variable displacement [26].

The increasing demand for affordable renewable energy technology over the last few years has lead to new research on fluid power technology as a means for energy transmission. Applications are researched and developed for wind, wave and tidal energy. The main motivations are:

- high torque to weight ratio, i.e. the compactness of the transmission reliability
- reputation for the ability to tolerate highly dynamic and stochastic loads.
- reputation for reliability
- reputation for low maintenance requirements
- the option of continuous variable transmission ratio, which excludes the need for frequency converters.

Considering these aspects, there is a case to be made that a hydraulic solution may offer solid economic benefits when compared with current geared solutions. The reason that multi-MW hydraulic drives wind turbines are not available yet is due to lack of demand, not technical feasibility.

Conceptual Designs of Fluid Power Transmission Systems for Offshore Wind Turbines

3.1 Introduction

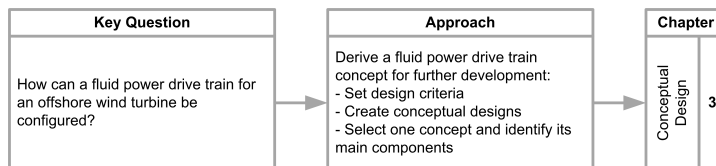


Figure 3.1: Flowchart for the objective and approach of chapter 3

3.1.1 Background

In the chapter 2 the arguments for considering fluid power transmission in large offshore wind turbines are presented.

Offshore wind turbines are situated in remote locations with harsh environments. Their sole purpose is to extract energy from the wind and convert it into electricity.

Horns Rev, commissioned in 2002, is widely considered as the first “real” offshore wind farm, due to its size (80× 2MW turbines) and its location (14km of the Danish coast). According to the EWEA: as of 30 June 2012, 1,503 offshore wind turbines

are fully grid connected in 56 wind farms across 10 countries, with a total capacity of 4,336MW [34]. The largest fully commissioned farm at this time was the UK's Greater Gabbard with 504MW of installed capacity. However development plans for the Dogger Bank in the North Sea mention a wind farm capacity of 1,800MW.

The development of an offshore wind farm is a highly complicated process. Over the years, many problems were encountered, such as issues with gearboxes, grouted connections and often seemingly simple installation logistics. Unfortunately these "lessons learned" are more often than not kept from the public by the project participants. The reluctance to share this information, which could be of great value to other wind farm developers, is due to fear of the eagerness of modern news media to publish bad news as a sensation and the immediate effect this has on political decisions.

3.1.2 Objective

The goal of the research presented in this dissertation is to find out whether the application of fluid power technology will lead to an improvement in the COE for offshore wind farms. The objective of the research presented in this chapter is to form conceptual designs in which this technology is applied and to select one for further analysis.

3.1.3 Approach

The approach taken here is to start at wind farm level and narrow down through the turbine level and to the drive train level. In section 3.2 those offshore wind farm design considerations which are relevant for the design of the drive train are listed. The

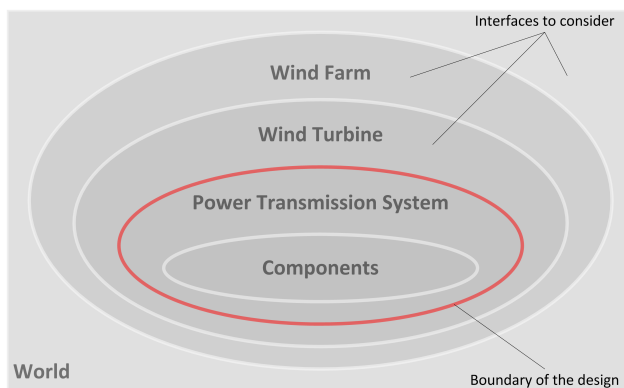


Figure 3.2: Surroundings and borders of the focus of the design process

next step (section 3.3) is to focus on the design considerations for the wind turbine drive train. From these considerations, design requirements for the hydrostatic drive train are derived in section 3.4.

The modularity of hydraulics make it possible to come up with many different designs for the drive train. In section 3.7.1, the design requirements are translated into a number of feasible configurations. Through multi-criteria analysis, the most suitable configuration is selected in section 3.7.2 which is subjected to further analysis in chapter 7. Next, the main power transmission components are selected for each main part of the conceptual design (section 3.8) of the transmission system.

3.1.4 Self-Imposed Constraints

The technology base, i.e. the technology that is considered for the system, corresponds to the current state of the art wind turbine technology and current state of the art fluid power technology. The properties of the main components are derived from commercial of the shelf (COTS) components. The selection process for the main component types is similar to the the process described in figure 3.3.

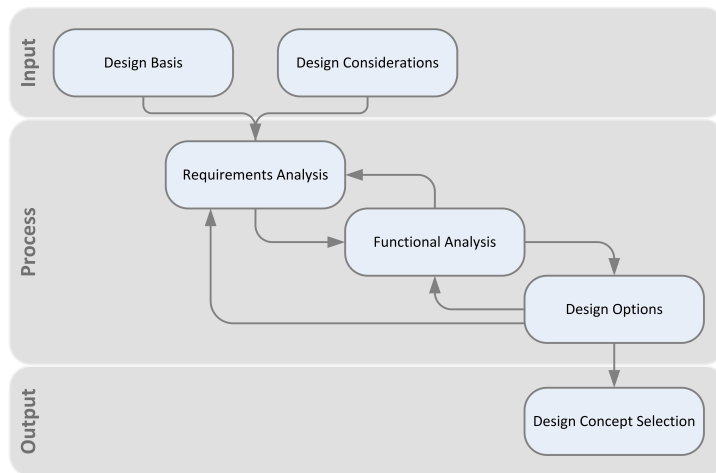


Figure 3.3: Conceptual design process

Design and certification standards set by parties such as Det Norske Veritas (DNV), International Organization for Standardization (ISO), Germanischer Lloyd (GL) and Lloyd's Register (LR) are to be consulted in later phases of product development.

For the purpose of simplicity the initial concept of operation is equal to that of a variable speed, pitch-controlled wind turbine. With the implementation of a (for wind turbines) new technology such as fluid power transmission, the existing design standards still have to be met. The purpose of introducing a new technology is essentially to improve the economic performance of a system. However, such an improvement may not lead to a degradation of standards in other aspects of the design. For instance the design lifetime still remains 20 years.

A fundamental requirement is that the implications of the design do not in any foreseeable way harm the environment. This means that there may be no pollution and that constraints are set on the sound level that is produced during installation and operation.

The primary functional requirements of a wind farm are:

- The harvesting of power from the collection of wind turbines and exporting it to the onshore grid.
- High reliability, thus requiring a minimum amount of visits per year to the wind farm. Typically the annual number of visits per turbine is around 6 [35]; 4 planned and 2 unplanned. According to [36] this should be less than one per turbine per year.
- High availability, thus minimum loss due to downtime in the power production. A typical number for the average availability is around 85% [2]. Some wind farm operators claim up to 98% availability, but this figure is achieved by leaving out scheduled maintenance.
- High power quality: the power from wind turbines is typically fluctuating due to the stochastic nature of wind. Voltage and frequency must be kept stable [37]. Although advances in power electronics have allowed for smoother power regulation, electricity from wind energy is still susceptible to voltage and current distortions due to harmonics. One of the solutions to improve the power quality is to use (short-term) storage to reduce fluctuations.

Note that ambiguous terms such as safe, simple, high, compact etcetera are used in reference to what is currently in publicly available literature.

3.1.5 The NREL 5MW Offshore Reference Turbine

The reference turbine is the NREL 5MW offshore baseline turbine [38]. This fictitious turbine has become the standard reference turbine for numerous academic studies. The main reason for this is that, in contrast to existing turbines, all its properties

are freely available. Some turbine parameters were arbitrarily selected using engineering judgment; others were selected to match those of the Repower 5MW turbine. For instance the EU-funded research project UpWind [39] also uses the NREL design. The only difference between the UpWind 5MW and the NREL 5MW turbines is that UpWind incorporates an industry standard controller developed by Garrad Hassan [40].

The properties assigned to the NREL turbine are aimed to represent the current state of the art for offshore wind turbines. This infers a drive train with a three-stage gearbox and an asynchronous high-speed generator as the principle components. Some characteristic properties of the reference turbine are given in table 3.1.

description	symbol	value	units
optimal tip speed ratio	λ	7.55	[-]
maximum power coefficient	$C_{P_{max}}$	0.48	[-]
No. of blades	N_{blades}	3	[-]
cut-in wind speed	v_{cut-in}	3.0	[m/s]
rated wind speed	v_{rated}	11.4	[m/s]
cut-out wind speed	$v_{cut-out}$	25.0	[m/s]
No. of gear stages:		3	
Control method:		variable pitch	

Table 3.1: NREL 5MW reference turbine properties

3.2 Offshore Wind Farm Design Considerations

3.2.1 Offshore Wind Farm Economics

The economic success of any power plant is determined by the cost (and the pricing) of energy.

The costs of an of any major system or structure are divided into the initial capital cost or capital expenditure (CAPEX) required to put the system in place and the operational cost (OPEX).

The CAPEX resides in fabrication, acquisition and installation. The cost of fabrication and or acquisition are essentially dependent on the mass, the complexity and the construction materials of the product. The cost of installation is dependent on the mass, complexity and maneuverability. The motivation for hydrostatic transmission is the foreseen reduced mass, complexity and cheaper materials.

For the wind farm operator, the aim is to produce maximum power output at the lowest OPEX. Cost depends on the wear of components and the required maintenance.

Another important economic aspect is the cost of money, i.e. interest rates, but this is considered to be outside the scope of this dissertation.

Prominent turbine manufacturers (Siemens, Vestas, Alstom, Mitsubishi) are all developing turbines with rated capacity larger than 6MW. Until recently, the design of a wind turbine for offshore was entirely separated from the design of an offshore wind farm. Currently, manufacturers are more and more addressing issues such as the tower-top mass, reducing the number of components, easy access methods for maintenance and the benefits of a higher tip speed ratio. It is safe to say that any offshore wind turbine (prototypes excluded) erected in the next 15 years will future be part of a farm. It therefore makes sense to optimize the design (in terms of the LCE) of the turbine from a farm point of view.

Offshore wind turbine designers should incorporate considerations and requirements of offshore wind farm design to minimize the levelized cost of energy (LCE).

3.2.2 The Competition for Space

The ideal site for an offshore wind farm has a favorable wind climate (high average wind speed, low turbulence), lies in shallow waters (approx. 20m) and is situated close to a port and close to a grid connection point.

The competition for space in shallow seas, close to a grid connection and with a favorable wind climate is fierce. A typical example of this is the Southern half of the North Sea. Typical stakeholders for such an area and the form of their stake are listed in table 3.2.2.

Stakeholder	Nature of claim for or occupation of space
the energy sector	offshore oil & gas infrastructure (incl. safety zones) offshore wind energy infrastructure (incl. safety zones) (international) electric power cables
communication sector	communication cables
the transport sector	shipping lanes anchoring sites (incl. safety zone)
the fishing industry	fisheries
flora and fauna	protected areas
seaside population and visitors	resistance against "visual pollution"

Table 3.2: Typical stakeholders for shallow seas, close to shore

3.2.3 Water Depth: Fixed versus Floating Turbines

So far, commercial offshore wind farms have been installed in relatively shallow waters using fixed support structures. Deeper waters require either a relatively larger support structure or a floating structure. Developments with floating wind turbines are still in an early phase of development. The water depth limit at which floating becomes the economically more attractive option is estimated between 80 and 100m [41].

In the hunt for offshore sites with favorable weather conditions near populated areas, the space in shallow seas is declining, whereas there remain plenty of deep water sites (Mediterranean/Norway/USA). Future wind farms will be placed in deeper waters and further away from the shore.

Space for offshore wind farms at locations with favorable wind climate	Shallow water (fixed structure)	Deep water (floating structure)
Near shore	Increasingly occupied	Ample space but visible
Far from shore	Targeted for future development	Ample space

Figure 3.4: Offshore wind farm location matrix

3.2.4 Distance to Port & Onshore Grid

The distance to port is important to consider for installation and maintenance. A large distance to port combined with a large wind farm might complicate logistics of maintenance to such an extend that an offshore servicing station is required.

The distance to shore defines cabling costs and the selected power transmission options. The typical setup of an offshore wind farm is to have an in-farm grid which connects the power lines from the turbines to a transformer station, where the voltage is boosted to reduce transport losses. High voltage power cables connect the wind farm to the onshore grid. Close to shore such as the OWEZ wind farm (10 to 18km from the coast), an offshore transformer station is not required.

3.3 Design Considerations for the Fluid Power Transmission System

3.3.1 Resonant Frequencies

To prevent resonance from occurring, the natural frequencies of the wind turbine components must be designed outside the ranges of normal operating frequencies. Operating frequencies to consider are:

1. The rotor speed: the range of rotational speeds, the so-called 1P region.
2. The blade passing frequency: the related range of frequencies at which a blade passes the turbine tower. The tower is an obstacle in the air flow. Pressure builds up in front of it, causing a local reduction in wind speed. When a blade passes through this area with reduced wind speed, it has an effect on the torque produced by the blade. This phenomena is visualized by figure 4.8(a). For a three bladed turbine this is referred to as the 3P region.
3. The hydraulic circuit frequencies. For a system where the pump coupled to a rotor, the natural frequency is determined by the combined mass moment of inertia of the rotor and the rotating parts of the pump and the stroke volume of the pump (see section 4.4.4).
4. The piston reciprocation frequencies of the pump and motor (see section 3.3.2).
5. Hydraulic piping: the fluid inertia in pipelines can cause hammering (see section 4.4.1).

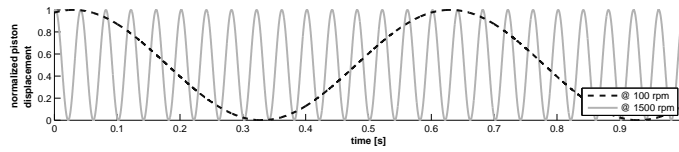
Due to the large number of components and/or modeling inaccuracies, it can happen that resonance does occur. This was for instance observed during the experiments described in section 5.4. Here the frame which supported the test facility resonated when the low speed shaft of the test bench rotated at around 24rpm. Fortunately, the resulting vibrations were small enough to ignore.

A mitigating measure is the manipulation of the control settings to avoid certain operating frequencies. This “frequency skipping” already happens with commercial turbines such as the Areva M5000 where the natural frequency of the support structure lies within range of operational frequencies of the turbine.

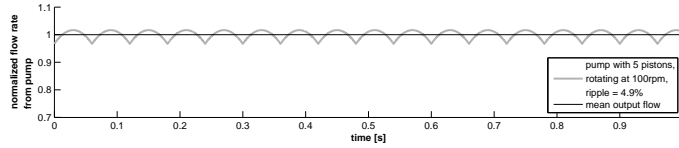
3.3.2 Flow Ripple

Radial piston pumps such as the one displayed in figure 2.4(a) have multiple pistons acting in parallel, with shifted phases. Each piston makes a sinusoidal motion. This

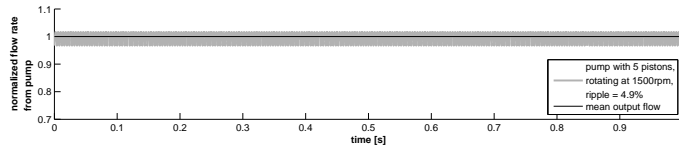
generates a near sinusoidal flow in (low pressure) and out (high pressure) of each cylinder. The shape of the this sinusoidal is perturbed by the effort it takes the piston to compress the fluid in a cylinder chamber to the point that the pressure in the chamber exceeds the line pressure and the non-return valve opens to let the fluid out of the chamber and into the high pressure line.



(a)



(b) the pump rotates at 100rpm



(c) the pump rotates at 1500rpm

Figure 3.5: Examples of flow ripple for an ideal pump (no leakages) with 5 pistons, rotating at 100rpm and 1500rpm

The flow into the circuit from each piston is thus either zero or shaped similarly to the upper half of a sinusoidal. The flow ripple is defined as the percentage of maximum difference in flow from the pump at an arbitrary rotation speed:

$$ripple = \frac{Q_{max} - Q_{min}}{mean(Q)} \times 100 \quad (3.1)$$

It leads to a pulsating flow in the pipe. If a hydraulic line is coupled to a pump with only one piston, the ripple is 100%. In principle it holds that the greater the amount of pistons operating in parallel (with shifted phase), the smaller the ripple. The speed of the pump and the number of pistons and their motion relative to each

other determine the frequency of the ripple. Hence a pump with only 5 pistons may have a ripple of 4.9%, but if the rotation speed is sufficiently high, the effect of this ripple becomes less pronounced.

The optimum configuration of a pump is that where the flow ripple is minimum for a minimum number of pistons. An example of flow ripple is given in figure 3.5. More elaborate explanations on the functioning of a radial piston pump and the flow ripple are given in [42, 43].

3.3.3 Heat Management

In fluid power systems, energy losses are predominantly converted into heat. The energy transferred from the wind turbine rotor is thus converted to useful work and heat by the hydrostatic drive train. The relation between the useful work and the produced heat is a measure of the system's energy efficiency. The main energy losses will occur due to the mechanical and volumetric efficiencies of the hydraulic drive systems. Volumetric efficiencies are associated with internal (cross-port) and external fluid leakages in pump and motor. Heat is lost through conduction, convection and radiation.

A standard solution for the cooling of a fluid power circuit is by running the return flow through a heat exchanger which is in contact with to the outside environment. In some cases a fan is used to improve convection.

For the design of a heat management system it is important to consider that the wind turbine should function on a cold winter's night (-20°C), a hot summer's day ($+30^{\circ}\text{C}$) and anywhere in between.

3.3.4 Choice of Fluid

For the choice of hydraulic fluid the following aspects should be considered.

- *Hydraulic stiffness*: for a circuit with relatively long lines it could be beneficial to use a fluid with a relatively high stiffness. The compressibility of a fluid (the inverse of the stiffness) and the total volume determine the speed of the response of a system. This is discussed more elaborately in section 4.4.
- *Viscosity*: the design value of the viscosity is a trade-off between friction losses and leakage (volumetric efficiency), see section 4.3.1.
- *External leakage*: it is safe to assume that every hydraulic circuit experiences some form of external leakage at some stage. Whether it is leakage due to insufficient sealing or spillage during installation or maintenance, the hydraulic fluid will come into contact with the surrounding environment. Although the

quantity is likely to be minute, there should be no harmful impact on the environment.

3.3.5 Seawater as Hydraulic Fluid

About 97% of the water on Earth is seawater. Almost every natural substance known to man is found in the world's oceans and seas, mostly in very small concentrations [44]¹ (see table 3.3). The most notable characteristic component of seawater with

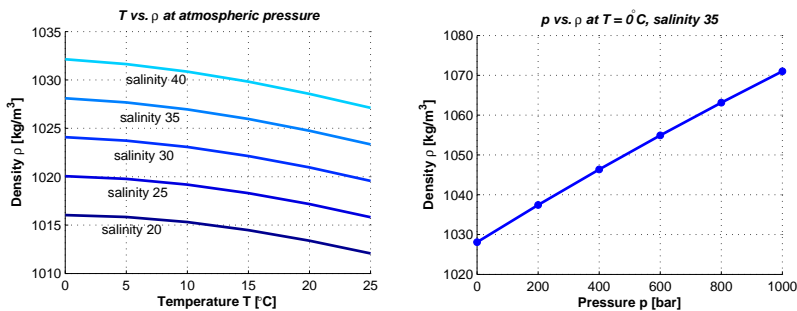


Figure 3.6: Density changes of seawater with temperature and pressure [46]

respect to freshwater is its salt. The salinity of seawater is a measure for its hardness and thus indicates its erosive potential. Although the vast majority of seawater has a salinity of between 3.1% and 3.8%, this number can vary significantly, for instance in response to addition of freshwater from rain and runoff, and removal of freshwater through evaporation.

Despite small compositional irregularities, seawater behaves as a Newtonian fluid, which is beneficial in terms of performance as a power fluid. For the use as hydraulic fluid, it is important to note that seawater contains suspended solids, organic substances, and dissolved gases (such as oxygen and chlorine which cause corrosion).

The density of surface seawater ranges from about 1020 to 1029 kg/m³, depending on the temperature and salinity (see figure 3.6).

Seawater density depends on temperature, salinity and pressure. Colder water is denser. Saltier water is denser.

According to [7]: *Water is a poor hydraulic fluid because of its restrictive liquid range, low viscosity and lubricity and rusting capability.* Recently though, the use of

¹Magnesium, bromine and sodium chloride (table salt) are all extracted from the sea on a global scale. In theory desalted seawater can provide a limitless supply of drinking water. So far this has been restricted due to the high processing costs.[45]

Element	Mass distribution [%]	Element	Mass distribution [%]
Oxygen	85.84	Sulfur	0.091
Hydrogen	10.82	Calcium	0.04
Chlorine	1.94	Potassium	0.04
Sodium	1.08	Bromine	0.0067
Magnesium	0.1292	Carbon	0.0028

Table 3.3: Seawater composition (salinity= 35) [44]

freshwater for high pressure hydraulics has gained new interest. With health, safety and environment becoming ever more important in modern industry, water-based hydraulics will likely see the number of applications grow. As discussed in [47], water is environmentally friendly (thus readily disposable), non-toxic, non-flammable, inexpensive, and readily obtained. Due to higher thermal conductivity, water systems require less cooling capacity than oil systems.

Low viscosity is generally regarded as the main disadvantage of water hydraulics. The reason for this is leakage flows in the drive systems. For equal geometry of leakage paths, water leakage is around 30 times larger than for oil [47]. Therefore it is essential for water power drives to minimize these paths further without increasing wear.

Fluids also have a property known as hardness, which is a measure for the mineral content. The relatively high concentrations of calcium and magnesium in seawater give it a high degree of hardness and thus its erosive nature [48].

3.3.6 Sources of Charge Pressure for a Pump at Hub-Height

Avoiding Cavitation

Cavitation is the occurrence of cavities in a liquid. This phenomenon occurs when the feed flow to a pump, which is not self-priming, is insufficient. The formation of a cavity and the subsequent implosion of it are an important cause of wear in hydraulic drives. To avoid cavitation, the charge pressure to the pump should be sufficient.

Closed Circuit Fluid Power Transmission

The hydraulic pump is coupled to the rotor shaft. The torque of the rotor shaft is equal to that of the rotor minus bearing friction losses. The closed-loop fluid power circuit has a similar function to that of the gearbox in a conventional drive train. The main components of this subsystem are:

- The positive displacement pump: directly coupled to the rotor shaft, the pump transforms mechanical power of the rotor into fluid power. The radial piston pump is the most suitable pump-type for the kind of applications required by the DOT [29]. The structural properties (stiffness & impermeability) of steel enable fluid power drive systems to operate at high pressure p . Using high pressure in relatively low weight drive systems yields a high power density.
- The hydraulic motor: located at the base of the turbine is a hydraulic motor which converts the pressure flow back into mechanical power.
- The vented reservoir & filter: for filtering and storage of hydraulic fluid.
- The boosting system: an auxiliary pump is used to add an extra pressure to the return line. This boost pressure enables continuous flow through the pump and prevents cavitation.
- The safety valve: to avoid exceeding the maximum allowable pressure.

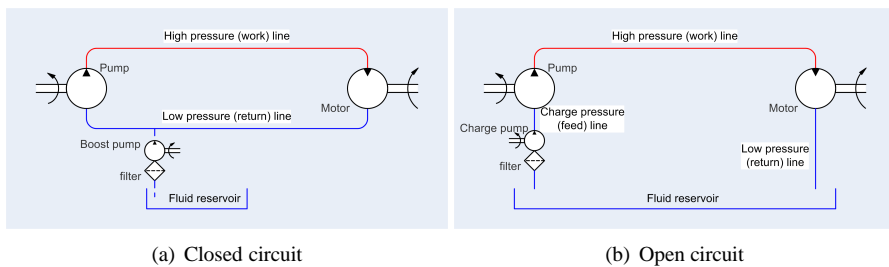


Figure 3.7: Diagrams of closed and open circuit hydraulic transmission systems

Open-Circuit Fluid Power Transmission

Here, an open circuit is considered, hence with seawater as hydraulic medium. Again, the hydraulic pump is coupled to the rotor shaft. To avoid cavitation at the pump an additional pumping system is required to force the seawater in the feeding line up to the non-self priming pump. Assuming that the main hydraulic pump will be less than 100m above the boost system, a centrifugal type boost pump capable of overcoming 20bar will suffice. The energy required to pump up this water is largely recaptured if the electricity generator is close to sea level. The main components of this fluid power circuit are the boosting system, the main hydraulic pump, the safety valve and the hydraulic motor or hydro turbine which converts the fluid power into mechanical power.

3.4 Design Requirements for the Fluid Power Transmission System

3.4.1 Functional Requirements

The primary functions of an offshore wind turbine are:

1. Extract kinetic energy from the wind and transform it into electrical energy
2. Feed the electrical energy generated by the generator to the electricity grid.
3. Operate safely and reliably during its design life (20 years), considering dedicated and acceptable maintenance.

The primary function of the transmission system is to convert mechanical power of the rotor into electricity. The aerodynamic rotor drives a positive displacement (PD) pump which converts the mechanical power into hydraulic power. At some stage the hydraulic power is converted back into mechanical power, which is converted to electric power.

	mode of operation	functional requirement
1	normal	Efficient operation throughout rotor performance envelope (low start-up torque required)
2	normal, $U_{\infty} < v_{rated}$	Control rotor speed: provide braking torque in order for the total system to operate at maximum energy efficiency between cut-in and rated wind speed
3	normal, $U_{\infty} \geq v_{rated}$	Limit rotor torque: provide braking torque in order for the total system to operate at nominal drive train torque between rated and cut-out wind speed
4	emergency stop	Force safe and controlled emergency shutdown: redundancy required either by drive train or via blade-pitch system

Table 3.4: Operational functions of the drive train

3.4.2 General Requirements

The requirements for the transmission system, as listed in chapters 1 and 2, are that throughout its design life (20 years) it is safe, sustainable, simple to install, operate and maintain/service, reliable (robust), compact and energy efficient, as well as requiring little and simple maintenance. These hold for every component/aspect of the design.

Installation Requirements

Installation should be fast en cheap. Hence the system must be easy to handle and simple to install. The aim is therefore to have the simplest configuration, i.e. minimum number of (sub)components, with size & minimum mass.

Operational Requirements

To maximize the power output of a turbine it is desirable to have maximum availability when the mean wind speed at hub height is between cut-in and cut-out wind speed.

The condition of the system should be observable at all times. Hence monitoring sensors (wind speed, rotor speed, pressures and temperatures) and interfaces are required.

Maintenance Requirements

The cost of operation and maintenance is estimated to be between 18% and 32% of NPV total wind farm costs [49, 16]. Considering the accessibility of wind turbines offshore and the traveling time from and to port, it is desirable that repair and maintenance are required as little as possible. When it is needed it should be simple and fast. Drive train components which are most likely to require regular replacement are filter cartridges and control valves (wear). Even for a 5MW hydraulic circuit, these components are likely to be sufficiently small and lightweight compared to the gearbox of existing wind turbines.

Verification Requirement

To present a business case for this new technology, the cost of energy should be significantly ($> 10\%$) less than for competing technologies.

3.5 Hydraulic Circuit Configuration Options

3.5.1 Variable Speed Operation

The reference technology described in section 3.1.5 is a variable speed wind turbine, designed to run at the optimal tip speed ratio between cut-in and close to rated wind speed. Between rated and cut-out wind speed the rotor speed is kept constant. Hence variable speed operation is a drive train design condition. For speed control at wind speeds greater than rated, pitch control is assumed in this dissertation.

3.5.2 Options for Closed-Circuit Hydraulics

The method of drive train torque control is typically determined by the type of generator. A hydraulic drive train is configured with either a fixed or a variable transmission ratio. In combination with a variable speed turbine with blade pitch control, the following options for the configuration of the closed-circuit transmission are identified. Their influence on the steady state performance of the rotor of the NREL 5MW reference turbine [38] are shown in figure 3.9.

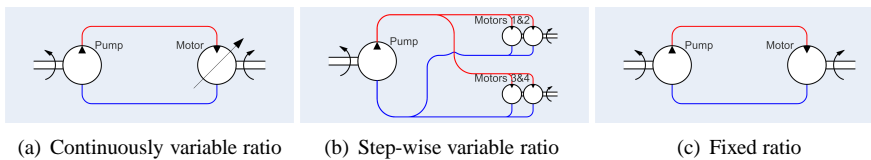


Figure 3.8: Configurations options for closed-circuit hydraulic transmission systems

Continuously Variable Transmission Ratio

A variable speed turbine with a synchronous generator (rotating at constant speed, synchronous to grid frequency) requires a variable transmission ratio. The standard hydraulic solution for this is to manipulate the stroke volume (swash plate angle) of either the pump(s) or the motor(s) or both. See figure 3.8(a)

Step-Wise Variable Transmission Ratio

An alternative solution is to have multiple fixed displacement motors coupled to one or more generators, which are activated through valve control [27]. The configuration in figure 3.8(b) has four motors, which are independently activated using control valves. When two motors are connected to one generator and only one is activated the other is idling.

Fixed Transmission Ratio

A variable speed turbine with an a-synchronous generator requires a fixed transmission ratio. Here the hydraulic circuit is externally controlled by the generator torque. Hence pump(s) and motor(s) with fixed volumetric displacement suffice.

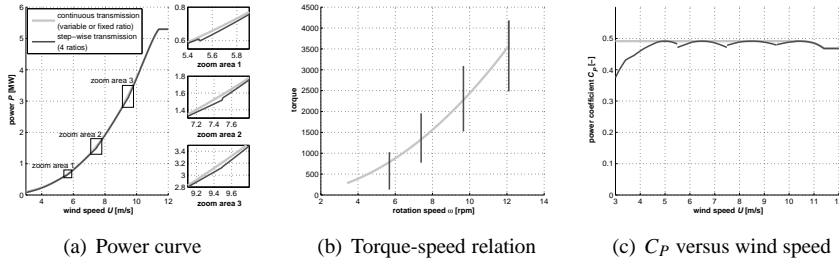


Figure 3.9: Steady state performance diagrams of the aerodynamic rotor for various types of drive train combinations, divided in continuously and step-wise (4 steps) variable transmission ratio; note the zoomed areas in figure 3.9(a) which indicate the switching in the number of active hydraulic motors

3.5.3 Options for Open-Circuit Hydraulics for Centralized Electricity Production

Seawater is used as a medium to transfer energy from each turbine to the generator platform. The ideal solution here would be to have a self-priming seawater hydraulic pump coupled to the rotor via the low speed shaft, such as shown in figure 3.10.

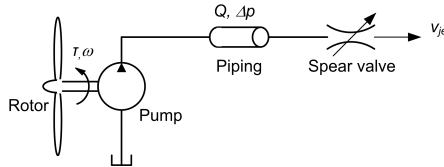


Figure 3.10: Simplified hydraulic diagram of an ideal but unrealistic solution for the open circuit configuration

However, commercially available positive displacement pumps suitable for seawater are neither self-priming nor designed for low speed operation. Although the technology of the Hydrowatt pumps could be combined with the cam solution of the Hägglunds motors (see section 2.3), this pump-type is not a reality at this time and is therefore neglected as an option. Hence, an additional fluid power circuit is applied between the low speed rotor shaft and the high speed seawater pump. This transmission thus essentially acts as a gear.

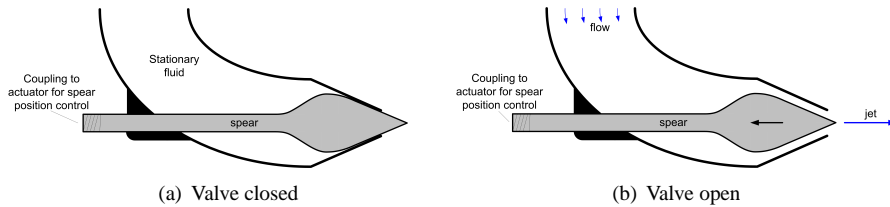


Figure 3.11: Diagrams of a spear valve

Variable Transmission Ratio

The transmission ratio is made variable using a spear valve, which guides a jet onto a fixed speed hydro turbine, which is coupled to a synchronous generator. The cross-sectional area of the spear valve outlet determines the pressure in the system. By moving the spear away from or towards the outlet, the outlet area is increased or reduced.

Similar to wind turbines, hydro turbines have an optimal speed ratio between the flow velocity and the angular velocity of the hydro turbine. For a constant speed ratio, constant pressure is required. This is achieved by controlling the outlet cross section of the spear valve. Constant pressure and variable speed operation mean the flow must vary. Hence, a variable displacement seawater pump is required.

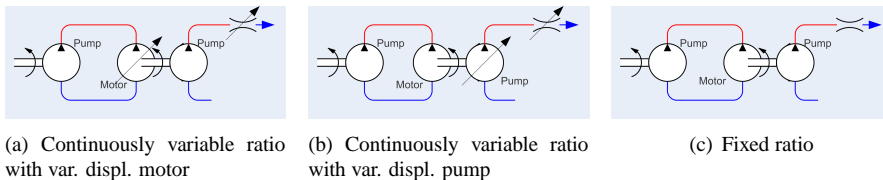


Figure 3.12: Configurations options for open-circuit hydraulic transmission systems

Fixed Transmission Ratio

The transmission ratio is kept constant by using a nozzle or spear valve (with fixed outlet area), which directs the jet onto a variable speed hydro turbine, which is coupled to an asynchronous generator. A frequency converter is required to synchronize the power output with the onshore electricity grid.

Although in theory a simple nozzle will suffice, using a spear valve has the added benefits that (1) small adjustments can be made to optimize power production and (2)

no additional valve is required for shutdown (i.e. cutting off the flow completely).

In the configuration presented in figure 3.10, the high pressure line connects the pump to a spear valve. A horizontal-axis wind turbine rotor drives a pump with torque τ . The rotation ω of the pump shaft creates a volume flow Q . The pressure difference Δp over the pump is determined by the size of the outlet area of the spear valve. The spear valve converts the high pressure/low speed flow into low pressure/high speed jet (v_{jet}), i.e. hydrostatic to hydrodynamic power.

The correlation between the pressure build up in the system as a result of flow speed and the optimal aerodynamic torque means that maximum power production is possible with a fixed displacement pump. This solution is described in chapter 6, along with the experiments that prove its functionality.

3.6 Control Options

3.6.1 Control of Hydrostatics

The controllable parameters of a hydraulic transmission system are pressure, flow rate, torque and rotation speed. Control is enforced by changing the volumetric displacement or through control valves. External control is enforced by changing speed and/or torque. A spear valve is also a form of control valve.

3.6.2 Option 1: Maximum Power Point Tracking

Through continuous adjustment, operation at $C_{P,max}$ is ensured.

The main advantage of this option is that no reference values are required. Blade properties change over time. Composite materials age, which alters their stiffness. Dirt and erosion change the airfoil. When damage or dirt changes the aerodynamic behavior of the rotor, the $C_P - \lambda$ relation changes. Since no reference values are used, there is no need to reconfigure these values.

Wind is never constant. To get the maximum power out of the wind requires continuous adjustment to the braking torque.

Sensors measure the power P extracted from the wind by the rotor in the form of torque and speed. If the new P is greater than the old P , the braking torque is increased. If the new P is less than or equal to the old P , the braking torque is decreased. When P approaches P_{rated} , the control of the rotor blades takes over and the braking torque is kept constant.

This principle works with a black-box system, provided that the nominal speed and torque are given.

3.6.3 Option 2: Model-Based Control

Here, knowledge of the rotor aerodynamics is required as input, in particular the relation between the tip speed ratio and the power coefficient. From this the optimal speed-torque curve is derived and used as a lookup table. The drive train torque is then simply a function of the rotor speed. This form of control is common in wind turbines [40], despite the obvious drawback that the effect of a change to the aerodynamic properties of the rotor cannot be minimized by the controller.

3.7 Design Concept Selection

3.7.1 Overview of Feasible Concepts

Three feasible transmission layouts have been derived, see figure 3.13. For each a subdivision of hydraulic component configurations is made.

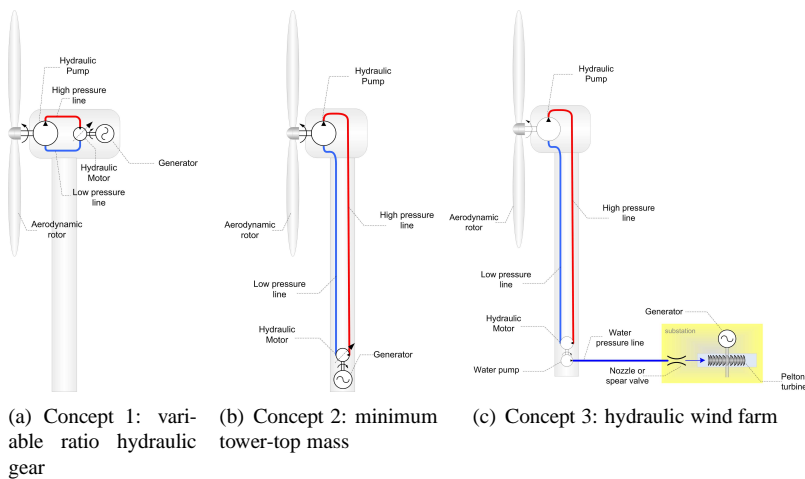


Figure 3.13: Three feasible concepts for hydraulic drive trains in offshore wind turbines

Concept 1: Variable Ratio Hydraulic Gear

This concept comes closest to the replacement of the gearbox in a conventional wind turbine offshore. The complete transmission system is located in the nacelle. A simplified breakdown of the transmission configuration in three parts:

- A The rotor, converting wind power into torque and angular velocity.
- B The closed-loop hydraulic circuit.
- C The generator and power electronics.

Several options for the configuration of motors and generators are possible, yielding a subdivision into concepts 1a, 1b and 1c (see table 3.5).

Concept 2: Minimum Tower-top Mass

Of the hydraulic circuit, only a pump is located in the nacelle. The motor, generator, filters, cooling and boost systems are placed at the base of the turbine.

The simplified breakdown of the transmission configuration in three parts is similar to concept 1:

- A The rotor, converting wind power into torque and angular velocity.
- B The closed-loop hydraulic circuit, running from nacelle to the base of the turbine tower.
- C The generator and power electronics.

Again, the various options of the hydraulic-electric component configurations yield concepts 2a, 2b and 2c (see table 3.5).

Concept 3: Hydraulic Wind Farm

Concept 3 comprises two hydraulic circuits. The first is a similar circuit to that of concept 2, with only a pump in the nacelle. The second is an open circuit whereby seawater is pumped to a substation where the hydraulic power is converted into electric power by a hydro turbine.

The primary reason to not have the rotor shaft directly connected to the seawater pump is that the technology for such a slow turning is not yet available. Hence the hydrostatic transmission acts as a gear with fixed ratio.

3.7.2 Selection of the DOT Concept for Further Development

An overview of the main components of the respective hydraulic transmission concepts is given in table 3.5. From a wind turbine point of view, concepts 1b, 2b and 3a have the minimum number of ticks up to the substation. Of these, 2b and 3a yield the minimum tower-top mass.

	Ref.	Concept 1			Concept 2			Concept 3	
		a	b	c	a	b	c	a	b
Nacelle									
Gearbox, three stage	✓	-	-	-	-	-	-	-	-
PD pump, fixed displacement	-	✓	✓	✓	✓	✓	✓	✓	✓
Motor, fixed displacement	-	✓	-	-	-	-	-	-	-
variable displacement	-	-	✓	-	-	-	-	-	-
multiple fixed displacement	-	-	-	✓	-	-	-	-	-
Generator, variable speed	✓	✓	-	-	-	-	-	-	-
fixed speed	-	-	✓	-	-	-	-	-	-
multiple, fixed speed	-	-	-	✓	-	-	-	-	-
Frequency converter	✓	✓	-	-	-	-	-	-	-
Voltage transformer	✓	✓	-	-	-	-	-	-	-
Cooling/boost/filter systems	✓	✓	✓	✓	-	-	-	-	-
Interface Nacelle to Tower Foot									
MV/HV electricity cables	✓	✓	✓	✓	-	-	-	-	-
Piping	-	-	-	-	✓	✓	✓	✓	✓
Tower Foot									
Motor, fixed displacement	-	-	-	-	✓	-	-	✓	-
variable displacement	-	-	-	-	-	✓	-	-	✓
multiple fixed displacement	-	-	-	-	-	-	✓	-	-
Generator, variable speed	-	-	-	-	✓	-	-	-	-
fixed speed	-	-	-	-	-	✓	-	-	-
multiple, fixed speed	-	-	-	-	-	-	✓	-	-
Frequency converter	-	-	-	-	✓	-	-	-	-
Voltage transformer	-	-	-	-	✓	-	-	-	-
Cooling/boost/filter systems	-	-	-	-	✓	✓	✓	✓	✓
Seawater PD pump, fixed displacement	-	-	-	-	-	-	-	✓	✓
Interface Wind Turbine to Substation									
HV electricity cables	✓	✓	✓	✓	✓	✓	✓	-	-
Piping	-	-	-	-	-	-	-	✓	✓
Substation									
Spear valves	-	-	-	-	-	-	-	✓	✓
Hydro turbines	-	-	-	-	-	-	-	✓	✓
Generator, variable speed	-	-	-	-	-	-	-	✓	✓
Frequency (and/or AC/DC) Converters	-	-	-	-	-	-	-	✓	-
Voltage Transformers	✓	✓	✓	✓	✓	✓	✓	✓	✓

Table 3.5: The main components of the considered drive train configurations

Variable displacement motors are less efficient than fixed displacement motors of the same type. Hydraulic pumps able to handle seawater are relatively expensive. However, concept 3a leads to a significant simplification of the offshore wind energy technology. This is why concept 3a is preferred. Hence forth it is referred to as the Delft Offshore Turbine (DOT) concept. In figure 3.14 the hydraulic diagram of the DOT is given. The entire system is divided into the following subsystems:

- A The rotor, converting wind power into torque and angular velocity.
- B The closed-loop circuit, where (a biodegradable) oil is the hydraulic fluid.
- C The open-loop circuit, where seawater is the hydraulic fluid.
- D The generator station, where one or more Pelton turbines, each coupled to a synchronous generator, convert the seawater pressure flow into electricity.

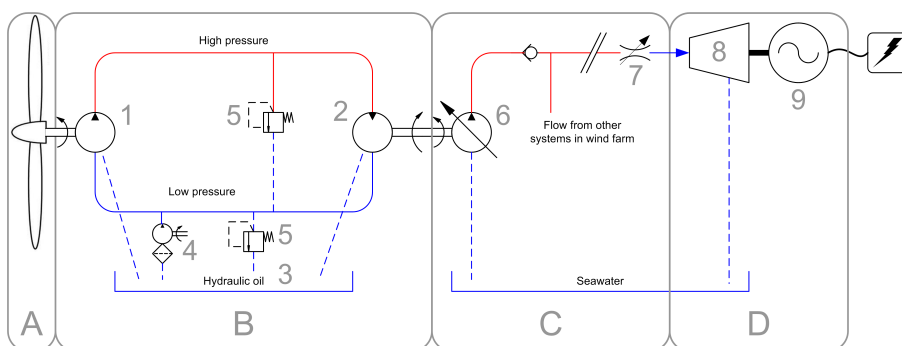


Figure 3.14: Schematic of the Delft Offshore Turbine power transmission: parts: (A) rotor, (B) closed-loop hydraulic circuit, (C) open-loop hydraulic circuit, (D) turbine generator components: (1) pump, (2) motor, (3) reservoir, (4) booster & filter, (5) pressure relief valve, (6) seawater pump, (7) spear valve, (8) hydro turbine, (9) synchronous generator

3.8 Selection of main component types

3.8.1 PD Pump

The different positive displacement (PD) pump options available on the market are shown in table 3.6. In this table the pumps are also compared to each other this is

done by indicating how good the pump fulfills each of the 4 main design objectives [50]. The pump option that gets the best total score in this comparison is the constant displacement axial piston pump. This is also the final pump used in the design for both the hydraulic oil pump and the water pump.

Type of pump	Size range [cm ³ /rev]	Maximum pressure [bar]	Compact energy transfer	Simplicity	Costs	Efficiency for large range of pressure
External gear	3-100	250	+	+	+	+
Internal gear	25-50	210	+	+	+	+
Vane-type	10-36	175	+	+	+	-
Radial piston	0.4-20	700	+	+	+	+
Axial piston	10-1000	400	+	+	+	+
Variable vane-type	8-125	160	+	-	-	-
Variable axial piston	20-1000	315	+	+	+	+

Table 3.6: Comparison of the pump options, + = reasonable, ++ = good, +++ = very good [50]

The radial piston pump is the design of choice. An overview of possible configurations of pistons and cams is given in figure 3.15. Such pumps can consist of multiple adjacent rings of pistons. Note that the number of pistons in one ring significantly influences the diameter of the ring and hence the size of the pump. The lower the operation speed, the more cylinders and cams are required, hence the larger the pump diameter.

3.8.2 Hydraulic Motor

The options considered for the hydraulic oil motor are also only positive displacement motors. They are compared in similar manner as the pumps, see table 3.7. The motor option that thus scores the best is the fixed displacement axial piston motor. The required speed of the hydraulic motor is typically as high as possible, to minimize the required size (volumetric displacement) of the motor and the pump to which it is connected. Due to the compatibility with 4-pole generators operating at grid frequency (50Hz in Europe/60Hz in USA), most fixed displacement pumps and motors are designed to have a nominal speed of 1500 to 1800rpm.

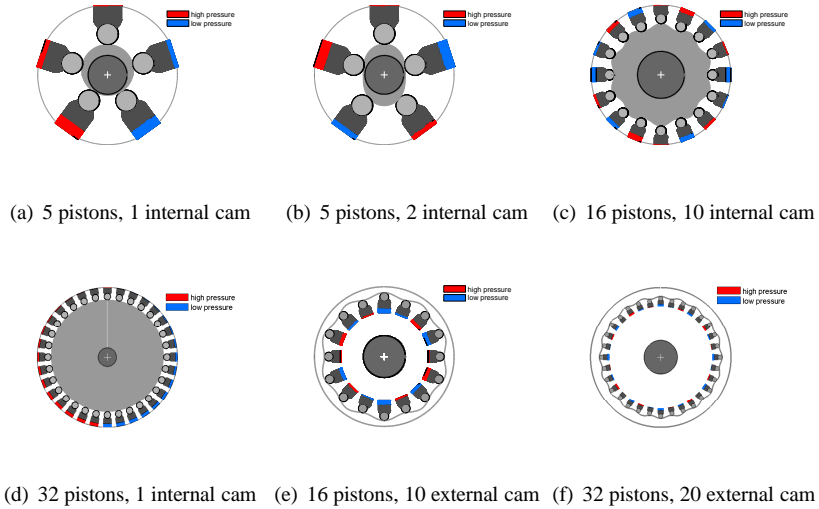


Figure 3.15: Radial piston pump configurations. Note that the center circle, representing the main shaft, is the same size for all configurations

Type of motor	Size range [cm ³ /rev]	Maximum pressure [bar]	Compact energy transfer	Simplicity	Costs	Efficiency for large range of pressure
Gear	6-38	250	++	++	+++	-
Radial piston	190-7000	420	+++	++	-	++
Axial piston	10-1000	400	+++	++	++	++
Variable radial piston	190-7000	420	+++	-	-	+
Variable axial piston	28-355	315	+++	-	-	+

Table 3.7: Comparison of the motor options, + = reasonable, ++ = good, +++ = very good [50]

3.8.3 Hydro Turbine

One of the main characteristics of the DOT is the idea of a centralized electricity generation. At the generator station, the pressurized seawater from all wind turbines is distributed over several hydro turbines.

The power capacity of offshore wind farms currently approaches the output rating of other large scale electric power plants. Thus the switch is made from having individual wind turbine electricity generators (eg. 100 generators of 5MW for a 500MW wind farm) to just a few central electricity generators. A few central generators will facilitate compliance with typical grid connection requirements for wind power plants (i.e. behavior during disturbances in the grid and control of the power quality).

Hydro turbines are a well explored technology that has allowed hydro power to achieve the highest operating efficiencies of all known generation systems, with capacities up to 1 GW per unit [51]. In a typical hydro power plant, the hydro turbine transforms the high water potential energy into mechanical rotational energy. For the DOT, this idea is also applied for the central generator platform, with the advantage that hydro turbines are used without the need of large reservoirs or dams due to the fact that the seawater is already pressurized from the individual pumping systems.

For an offshore wind farm, wake effects represent typically a power loss in the range of 10 to 23% of the power output [52]. From a centralized generation point of view, this means that if these losses are properly taken into account in a preliminary design phase, a size reduction of the central generator is possible, leading to economical benefits and higher capacity factor of the entire wind farm.

Hydro turbines are the prime movers that transform the energy content of the water into mechanical energy and whose primary function is to drive an electric generator. Depending on their working principle hydro turbines are classified into:

- *Impulse turbines*: in which the driving energy is supplied by the water only in kinetic form. The water pressure is converted into kinetic energy in the form of a high speed jet that hits the runner.
- *Reaction turbines*: in which the driving energy is supplied partly in kinetic and partly in pressure form. Water pressure can apply a force on the face in the runner blades and decreases as it proceeds through the turbine.

The first criteria for a turbine selection is the available pressure.²

Of the existing hydraulic turbines, the Pelton turbine is the most suitable for high pressures/high velocity jets.

²In hydro power terminology it is common to refer to pressure in terms of the height of the fluid column, known as “head”. Since the pressure in the seawater pipelines is not caused by elevation, but by wind power, the use of “head” is not considered appropriate, but merely confusing.

Turbine type	Pressure difference range [bar]		
Kaplan and Propeller	0.2	$< \Delta p <$	4
Michelli-Banki	0.3	$< \Delta p <$	25
Francis	1	$< \Delta p <$	35
Turgo	5	$< \Delta p <$	25
Pelton	5	$< \Delta p <$	185

Table 3.8: Range of operating pressure differences for hydro turbines [53]

From table 3.8 it is seen that for high pressure applications, the Pelton turbine is the most suitable. In this type of turbine, the high pressure water is converted into high velocity water jets by a set of fixed nozzles. Mechanical torque is produced at the turbine shaft when the high-speed water jets hit the bowl shaped buckets (spoons) placed around the turbine runner. The needle is actuated by the turbine governor with a servomotor.

An important advantage of the Pelton turbine is the ability to perform efficiently not only at rated and partial loads, but over a wide range of flow rates starting from 10% of the rated flow. The Pelton turbine used in the Bieudron hydroelectric power station in the Swiss Alps has a power capacity of 423MW per unit with 1,883m head ($\approx 185\text{bar}$) and $25 \text{ m}^3/\text{s}$ flow [53].

High rotation speed combined with high torque enable a compact design. Hence, a DOT farm requires only one or a few generators to produce electricity, using technology that is similar to what is used in hydro power plants.

Coupling Rotor Aerodynamics and Fluid Power Transmission

4.1 Introduction

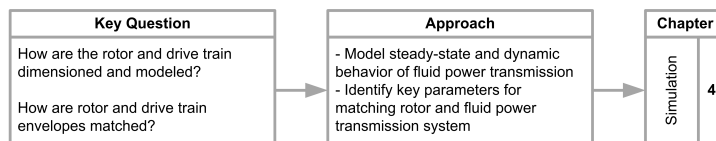


Figure 4.1: Flowchart for the objective and approach of this chapter

4.1.1 Torque Balance

In chapter 3 conceptual designs are formed of how fluid power transmission may be applied in offshore wind turbines. In all three designs shown in figure 3.13 the wind turbine rotor is directly coupled to a positive displacement pump. The rotation of the rotor causes the pump to displace fluid, creating a flow. The hydraulic motor converts the flow back into rotation. The resistance to rotation experienced by the motor is the required motor torque. This required torque determines the pressure in the line from the pump to the motor. At the pump, the pressure determines the torque that is experienced by the rotor as the resistance to rotation.

In order to efficiently and safely extract power from the wind, the speed of the rotor has to be controlled. The source of the rotor torque is free stream wind which

cannot be controlled. Hence, the braking torque must control the speed.

The design operating speed of the rotor of a wind turbine is limited by the airspeed of blade tips.¹ For large wind turbines the mechanical power thus exists in the form of low speed high torque. The balance between the rotor torque τ_{rotor} and the braking torque τ_p provided by the hydraulic circuit (pump) determines the speed ω of the rotor, as describe by equation 4.1.

$$J_t \dot{\omega} = \tau_{rotor} - \tau_p \quad (4.1)$$

Here, friction from the rotor bearings is neglected. J_t is the combined mass moments of inertia of the pump and the aerodynamic rotor.

Assuming the pump to have fixed volumetric displacement, equation 4.1 is the equation of motion of the rotor in the rotor plane.

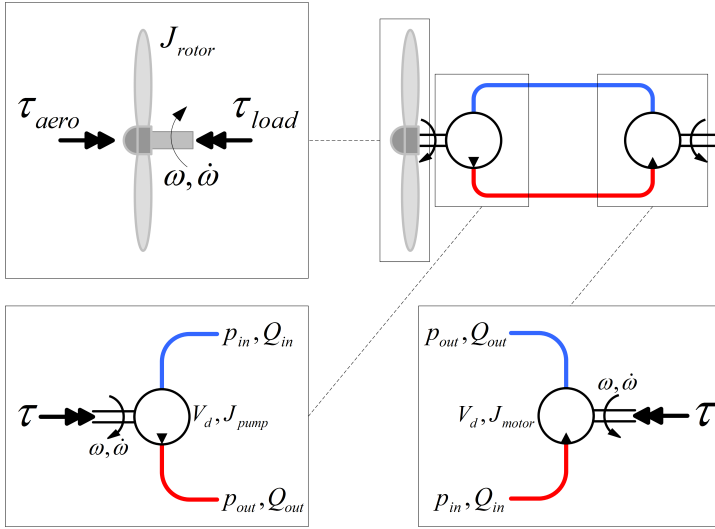


Figure 4.2: Free body diagrams of a fluid power circuit coupled to a rotor

The performance of a rotor is predominantly a function of the tip speed ratio λ and the blade pitch angle θ . The performance of a pump is predominantly a function of the rotation speed ω , the pressure p and the state of the hydraulic fluid. In order to have both pump and rotor operate as energy efficiently as possible, their performance envelopes have to match.

¹The design speed of the blade tips in the rotor plane is usually around 80m/s for larger wind turbines [1].

To model the behavior of the complete system, equation 4.1 must be solved. To solve this equation the following must be understood and for both wind turbine rotor and hydraulic circuit:

- how torque is produced
- how torque and speed are controlled
- what the optimal operating conditions are
- which properties are characteristic, i.e. which have a strong influence on the performance
- how the dynamic behavior is modeled
- which properties influence the dynamic behavior and how

4.1.2 Objective & Approach

This chapter describes how the steady state and dynamic performance of the rotor and the hydraulic circuit are modeled, based on well-established theoretical and empirical relations.

The simulation techniques described in this chapter have served to define a model for the entire transmission as presented in the conceptual design. The theory on rotor aerodynamics has been taken from [54] and [55]. The theoretical modeling of hydraulic drives has been extensively developed. The relations between the physical parameters and their performance used for this dissertation was derived from [7], [56] and [57].

The validation of (parts of) the modeling techniques is presented in chapter 5. Together with the control method presented in chapter 6, they form the basis for the preliminary design in chapter 7.

4.1.3 Macroscopic vs. Microscopic Approach to System Modeling

The analysis of fluid flow systems is typically done in one of two manners:

1. Microscopic - defining differential relations for fluid flow analysis [58]. The differential analysis method is used when a detailed flow pattern is required. A popular approach is the numerical analysis of the differential equations, also known as computational fluid dynamics.

2. **Macroscopic** - defining integral relations for a control volume analysis. The control volume analysis method is based on average property values (such as mass flow, induced force, energy exchange) at the boundaries of the control volume. This method is specifically useful for one dimensional fluid flow systems. It gives good engineering estimates of the systems properties.

In modeling rotor aerodynamics and fluid power transmission systems, the goal is to approximate the behavior of real life systems. The focus of this dissertation is on design synthesis and overall power transmission system performance. Detailed flow patterns in (parts of) the system are not of interest here. The differential analysis method will result in an overly detailed and complex model. Hence, the more suitable method is the control volume analysis.

4.1.4 Three Governing Equations

For both approaches described in section 4.1.3, three principles hold:

- **Conservation of mass** - In a mechanical system, the system is defined as a fixed quantity of mass m . Everything outside the system boundaries is called the surroundings. The law of conservation of mass states: *mass can neither be created nor destroyed*

$$\frac{dm}{dt} = 0 \quad (4.2)$$

- **Conservation of linear momentum** - Newton's second law states that the system will accelerate when a force F from the surroundings is exerted on the system: *force equals the time rate of change of momentum*

$$F = m \frac{du}{dt} \quad (4.3)$$

- **Conservation of energy** - the first law of thermodynamics states that the systems energy E will change when work W is done by the system or heat Q is exchanged with the surroundings: *energy can neither be created nor destroyed; it can only change form.*

$$\frac{dE}{dt} = \dot{Q} - \dot{W} \quad (4.4)$$

4.1.5 Assumptions & Conditions

Pipeline dynamics are neglected. The main reason to incorporate pipeline dynamics is to analyze the possibility of “hammer” occurring due to a sudden large pressure fluctuation. The change in fluid inertia created by a wind turbine rotor is assumed sufficiently low to not encounter this “hammer” phenomenon. This assumption is backed up by the findings in [59].

4.2 Modeling Rotor Aerodynamics

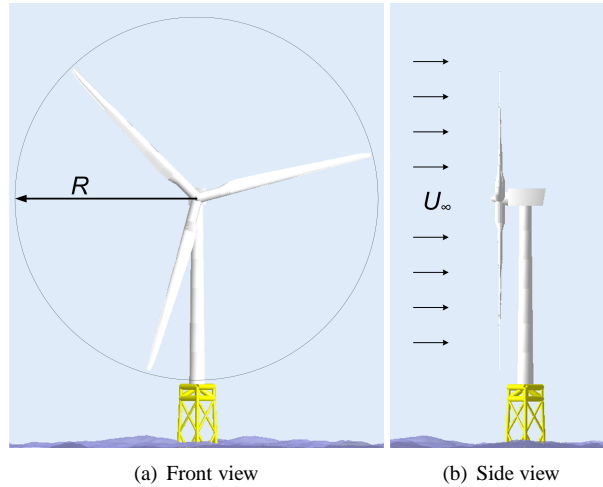


Figure 4.3: Wind turbine front view and side view

4.2.1 Blade Element Momentum (BEM) Theory

Consider a rotor (actuator disk) placed in the flow of air through a cylindrical control volume. The airflow before the rotor has a velocity U_∞ and pressure p_∞ . When the air flow reaches the rotor, kinetic energy is extracted from it, causing a reduction in flow velocity. Since the total mass flow in and out of the control volume must be equal, the cross section of the flow area must increase.

The rotor acts as a permeable barrier: the pressure will increase (p_D^+) just before the rotor and decrease (p_D^-) directly after. After that, the pressure of the wake p_W

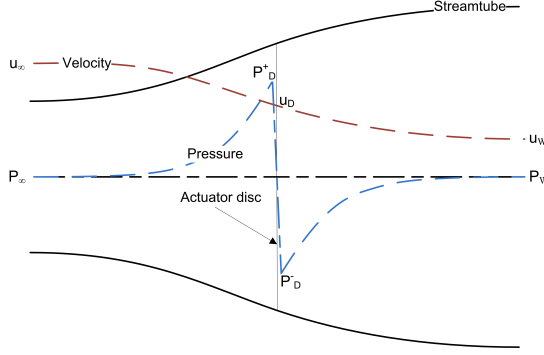


Figure 4.4: Wind speed, pressure and area of the air flow around a wind turbine modeled by an actuator disc

will gradually increase to the level of the free-stream static pressure p_∞ . Figure 4.4 visualizes the speed and pressure changes around the rotor.

Based on the law of conservation of momentum, the “Momentum Theory” is used for modeling the wind passing through the rotor swept area A_D . This specific application is also known as the “Actuator Disc Theory”. In combination with the “Blade Element Theory” it yields the axial (and related tangential) induction factors which serve as corrections to the airspeed at the rotor disc.

In the “Momentum Theory”, the axial induction factor a for a blade section is the ratio between the reduction in wind speed at its location in the actuator disc ($U_\infty - U_D$) and the free-stream wind speed U_∞ at that location. For the whole rotor:

$$a = \frac{U_\infty - U_D}{U_\infty} \Rightarrow U_D = U_\infty(1 - a) \quad (4.5)$$

The power coefficient C_P is the relation between the power extracted by the rotor P_{rotor} and the power in the free-stream wind P_{wind} through the same area A_D .

$$C_P = \frac{P_{rotor}}{P_{wind}} = \frac{2\rho A_D U_\infty^3 a(1-a)^2}{\frac{1}{2}\rho_{air} U_\infty^3 A_D} = 4a(1-a)^2 \quad (4.6)$$

The thrust coefficient C_T is similarly defined as:

$$C_T = 4a(1-a) \quad (4.7)$$

The theoretical maximum value of C_P is $\frac{16}{27} \approx 0.593$ and it occurs when $a = \frac{1}{3}$. This is known as the Lancaster-Betz Limit [60, 61, 62].

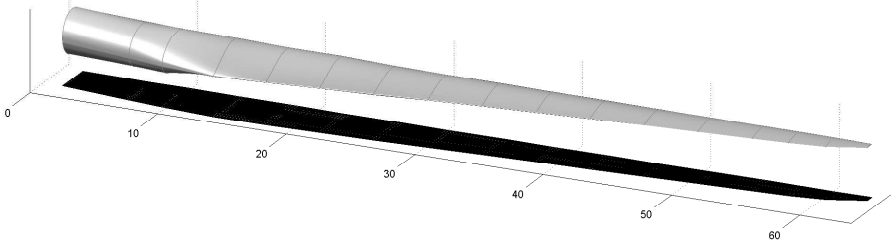


Figure 4.5: 3D drawing of a rotor blade of the NREL 5MW Offshore reference turbine [38]

As the name suggests, “Blade Element Theory” considers a 2D flow over each of a finite number N_s of blade sections. It is used to calculate the lift and drag forces on a blade, whether it is an airplane wing, propeller or wind turbine blade. For a wind turbine rotor, the summation of the lift and drag contributions of each section of each blade yields the rotor torque τ_{rotor} and thrust force F_T . Figure 4.6 shows that the 2D airflow experienced by a blade section consists of two components, the incoming wind speed U_D at the rotor disk and the airspeed due to the rotation of the rotor U_{rot} , which together make up the effective relative velocity U_e .

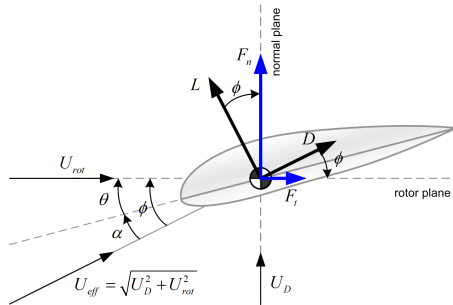
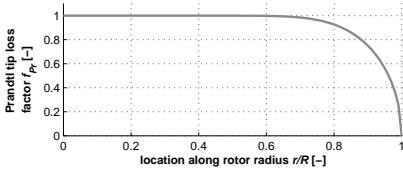


Figure 4.6: The flow angles, velocity components and forces on an airfoil

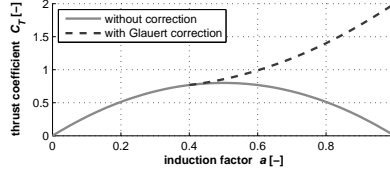
These velocities are subsequently used to calculate new values of a and a_{tg} . This iterative process continues until the values of a and a_{tg} converge to within a specific tolerance, or until an iteration threshold is reached. So, for each element of each blade the value of a is calculated at each iteration step.

Based on empirical evidence [55, 54], a number of corrections have been developed for BEM to incorporate aerodynamic phenomena that have significant influence. Two important corrections are:

1. The Prandtl tip-loss factor - A limitation of the BEM theory is that the influence from vortices shed at the blade tip are not taken into account when calculating the induced velocity. To correct for this effect, the Prandtl tip-loss factor f_p is calculated. An example of its value for different radii along the blade length is shown in figure 4.7(a).



(a) Typical values of the Prandtl tip loss factor f_p .



(b) Glauert correction

Figure 4.7: Examples of Prandtl & Glauert corrections for BEM

2. The Glauert high load correction - The blade element momentum theory is only accurate with axial induction factors which are smaller than approximately 0.5. If a transcends this value, the influence of wake turbulence becomes apparent, according to [55, 54]. The “Modified Glauert High Induction Correction” is an empirically derived relation to approximate this influence. So, for each blade section section, if $a_i \geq 0.5$, a correction factor is determined.

The Glauert high load correction and the Prandtl tip-speed correction are applied to calculate the new values of a .

4.2.2 Model Extensions for Dynamic Simulation

To improve the accuracy of the time-simulation of the wind turbine response to dynamic wind loads, the following corrections to the aerodynamic model have to be applied.

1. **Tower shadow** is a phenomenon that occurs when a rotor blade passes the tower of a wind turbine. The presence of the tower in the airflow causes the build up of air pressure in front of the tower. As the rotor blade moves in front of the tower it experiences a change in air pressure, i.e. a change in airflow. This drop in the momentum results directly in a drop of U_D , the wind speed

at the rotor disk. Using potential flow theory, the effect of tower shadow is modeled by calculating the change in U_D .

2. **Dynamic inflow** refers to sudden changes in the inflow speed, which may originate from a fast change in wind speed (turbulence) or from a sudden change in the blade pitch angle θ . The essence of the model used in this dissertation is that the induced velocity on the blade section is re-determined using empirical relations. Details of the model are explained in [63].
3. **Dynamic Stall** occurs when the angle of attack of an airfoil is rapidly changing. As with dynamic inflow, the cause of this non-linear unsteady aerodynamic effect may be turbulence or a change in pitch angle. Induced vortices around the airfoil influence the flow along the skin such that the lift (coefficient) increases or decreases, depending on the sign of the time rate of change of the angle of attack $\dot{\alpha}$. The modeling of dynamic stall is done by redefining the lift coefficient C_l .
4. **Flapwise bending** is the bending of the blade due to thrust forces, i.e. in the direction perpendicular to the rotor plane. The deflection of the blades due to the bending moment creates a changes in the local angles of attack. This influences the behavior of the blade.

4.2.3 $C_P - C_\tau - \lambda$ Relation

The tip speed ratio λ is defined as the ratio between the speed of the rotor blade tip $\omega \times R$ (in plane) and the free stream wind speed U_∞ (out of plane).

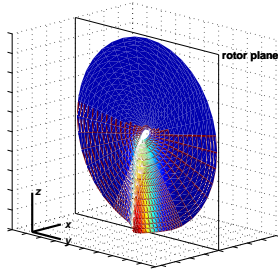
$$\lambda = \frac{\omega R}{U_\infty} \quad (4.8)$$

The optimal tip speed ratio λ_{opt} is the ratio between the incoming wind velocity and the blade tip speed for which the rotor extracts energy from the wind at maximum efficiency. It is therefore a characteristic property of any aerodynamic rotor.

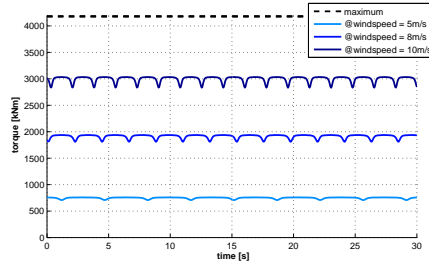
The values of the lift and drag coefficients of an airfoil depend on the angle of attack of the airflow. The angle of attack α depends on the angle of incidence γ and the pitch angle θ of the airfoil, both defined with respect to the rotor plane.

$$\gamma = \arctan\left(\frac{U_D}{U_{rot}}\right) = \arctan\left(\frac{U_\infty(1-a)}{\omega R(1+a_{tg})}\right) \quad (4.9)$$

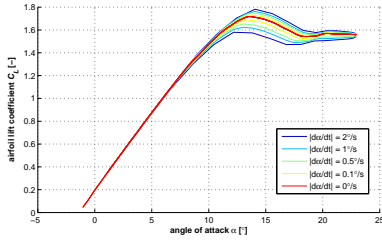
$$\alpha = \gamma - \theta \quad (4.10)$$



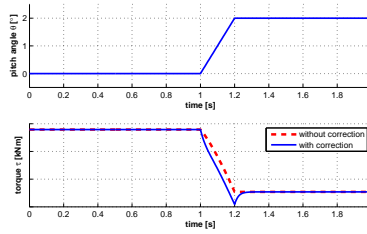
(a) 3D animation of tower shadow



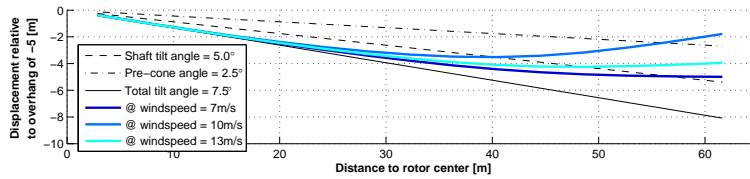
(b) Effect of tower shadow on rotor torque for the NREL 5MW reference turbine [38] under constant wind speed conditions



(c) The effect of dynamic stall on the lift coefficient.



(d) The effect of dynamic inflow on the rotor torque.



(e) Flap wise bending of the rotor blades operation at the wind speed related design tip speed ratio.

Figure 4.8: Visualization of corrections to the aerodynamic model to improve the accuracy of the dynamic response

Since the rotor blade rotates, the speed due to rotation differs along the blade, altering the angle of incidence γ with respect to the rotor plane. To ensure the optimal aerodynamic performance, the blade is twisted by angle $\theta_{twist}(r)$ along its length. Thus, for the same optimal tip speed ratio λ , the angle of attack at each section is optimal and yields a maximum C_l/C_d ratio.

$$\theta = \theta_B + \theta_{twist} \quad (4.11)$$

Hence, the value of the power coefficient C_P depends on the tip speed ratio λ and blade pitch angle θ . For each blade pitch angle θ there is an optimal tip speed ratio λ_{opt} . The relation between C_P , λ and θ for the rotor blades of the NREL 5MW Baseline offshore turbine is given in figure 4.9. So, to capture maximum power at

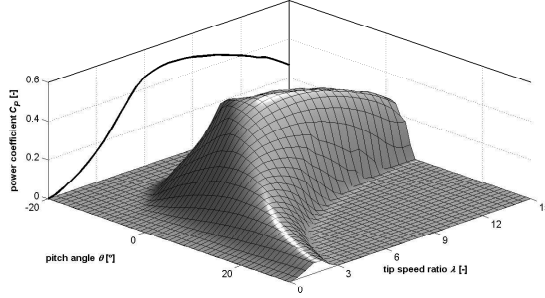


Figure 4.9: C_P - λ - θ relation for the NREL 5MW offshore baseline turbine [38]

a given wind speed, the rotation speed of the rotor should be controlled as to maintain a constant optimal value of the tip speed ratio. Optimal aerodynamic efficiency thus implies a linear increase in the rotational speed of the rotor with respect to wind speed. Hence, the optimal aerodynamic torque rotor is proportional to the second power of the free-stream wind speed.

$$\omega \propto U_\infty \quad (4.12)$$

$$\tau_{rotor} \propto U_\infty^2 \quad (4.13)$$

$$\tau_{rotor} = C_\tau(\lambda) \frac{1}{2} \rho_{air} U_\infty^2 \pi R^3 \quad (4.14)$$

$$P_{rotor} = C_P(\lambda) \frac{1}{2} \rho_{air} U_\infty^3 \pi R^2 \quad (4.15)$$

The expression for the power coefficient C_P in equation 4.6 is redefined as:

$$C_P = \frac{P_{rotor}}{P_{wind}} = \frac{\tau_{rotor} \omega}{\frac{1}{2} \rho_{air} U_{\infty}^3 \cdot \pi R^2} \quad (4.16)$$

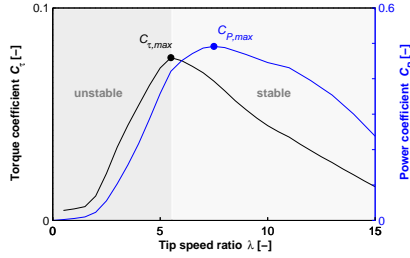
Similarly, the aerodynamic torque is described through the non-dimensional torque coefficient C_{τ} :

$$C_{\tau} = \frac{\tau_{rotor}}{\frac{1}{2} \rho_{air} U_{\infty}^2 \cdot \pi R^3} \quad (4.17)$$

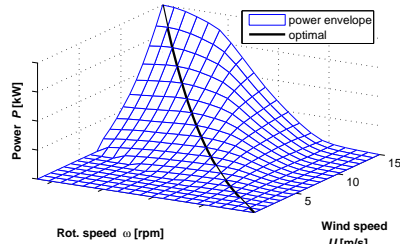
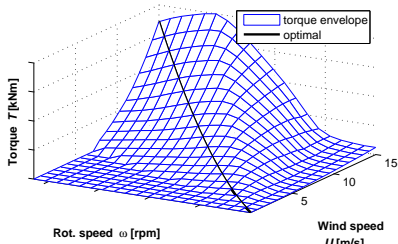
Using equations 4.8, 4.16 and 4.17, the following relationship is derived:

$$C_{\tau} = \frac{C_P}{\lambda} \quad (4.18)$$

An example of the typical relationships between the power coefficient, torque coefficient and tip speed ratio for a three-bladed horizontal axis wind turbine rotor with fixed pitch angle, is given in figure 4.10.



(a) C_P - λ and C_{τ} - λ curves



(b) ideal torque - wind speed - rotor speed relation (c) ideal power - wind speed - rotor speed relation

Figure 4.10: The aerodynamic performance of a conventional wind turbine rotor

From figure 4.10(a) it is observed that the maximum value of the power coefficient occurs for only one value of the tip speed ratio. Thus, the rotor of a variable speed wind turbine is designed so that, with a fixed blade pitch angle, the maximum power coefficient $C_{P,max}$ occurs at the optimal tip speed ratio λ_{opt} independent of the wind speed as observed in figure 4.10(c). This implies that in order to operate at constant tip speed ratio, two relationships are determined: a linear relationship between the rotational speed of the rotor and the wind speed, and a squared relationship between the aerodynamic torque and the wind speed (or rotational speed since they have a linear dependence).

4.2.4 The Power Curve

The ideal shape of the power curve of an arbitrary horizontal-axis, variable speed, pitch controlled wind turbine is given in figure 4.11. This power curve exhibits different regions mainly delimited by the cut-in wind speed v_{ci} , the wind speed for rated rotor speed v_{ω} , rated v_{rated} and cut-out v_{co} wind speeds. Each of these regions have different objectives in both terms of operation and power extraction [64, p.51].

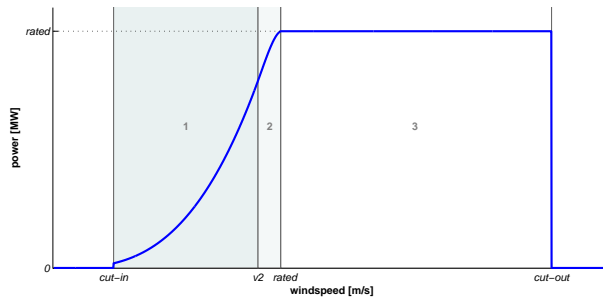


Figure 4.11: The ideal power curve of an arbitrary wind turbine and the 3 zones of control

Below cut-in speed, the available energy in the wind is insufficient to keep the wind turbine running cost-effectively. Around cut-in wind speed, the available energy in the wind is used to accelerate the rotor to the point where the tip speed ratio is optimal. In region 1, between cut-in wind speed and the wind speed v_2 where the nominal rotation speed is reached, the wind turbine operates at maximum efficiency, i.e. at the optimal tip speed ratio and the corresponding maximum power coefficient. In region 2, between v_2 and the rated wind speed, the torque is increased until the nominal power output is achieved. In region 3, between the rated and the cut-out

wind speeds, the speed and torque (and hence power output) are kept constant. The rated wind speed of wind turbines offshore ranges between 11 and 15m/s. Note from figure 4.12 that wind speeds higher than these occur only sporadically. Hence, the impact on the annual energy production of not fully exploiting these high wind speeds is minimal. Beyond cut-out wind speed the turbine is shut down to prevent structural overload.

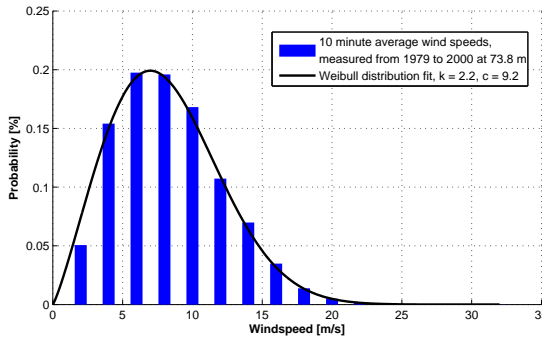


Figure 4.12: Weibull distribution of the wind speed at the North Sea sector K13

4.3 Modeling Fluid Power Transmission Components

4.3.1 Important Fluid Properties

Density, Compressibility and Thermal Expansion

The state of a fluid, i.e. the fluid's condition, determines to the large extend the performance of a hydraulic system. It is defined by the relation between the fluid's temperature, volume (or density) and pressure. The density ρ of a fluid is thus a function of both pressure p and temperature T .

$$\rho = f(p, T) \quad (4.19)$$

For a matter in liquid state, changes in density are small. Liquids are often assumed to be incompressible, meaning no changes in density occur as a result of pressure variation. However, in hydraulics, the degree of pressure variation is such that it does have a significant effect on the fluid density.

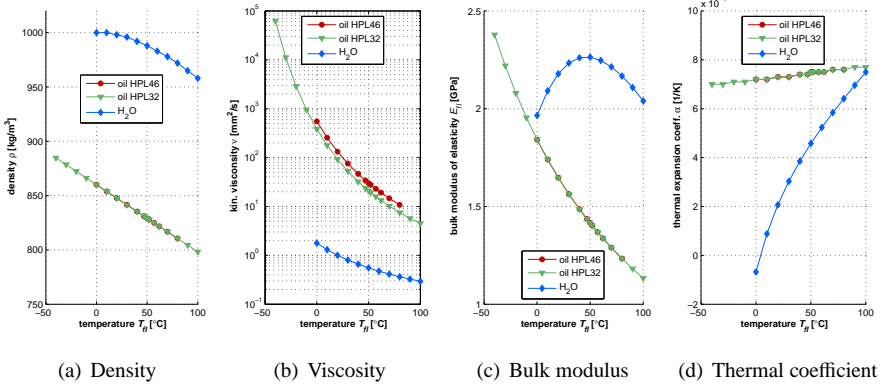


Figure 4.13: Fluid properties of water and hydraulic oils used for modeling and experiments throughout this dissertation

Consider an initial volume of fluid V_0 with mass m_0 at temperature T_0 and pressure p_0 . If the mass stays the same, but the volume increases by ΔV , the density ρ will decrease and vice versa.

$$\rho_0 = \frac{m_0}{V_0} \quad (4.20)$$

$$\rho = \frac{m_0}{V_0 + \Delta V} \quad (4.21)$$

Within a system, density increases with increasing pressure and decreases with increasing temperature. Equation 4.22 represents the isobaric volume change as a function of temperature change. Equation 4.23 represents the isothermal volume change as a function of pressure change.²

$$\Delta V(T) = V_0 \alpha (T - T_0) \Rightarrow \rho = \frac{\rho_0}{1 + \alpha \Delta T} \quad (4.22)$$

$$\Delta V(p) = -V_0 \beta (p - p_0) \Rightarrow \rho = \frac{\rho_0}{1 - \beta \Delta p} \quad (4.23)$$

Here, α is the thermal expansion coefficient. The compressibility β is the inverse of the fluid bulk modulus E_{fl} . The bulk modulus of elasticity of a fluid is a measure for

²Note that here the delta (Δ) is used to symbolize exact difference. In Δx the delta symbolizes the difference. In dx the d symbolizes the derivative (with respect to another dependent variable). In δx the delta symbolizes the differential with respect to another dependent variable (infinitesimal change). [65].

its volumetric elasticity.

$$\beta = \frac{1}{E_{fl}} \quad (4.24)$$

The fluid bulk modulus E_{fl} is modeled as the sum of the reference fluid bulk modulus $E_{fl,0}$ (at atmospheric pressure) and a pressure dependent gain $G_p p$.

$$E_{fl} = E_{fl,0} + G_p p \quad (4.25)$$

Here, gain constant $G_p = 10$ is assumed [66, p.118]. In figure 4.13 the temperature dependence is shown of properties ρ , ν , E and α of fluids used in experiments conducted as part of the research for this thesis. What these graphs show is that, in comparison to the hydraulic oils, water has:

- greater mass density ρ
- lower kinematic viscosity ν
- greater stiffness E
- less tendency for thermal expansion

Combining expressions 4.22 and 4.23 as the total change in volume ΔV as a function of pressure and temperature, yields equation 4.26 for the fluid density.

$$\rho = \frac{\rho_0}{(1 - \beta \Delta p)(1 + \alpha \Delta T)} \quad (4.26)$$

Viscosity

Viscosity is the resistance of a fluid against deformation by shear or tensile stress. The choice of the design operating fluid viscosity for an industrial pump is a compromise between leakage losses and friction losses (lubrication). The ideal operating viscosity for industrial pumps is typically between 20 and 25cSt.

The absolute or kinematic viscosity ν is a temperature dependent fluid property.

$$\nu = f(T) \quad (4.27)$$

In axial or radial piston pumps & motors, the pistons and cylinders have close-fitting surfaces in relative motion. The leakage in between piston and cylinder depends on the tolerance between these surfaces, the properties of the seals and the fluid viscosity. Low fluid viscosity thus implies greater leakage flows and vice versa.

In hydraulic lines, the fluid experiences friction with the container walls. The degree of friction is dependent on the Reynolds number Re and the surface roughness of the container walls. The value of Re depends on the viscosity ν and the fluid velocity u .

$$Re = \frac{u D}{\nu} \quad (4.28)$$

Considering the dependency of viscosity on temperature, the operating conditions of the hydraulic circuit thus have to be known before a fluid is selected.

4.3.2 The Effective Bulk Modulus

The effective bulk modulus of elasticity E_e is a defining property in determining the dynamic performance of hydraulic systems, because it relates to the “stiffness” of the system. This is an important parameter because it relates to the speed of the response of a hydraulic system.

$$\partial p = E_e \frac{\partial V}{V} \quad (4.29)$$

The stiffness of the system will increase with pressure.

A system has the following volumes [7, p.16]:

- Instantaneous container volume V_c
- Total container volume V_t
- Initial volume of gas V_g
- Initial volume of liquid V_l

The assumption made here is that the circuit is completely filled with one type of fluid $V_{fl} = V_l + V_g$.

$$V_c = V_t = V_{fl} \quad (4.30)$$

A change in the initial volumes of either the container, the liquid or both results in a change in the total container volume.

$$\Delta V_t = \Delta V_{fl} + \Delta V_c \quad (4.31)$$

The effective bulk modulus E_e is defined as:

$$\frac{1}{E_e} = \frac{1}{E_c} + \frac{1}{E_{fl}} \quad (4.32)$$

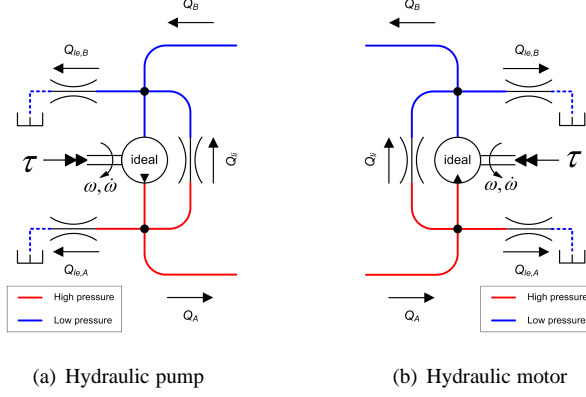


Figure 4.14: Flow components of hydraulic pumps & motors [66]

4.3.3 Modeling a Hydraulic Pump

The primary function of hydraulic pumps is to convert mechanical energy into hydraulic energy. Pumps are characterized by their volumetric displacement V_p . This parameter describes the volume of fluid that is displaced per rotational displacement of the driving shaft. It also defines the specific torque, i.e. the torque gradient in relation to pressure.

Generated Flow

Figure 4.14 shows the flow components of a pump such as they are modeled here. The ideal flow Q_{id} from the pump is the product of its volumetric displacement V_p and its rotational velocity ω .

$$Q_{id} = V_p \omega \quad (4.33)$$

The net flow Q_{net} from a pump is expressed as:

$$Q_{net} = Q_{id} - Q_s \quad (4.34)$$

$$= V_p \omega \eta_v \quad (4.35)$$

Here Q_s represents the total slip flow due to leakages. Two types of leakage are distinguished at a pump or motor:

1. the internal leakage Q_{li} (also known as cross-port leakage) between the high and low pressure lines.

2. the external leakage Q_{le} from the internal chambers to the case drain.

Due to the small clearances inside a pump or motor, the leakage flows are usually laminar and are described as a function of pressure p and/or rotational speed ω . A general schematic of the different leakage losses that occur in hydraulic pumps and motors is shown in figure 4.14.

Complex models have been developed to consider a turbulent leakage flow [56, 57]. However, for the purpose of this study and for simplicity of analysis, a simple description assumed, where the total leakage (or slip) flow Q_s is directly proportional to the pressure difference Δp across the hydraulic pump/motor in terms of a laminar leakage coefficient C_s [67].

$$Q_s = C_s \frac{\Delta p}{\mu} \quad (4.36)$$

Transmitted Torque

The ideal torque of a pump is the product of the pump volumetric displacement V_p and the pressure difference Δp across it. The effective torque of the pump τ_p is the total torque at its input shaft. It is modeled as:

$$\tau_p = V_p \Delta p + \tau_d + \tau_f \quad (4.37)$$

The damping torque τ_d is a torque loss required to shear the fluid in the small clearances between mechanical elements in motion [7]. It is independent of the load and is assumed to be proportional to the pump speed ω , viscous damping coefficient C_d and the dynamic viscosity μ .

$$\tau_d = C_d \mu \omega \quad (4.38)$$

The friction torque τ_f simulates the effect of dry friction forces on the pump pistons that oppose their motion. The resulting friction torque is proportional to the volumetric displacement and the pressure difference across the hydraulic pump/motor. For a quasi-static analysis a constant Coulomb friction coefficient C_f is defined to describe the friction torque independently of the speed [7]:

$$\tau_f = C_f V_p \Delta p \quad (4.39)$$

Hence equation 4.37 becomes

$$\tau_p = (1 + C_f) V_p \Delta p + C_d \mu \omega \quad (4.40)$$

$$= \frac{V_p \Delta p}{\eta_m} \quad (4.41)$$

4.3.4 Modeling a Hydraulic Motor

A hydraulic motor converts fluid power into rotating kinetic power. The modeling techniques are essentially the same as for the hydraulic pump. The main difference is the modeling equations is due to the reversal of the power conversion function.

Generated Pressure

The load applied to the motor determines the required effective motor torque τ_m and hence the required line pressure.

$$\tau_m = \Delta p V_m - \tau_f - \tau_d \quad (4.42)$$

$$\Delta p = \frac{1}{V_m} (\tau_m + \tau_f + \tau_d) \quad (4.43)$$

Generated Speed

The effective flow Q_m through the motor is the difference between the flow Q_{in} from the high pressure line and the leakage flow Q_s . The effective flow determines the speed of the motor.

$$Q_{net} = Q_{in} - Q_s \quad (4.44)$$

$$\omega = \frac{Q_{net}}{V_m} \quad (4.45)$$

4.3.5 Efficiencies of Hydraulic Pumps

The volumetric efficiency η_v of a pump is defined as the ratio of real flow Q_{net} to the ideal flow $V_p \cdot \omega_p$ from the pump. The volumetric efficiency describes internal and external leakages and the losses through the compression work. Using 4.34, the volumetric efficiency becomes:

$$\eta_v = \frac{Q_{net}}{V_p \omega} = 1 - C_s \frac{\Delta p}{V_p \mu \omega} \quad (4.46)$$

The mechanical efficiency or torque efficiency η_m of a pump is the ratio between the effective torque $V_p \Delta p$ and the torque that is applied τ_p .

$$\eta_m = \frac{V_p \Delta p}{\tau_p} = \frac{V_p \Delta p}{V_p \Delta p + \tau_d + \tau_f} \quad (4.47)$$

$$= \frac{1}{1 + C_d \frac{\mu \omega}{\Delta p} + C_f} \quad (4.48)$$

The total pump efficiency η_{tot} is defined as the ratio between the hydraulic power (output) and the mechanical power (input). It is the product of the volumetric and mechanical efficiencies.

$$\eta_{tot} = \frac{P_{hyd}}{P_{mech}} = \eta_v \eta_m \quad (4.49)$$

$$= \frac{Q \Delta p}{\omega \tau_{rotor}} \quad (4.50)$$

$$= \frac{1 - C_s \frac{\Delta p}{\mu \omega}}{1 + C_d \frac{\mu \omega}{\Delta p} + C_f} \quad (4.51)$$

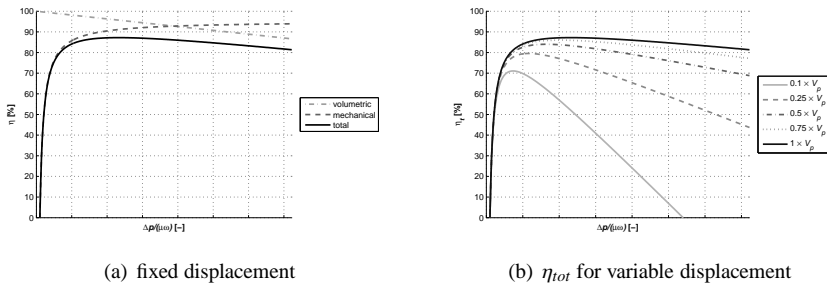


Figure 4.15: The simulated efficiency curves of an arbitrary pump

4.3.6 Efficiencies of Hydraulic Motors

The volumetric efficiency of a motor is defined as:

$$\eta_v = \frac{Q_{net}}{Q_{in}} \quad (4.52)$$

The mechanical efficiency of a motor is defined as:

$$\eta_m = \frac{\tau_m}{\Delta p V_m} \quad (4.53)$$

The total motor efficiency η_{tot} is defined as the ratio between the mechanical power (output) and the hydraulic power (input).

$$\eta_{tot} = \frac{P_{mech}}{P_{hyd}} = \eta_v \eta_m \quad (4.54)$$

$$= \frac{\omega \tau_m}{Q_{in} \Delta p} \quad (4.55)$$

$$= \frac{1 - \frac{C_d \mu \omega}{\Delta p} - C_f}{1 + \frac{C_s \Delta p}{\mu \omega}} \quad (4.56)$$

The theoretical static performance of pump and motor is defined here by coefficients C_s , C_d , C_f , fluid viscosity μ and operational conditions Δp and ω_p . Since the coefficients are assumed constant, the efficiency is a function of $\Delta p/(\mu \omega_p)$. The efficiency curves of a pump with constant volumetric displacement are given in figure 4.15(a).

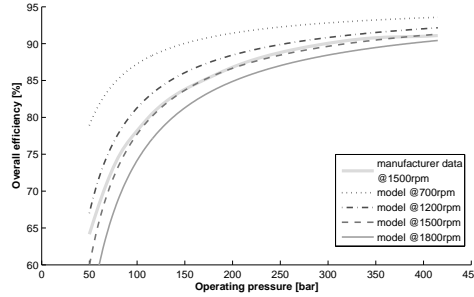


Figure 4.16: Comparison between simulation results and manufacturer data of the Hydrowatt R250/250 pump

In figure 4.16 the measured efficiency of a radial piston pump (suitable for pumping seawater) is compared to the efficiency which is simulated using equation 4.51. The displayed curves for operation at 1500rpm are in close proximity for a wide range of operation.

In order to obtain the maximum efficiency in the mechanical to hydraulic power conversion, it is desirable to operate in the maximum point of the total efficiency curve. Once the pump parameters are established, the maximal theoretical efficiency and corresponding required conditions for steady-state performance are obtained. It is important to notice from the efficiency curve in figure 4.15(a) that there is only one point where maximum efficiency is achieved for a pump with fixed volumetric displacement.

Pumps with variable displacement are able to operate with different efficiency curves, as shown in figure 4.15(b). The total efficiency of the pump increases for higher volumetric displacements. This is explained by the fact that for otherwise similar conditions, greater displacement V_p leads to a lower slip coefficient value C_s . Larger stroke volumes thus result in relatively lower leakage.

It is also observed that the maximum efficiency for each displacement corresponds to a different value of $\frac{\Delta p}{\mu \omega}$. Hence for every operating value of this parameter, there is only one volumetric displacement at which maximum efficiency is reached.

Three similar plots for the operational envelope of the Häggblunds CA210 are shown in figure 4.17, in terms of torque, speed, flow and pressure for a given oil viscosities. Figure 4.17(a) is taken from the product folder. In the figure, flushing refers to the cooling of the pump/motor by forcing fluid through its casing. For this specific pump the maximum allowed operating power without flushing is 120kW. Figure 4.17(b) is the simulation result using the expressions given in this section. The

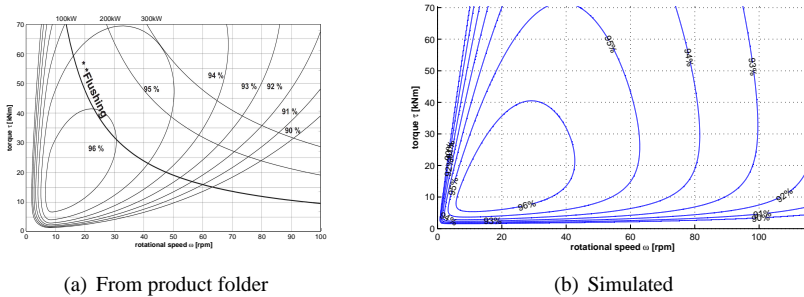


Figure 4.17: Contour plots of the total efficiency of the Häggblunds CA210 for oil with viscosity $\nu = 40\text{cSt}$

pump type of which the envelope is shown in figure 4.17 is used in the experiments described in chapter 5. The pump type of which the envelope is shown in figure 4.18 is used in the experiments described in chapter 6.

In both figures there is a noticeable difference between the data from the manufacturer and the simulated data. As long as the region of operation is well within the boundaries of these graphs, the deviation is never more than a few percent. Then the impact on the simulation of the hydraulic system is therefor minimal.

However, it is found that accurate modeling of the efficiency of a hydraulic pump or motor is not possible with the empirically derived equations presented here. In literature such as [66], the issue of modeling efficiency is omitted altogether. A common approach is to use lookup tables of measured values. That does however require

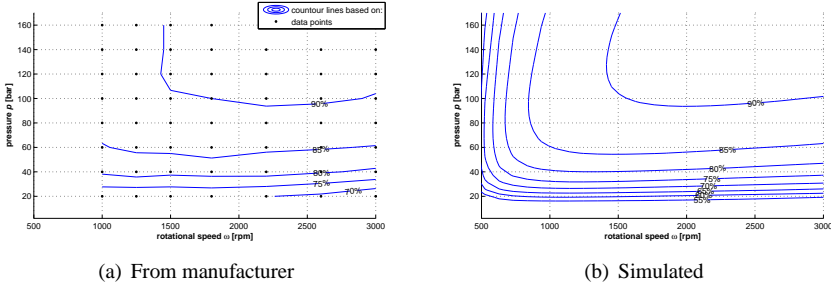


Figure 4.18: Contour plots of the total efficiency of the Danfoss PAH12.5 for tapwater with viscosity $\nu = 1.0040\text{cSt}$

the availability of accurate data.

4.3.7 Modeling Nozzle Flow

The concept depicted in figure 3.14 shows that the flow from the seawater pump travels to the generator platform. At the platform the flow is directed onto the buckets of a Pelton turbine runner by a valve. This valve (either a spear valve or a simple nozzle) changes the ratio between pressure and flow speed. The Bernoulli equation for dynamic pressure is derived from the law of conservation of energy.

$$p_1 + \frac{1}{2} \rho U_1^2 + \rho g z_1 = p_2 + \frac{1}{2} \rho U_2^2 + \rho g z_2 \quad (4.57)$$

Assuming that there is no height difference $z_1 = z_2$, the expression for the nozzle flow speed is:

$$U_{jet,id} = \sqrt{U_1^2 + \frac{2(p_1 - p_0)}{\rho}} \quad (4.58)$$

The volume of the nozzle is typically much smaller than the volume of the high pressure line of the hydraulic system. The corresponding fluid inertia and capacitance of the nozzle are thus much smaller and therefore deemed negligible. Only the resistance of the nozzle is taken into account.

Expressions 4.57 and 4.58 hold for ideal nozzle flow. The nozzle losses, that are caused by viscous effects of the fluid, are described by the velocity coefficient [58]. For well-designed nozzles the velocity coefficient ranges from 0.92 to 0.98 [58].

This then gives the following equation for the jet velocity.

$$U_{noz} = C_v \sqrt{U_{line}^2 + \frac{2\Delta p}{\rho}} \quad (4.59)$$

The diameter of the water jet out of the nozzle continues to converge until a certain minimum, the so called vena contracta, is reached. The effect of this on the jet velocity is that it keeps on increasing until the minimum diameter is reached. The vena contracta phenomenon does not influence the nozzle efficiency. The contraction coefficient C_c takes into account the effect of the vena contracta on the jet velocity. The jet velocity is determined by [68]:

$$U_{jet} = \frac{Q}{C_c A_{noz}} \quad (4.60)$$

Both the velocity and contraction coefficients depend on the geometrical shape of the nozzle. Both coefficients have an influence on the jet velocity.

$$p_{loss} = \Delta p_{jet} - \Delta p_{jet,id} \quad (4.61)$$

$$= \frac{1}{2} \rho \left(\frac{Q}{A_{noz}} \right)^2 \frac{1 - C_c^2 C_v^2}{C_c^2 C_v^2} \quad (4.62)$$

Only the velocity coefficient has an influence on the nozzle efficiency [68].

$$p_{loss} = \frac{1}{2} \rho \left(\frac{Q}{A_{noz}} \right)^2 \frac{1 - C_v^2}{C_v^2} \quad (4.63)$$

Assuming equal flow, nozzles with a larger resistance thus result in larger losses at the nozzle and an increase in the line pressure. The pressure loss at the nozzle is a non-linear function of the volume flow. The nozzle efficiency is determined by:

$$\eta_{noz} = 1 - \frac{p_{loss}}{p_{line}} \quad (4.64)$$

4.4 Modeling Fluid Power Transmission Dynamics

4.4.1 Inertia & Hydraulic Induction

Through a Pipeline - Fluid Inertia

When the fluid inertia is high and the de-/acceleration of the flow is high, the pressure peak will be high. The fluid inertia is modeled as:

$$I_{fl} = \frac{\Delta p}{\dot{Q}} = f_c \frac{\rho l}{A_{pipe}} \quad (4.65)$$

From the expression for fluid inertia, a distinction is made by [58, 66] between the fluid inertia of a laminar flow and a turbulent flow. For laminar flow a correction factor $f_c = 4/3$ is applied. Turbulent flow profiles have a more uniform shape and therefore the correction factor is much smaller and is usually neglected ($f_c = 1$), see figure 4.19 [58]. For a hydraulic line, the hydraulic induction is equal to the fluid inertia.

$$L_H = I_{fl} \quad (4.66)$$

The inertia of the fluid element is analogue to the mass in a mechanical system. From equation 4.65 it is concluded that the inertia of a fluid element is reduced when the density and length decrease or when the area increases.

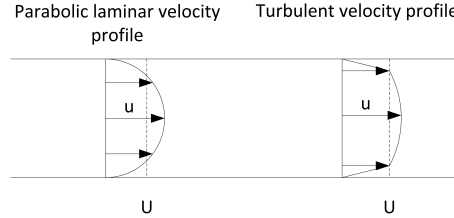


Figure 4.19: Laminar and turbulent flow profiles

From a Hydraulic Pump

The line pressure Δp is the pressure difference over the hydraulic pump/motor, i.e. the difference between the work pressure p_A in line A and the charge or return pressure p_B in line B.

$$\Delta p = p_A - p_B \quad (4.67)$$

For a frictionless, leakage free rotary actuator, the torque is equal to the product of the load pressure and the volumetric displacement.

$$\tau_p = \Delta p V_p \quad (4.68)$$

Assuming $\tau_{rotor} = 0$ and $\eta_{mec} = 1$, equation 4.1 is written as:

$$\Delta p V_p = J \dot{\omega} \quad (4.69)$$

Here, J is the sum of the mass moments of inertia of the rotating parts of the pump and the actuator that drives it, in this case an aerodynamic rotor. By multiplying both sides by V_p and using $Q = V_p \omega$, the flow rate of change appears.

$$\Delta p V_p^2 = J \dot{\omega} V_p = J \dot{Q} \quad (4.70)$$

The relation between the pressure in the system and the time rate of change in flow speed is known as the hydraulic induction L_H [66].

$$L_H = \frac{\Delta p}{\dot{Q}} = \frac{J}{V_p^2} \quad (4.71)$$

4.4.2 Compressibility & Hydraulic Capacitance

The oil in the piping that connects the pump and the hydraulic motor behaves similar to a mechanical spring. It is modeled as a constant volume with an effective bulk modulus associated to the compressibility of such volume. The spring stiffness equivalent C_o of a hydraulic fluid is the ratio between the change in force dF exerted on a fluid in a rigid container and the compression length of the fluid dL .

$$C_o = \frac{dF}{dL} \quad (4.72)$$

The addition or subtraction of an oil volume ΔV to a container with constant volume V_c will lead to a change in pressure Δp .

$$\Delta p = E_e \frac{\Delta V}{V_c} \quad (4.73)$$

This change with respect to time is the effective flow Q into or out of the system $Q_c = \frac{dV_c}{dt}$. Hence,

$$\frac{dp}{dt} = E_e \frac{dV_c/dt}{V_c} \quad (4.74)$$

$$\dot{p} = E_e \frac{Q_c}{V_c} \quad (4.75)$$

The effective bulk modulus E_e considers not only the fluid stiffness but also the material compliance [69]. The value of E_e may therefore vary considerably from the fluid bulk modulus E_{fl} , as is demonstrated in section 4.3.2.

The pumps used for the experiments described in section 5.4 are radial piston pumps. The pistons move along a cam ring so that they (dis)charge several times per

pump revolution, depending on the number of cams. The instantaneous volume V_i of oil in the pump, in open connection with the high pressure line, is on average half the pistons of the pump which are on average at half their stroke volume [70, p.135]. Hence,

$$V_i = V_p \frac{\pi}{2} \quad (4.76)$$

The instantaneous volume of the high pressure container is thus:

$$V_c = V_i + V_{pipe} \quad (4.77)$$

The instantaneous oil volume in the motor is deemed insignificantly small and is therefor not taken into account here. The inverse of the hydraulic spring stiffness C_o is known as the hydraulic capacitance C_H [66]. This capacitance is the relation between time rate of change of the pressure and the effective volumetric flow. It follows that:

$$C_H = \frac{Q_c}{\dot{p}} = \frac{V_c}{E_e} \quad (4.78)$$

Thus, the more oil, the greater the capacitance.

4.4.3 Hydraulic Resistance: Pressure & Flow Losses

Two types of hydraulic resistance R_H are recognized:

1. Resistance due to pressure loss
2. Resistance due to flow loss

In practice, the effect of flow loss is significantly larger than that of pressure loss.

Resistance due to Pressure Loss

The hydraulic resistance R_H is the change in pressure over the flow speed. For a pipe, the resistance R_H is defined by:

$$R_{H,p} = \frac{p_{loss}}{Q} \quad (4.79)$$

What this effectively represents is the relation between the pressure loss and the flow rate.

Pressure losses are associated to the energy dissipation from viscous effects of a fluid flow. They occur in two forms:

1. At the hydraulic pump/motors these losses occur due to the shearing of fluid between close fitting surfaces within the pump/motor. This shearing causes what is known as damping torque τ_d , see equation 4.38. So the pressure loss due to viscous damping at a pump/motor is modeled as:

$$p_{loss} = \tau_d / V_p = \frac{C_d \mu}{V_p} Q \quad (4.80)$$

2. By applying the Darcy-Weisbach equation for pressure losses due to friction, the pressure loss in the pipe is directly proportional to the flow rate when the flow is laminar.

$$p_{loss,pipe} = \frac{8 \mu L}{\pi R_{pipe}^4} Q \quad (4.81)$$

When the flow is turbulent this relation does not hold. To apply a second order model for the hydraulic transmission then requires linearization of the pressure loss.

Therefore,

$$R_{H,p} = \frac{C_d \mu}{V_m} + \frac{8 \mu L}{\pi R_{pipe}^4} \quad (4.82)$$

Additional losses occur due to valves (globe/check/gate), elbow corners, T-pieces etc. The losses due to these components are effectively modeled as extensions of the pipe through a factor K [58, 7]. The contribution of these additional losses is deemed negligible here and is hence not modeled for simplicity.

Resistance due to Flow Loss

This form of resistance occurs predominantly at the hydraulic pump/motors. These are assumed to be the only components experiencing leakage.

$$R_{H,Q} = \frac{\Delta p}{Q_{loss}} \quad (4.83)$$

The flow losses due to leakage at the pump and the motor are predominantly a function of pressure. C_s is the slip coefficient, hence:

$$Q_{loss} = (C_{s,p} + C_{s,m}) \Delta p \quad (4.84)$$

The hydraulic resistance due to leakage thus becomes.

$$R_{H,Q} = \frac{1}{C_{s,p} + C_{s,m}} \quad (4.85)$$

4.4.4 Derivation of the Characteristic System Equations

For a Hydraulic Line

The dynamic behavior of hydraulic systems is analogous with that of mass-spring-damper systems.

If the hydrostatic system is regarded as merely a single pipeline, its behavior is modeled in the same fashion as that of the linear system in figure 4.20(a). The hydraulic stiffness of this pipeline is derived from equations 4.72 and 4.73.

$$C_o = \frac{\Delta p A}{\Delta L} = \frac{\Delta p A^2}{A \Delta L} = \frac{E \frac{\Delta V}{V} A^2}{\Delta V} = \frac{E A}{L} \quad (4.86)$$

Setting $k = C_o$, the characteristic equation is defined by formulating the second order

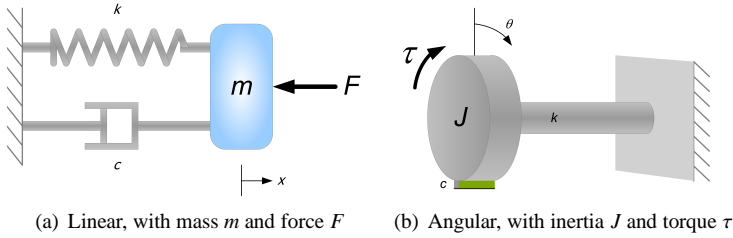


Figure 4.20: Mass-spring-damper systems, with stiffness k and damping coefficient c differential equation for the response of the system to an externally applied force F .

$$F = m \ddot{x} + c \dot{x} + k x \quad (4.87)$$

Using $F = p/A$, $v = \dot{x}$, $Q = A v$ and expressions 4.71, 4.79, 4.86 for the hydraulic induction L_H , resistance R_H and capacitance C_H , the system equation is found to be:

$$p = \frac{\rho L}{A} \dot{Q} + \frac{c}{A^2} Q + \frac{C_o}{A^2} \int Q dt \quad (4.88)$$

$$= L_H \dot{Q} + R_H Q + \frac{1}{C_H} \int Q dt \quad (4.89)$$

By setting $p = 0$, the characteristic system equation is defined:

$$L_H \dot{Q} + R_H Q + \frac{1}{C_H} \int Q dt = 0 \quad (4.90)$$

$$\dot{Q} + 2 \zeta \omega_n Q + \omega_n^2 \int Q dt = 0 \quad (4.91)$$

The natural frequency of the system is defined as:

$$\omega_n = \sqrt{\frac{1}{C_H L_H}} \quad (4.92)$$

$$(4.93)$$

The damping ratio with respect to pressure loss is given by:

$$\zeta_p = \frac{R_{H,p}}{2} \sqrt{\frac{C_H}{L_H}} \quad (4.94)$$

The pressure loss in the pipeline and hence this damping ratio is very low if the pipe is designed for the relevant flow regime.

For a Hydraulic Circuit with a PD Pump

The focus of the theory presented in this chapter and the research presented in chapters 5 and 6 is on the torque balance at the rotor. The system is therefore now modeled analogous to an angular mass-spring-damper system such as displayed in figure 4.20(b). The flow input to the system comes from the pump which is driven in this case by an aerodynamic rotor.

$$\tau = I \ddot{\phi} + c \dot{\phi} + k \phi \quad (4.95)$$

For simplicity, the charge pressure is assumed as zero here, so that $\Delta p = p$ and hence $\tau = V_p p$.

$$p = \frac{I}{V_p} \ddot{\phi} + \frac{c}{V_p} \dot{\phi} + \frac{k}{V_p} \phi \quad (4.96)$$

Using $\omega = \dot{\phi}$, $Q = V_p \omega$ and expressions 4.66, 4.85, 4.78 for the hydraulic induction L_H , resistance R_H and capacitance C_o , the system equation is defined as:

$$p = \frac{I}{V_p^2} \dot{Q} + \frac{c}{V_p^2} Q + \frac{C_o}{V_p^2} \int Q dt \quad (4.97)$$

$$= L_H \dot{Q} + R_H Q + \frac{1}{C_H} \int Q dt \quad (4.98)$$

Hence the same expression for the characteristic equation is derived as in equation 4.91, but with different definitions of L_H , R_C and C_H . The equations for natural frequency and damping ratio of the second order system are also maintained.

Rewriting equation 4.98 as a function of p yields:

$$Q = C_H \dot{p} + \frac{1}{R_H} p + \frac{1}{L_H} \int p dt \quad (4.99)$$

Note that the position of R_H has changed here with respect to the one in equation 4.85. The resulting characteristic equation yields the same expression for the natural frequency, but a different expression for the damping ratio. This is explained by the fact that the damping ratio due to leakage loss is different to the damping ratio due to viscous friction loss. The damping ratio with respect to volume flow loss is given by:

$$\zeta_Q = \frac{1}{2 R_{H,Q}} \sqrt{\frac{L_H}{C_H}} \quad (4.100)$$

The effective damping ratio ζ of the system is the sum of both pressure and flow related damping ratios:

$$\zeta = \zeta_p + \zeta_Q \quad (4.101)$$

The value of ζ_p is typically very small compared to ζ_Q .

4.4.5 Conversion to State Space

The mechanical-hydraulic conversion of the system is analytically described by a second order system. The first equation is obtained from the torque balance at the rotor shaft according to Newton's second law. Lumped constants for the rotor and a rigid shaft are assumed such that:

$$J_t \ddot{\theta} = \tau_{rotor} - \tau_p \quad (4.102)$$

$$= \tau_{rotor} - V_p (p_L + p_{loss}) - B_p \dot{\theta} - C_f V_p (p_L + p_{loss}) \quad (4.103)$$

The second equation of the hydrostatic transmission, including the pump, hose and hydraulic motor is developed based on the flow continuity equation for the high pressure line. The displacement of the motor V_m is controlled by input parameter e . Leakages of the pump and motor are included so that:

$$C_H \dot{p}_L = V_p \dot{\theta}_p - C_{s,p} (p_L + p_{loss}) - C_{s,m} p_L - e V_m \omega_m \quad (4.104)$$

$$= V_p (1 - R_H C_{s,p}) \dot{\theta} - (C_{s,p} + C_{s,m}) p_L - e V_m \omega_m \quad (4.105)$$

The linear dynamic equations of the proposed model are rewritten in state-space form:

$$\dot{\mathbf{x}} = \mathbf{A} \mathbf{x} + \mathbf{B} \mathbf{u} \quad (4.106)$$

$$\mathbf{y} = \mathbf{C} \mathbf{x} \quad (4.107)$$

Here, \mathbf{x} is the state vector, \mathbf{u} is the input vector and \mathbf{y} is the output vector. For the hydraulic transmission these vectors are defined as:

$$\mathbf{x} = \begin{bmatrix} \dot{\theta} \\ p_L \end{bmatrix}, \quad \mathbf{u} = \begin{bmatrix} \tau_{rotor} \\ e \end{bmatrix}, \quad \mathbf{y} = \begin{bmatrix} \dot{\theta} \\ p_L + p_{loss} \end{bmatrix} \quad (4.108)$$

The matrices A, B, C and D are defined as:

$$A = \begin{bmatrix} -\frac{B_p + V_p^2 (1 + C_f) R_H}{J_t} & -\frac{V_p (1 + C_f)}{J_t} \\ \frac{V_p (1 - R_H C_{s,p})}{C_H} & -\frac{(C_{s,p} + C_{s,m})}{C_H} \end{bmatrix} \quad (4.109)$$

$$B = \begin{bmatrix} \frac{1}{J_t} & 0 \\ 0 & -\frac{V_p \omega_m}{C_H} \end{bmatrix}, \quad C = \begin{bmatrix} 1 & 0 \\ R_H V_p & 1 \end{bmatrix} \quad (4.110)$$

With a linear mathematical model of this second-order system, the dynamic behavior is characterized through the eigenvalues of the matrix A; hence the natural frequencies and damping ratios are obtained.

4.4.6 Calculation of Natural Frequencies

Natural frequencies are determined by the magnitude of each pair of complex conjugated eigenvalues of matrix A. The resulting hydraulic natural frequency ω for the proposed second order system is then given by:

$$\omega_n = \sqrt{\frac{V_p^2}{C_H J_t}} K_i \quad (4.111)$$

With

$$K_i = \sqrt{(1 + C_f) (1 + R_H C_{s,m}) + \frac{(B_p) (C_{s,p} + C_{s,m})}{V_p^2}} \quad (4.112)$$

4.4.7 Calculation of Damping Ratios

Damping ratios are obtained from the ratio of the absolute value of the real part and the magnitude of each pair of complex conjugated eigenvalues of matrix A

$$\zeta = \left[\frac{(B_p)}{2 V_p} \sqrt{\frac{C_H}{J_t}} + \frac{(C_{s,p} + C_{s,m})}{2 V_p} \sqrt{\frac{J_t}{C_H}} \right] \frac{1}{K_i} \quad (4.113)$$

Generally the term $\frac{(B_p) (C_{s,p} + C_{s,m})}{V_p^2} \ll 1$ and $R_H C_{s,m} \ll 1$, thus giving little influence of the constant K_i over the natural frequency and damping ratio.

4.4.8 Acquiring Realistic Values of L_H , C_H , R_H

The hydraulic inertia L_H is usually relatively simple to determine. The volumetric displacement of the pump/motor is commonly provided by the manufacturer. If the mass moment of inertia of the rotor is known, an estimation can be made. When coupled to a wind turbine rotor, the contribution of the pump to the mass moment of inertia is negligible. The effect of friction from the main shaft bearings is also deemed negligible here.

Finding the hydraulic capacitance C_H is less straightforward. One should know the total contained volume in the high pressure line and the effective bulk modulus E_e . The bulk moduli that comprise E_e depend on pressure and temperature, though its range of values is small within the operational means of the hydraulic systems considered here. As is shown in section 5.4.5, the value of C_H can be determined experimentally.

The hydraulic resistance R_H is the most complicated to determine. Any change in (the state of) the equipment or the fluid has an effect on its value.

The simulation of the fluid power circuit could be improved by:

- implementing models on pipelines dynamics: a common tool is the “lumped” model where fluid mass is divided in lumps. The more lumps, the greater the accuracy. Another tool is the distributed parameters model which is an approximation model [71].
- applying discrete models of the hydraulic pumps/motors such as the one for radial piston pumps given in [43].
- incorporating thermodynamics: energy losses occur primarily in the form of generated heat. Temperature has a significant influence on the fluid viscosity.

However, for the purpose of general analysis of the behavior of fluid power transmission systems, the theory as presented in this section is deemed sufficient.

4.5 Matching Rotor and Hydraulic Pump Characteristics

4.5.1 Pump-Rotor Matching

When designing a wind turbine, the properties of the rotor and the drive train should match. For a hydraulic drive train, the pump coupled to the rotor is the interface between the rotor and the fluid power circuit. Its performance envelope should match

that of the rotor. The essential performance characteristics of both the rotor and the hydraulic pump are listed in table 4.1.

Aerodynamic Rotor		Hydraulic Pump	
Rotor radius	R	Volumetric displacement	V_p
Optimal tip speed ratio	λ_{opt}	Nominal operating pressure	p_{nom}
Max. power coeff.	$C_{P,max}$	Minimum operating speed	ω_{min}
Rated wind speed	v_{rated}	Nominal operating speed	ω_{nom}

Table 4.1: Characteristics parameters

If the power transmission system of a wind turbine or farm is to be designed, the key design input parameters are (1) how much electric power it should produce and (2) in which form. The form here refers to output frequency and voltage. Once these are known, all stages of the design are dimensioned so that the conditions on the power output are met. The rotor then is the last part to be designed.

An alternative approach is to start at the rotor. By estimating the losses, an initial estimate of the power production is possible.

Another approach to wind turbine design (which is more economically attractive for a purpose such as prototyping) is to use components-of-the-shelf (COTS). If the design of the rotor is given, the challenge is to find (or design) a suitable pump. If the design of the pump is given, the challenge is to find (or design) a suitable rotor. A necessary condition here is that either these rotor or pump characteristics are known.

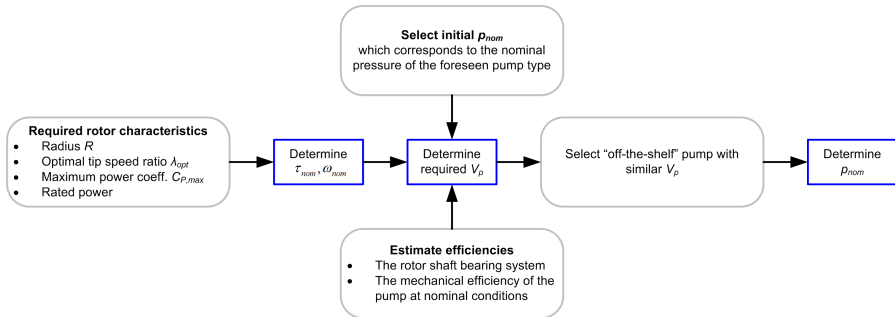


Figure 4.21: Flowchart for matching characteristics

In practice it is found that positive displacement pumps are often designed to operate at high rotation speeds. This is because they are assumed to be powered by an electric 50Hz 4 pole motor (1500rpm).

However, hydraulic motors are often required to operate at much lower speed (winches, ship propulsion, excavators). Some of these motors, such as the Häglunds CA, CB and CBP series, are also applicable as pumps.

Starting point of design example 1: the NREL 5MW rotor

- Known: - $C_P - \lambda$ curve, v_{rated} , R , P_{rated}
 Select: - design point: typically this is at nominal (rated) design conditions for the rotor
 - Δp_{nom} , the pressure difference which occurs at the design point
 Estimate: - the efficiency η_{bs} of the rotor shaft bearing system,
 - the volumetric η_v and mechanical η_m efficiencies of the pump at the design point

The nominal rotor torque is given by:

$$\tau_{rotor,nom} = C_{P,max} \frac{1}{2} \rho \frac{1}{\lambda_{opt}} v_{rated}^2 \pi R^3 \quad (4.114)$$

For steady state conditions it holds that:

$$\tau_{rotor,nom} = \tau_{pump} \frac{1}{\eta_{bs}} \quad (4.115)$$

Hence, using equation 4.37 the required volumetric displacement V_p of the pump in m^3/rad is:

$$V_p = \frac{\tau_{rotor,nom}}{\Delta p_{nom}} \frac{\eta_{bs}}{\eta_m} \quad (4.116)$$

The next step is to find a positive displacement pump with a similar volumetric displacement V_p , which is designed to operate efficiently for the same speed range. Applying the properties of this pump in equation 4.116, the expected nominal pressure difference Δp_{nom} is calculated.

From the NREL rotor, the key design parameters are listed in table 3.1. As described in section 2.3, the Häglunds motors are the state-of-the-art in low speed high efficiency hydraulic motors, which are also applicable as pump. Therefore, the characteristics of these motors are extrapolated to the 5MW range. The nominal operating pressure p_{nom} is set at 350bar. The related charge pressure $p_{ch,nom}$ is around 20bar. Using equation 4.116 the required volumetric displacement is calculated to be $0.812m^3/rev$.

Starting point of design example 2: the Hägglunds CBP840 radial piston motor applied as pump

An alternative approach is to find a rotor to match a specific pump or full transmission. The optimal tip speed ratio in combination with the selected rotor radius determine the speed range of the rotor. Hence to make optimal use of the operational envelope of the pump the matching optimal tip speed ratio must be selected.

Known: - p_{nom} , ω_{min} , ω_{max} , V_p ,
- efficiencies over full operational range η_v , η_m .

Select: - optimal tip speed ratio λ_{opt}

Estimate: - C_p

The nominal torque of the wind turbine rotor is determined using:

$$\tau_{nom} = V_p \Delta p \eta_m \quad (4.117)$$

Figure 4.22 displays the result of the steady state torque and speed operational ranges for several optimal tip speed ratios.

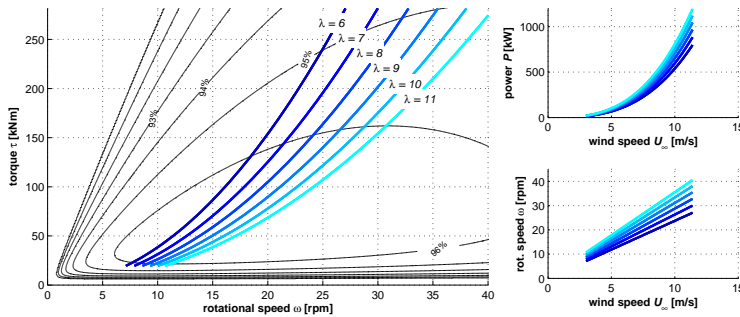


Figure 4.22: The simulated operational envelope of a Hägglunds CBP840 type radial piston motor (starting point of the design) and a corresponding range of rotor properties for $C_{p,max} = 0.48$, where the optimal tip speed ratios vary from 6 to 11 and rotor diameters vary from 59.1m to 48.2m respectively

4.6 Conclusion

The power performance of a wind turbine rotor is essentially a function of the tip speed ratio λ and the pitch angle θ of the wind turbine blades. In particular the presence of the turbine tower and the stochastic nature of wind introduce noise in the torque produced by the rotor.

A fluid power circuit, such as may be applied in the transmission of a wind turbine, essentially behaves as a second order system. To be able to describe a system in this way is beneficial for the simplicity of the analysis of its dynamic behavior. To accurately predict the response of a systems the values for L_H , C_H , R_H must be known.

To match an aerodynamic rotor to a given hydraulic pump requires the following parameters of the pump to be known: the volumetric displacement, the nominal pressure, the nominal speed. To match a hydraulic pump to a given aerodynamic rotor requires the following parameters of the rotor to be known: the rotor radius, the optimal tip speed ratio and the rated wind speed.

Dynamic Response Analysis of Fluid Power Drive Trains

5.1 Introduction

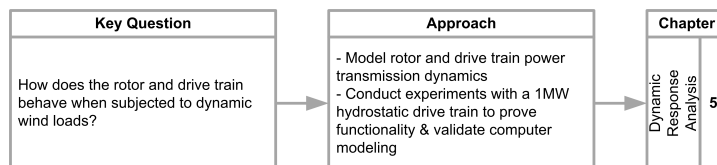


Figure 5.1: Flowchart for the objective and approach of this chapter

5.1.1 Background & Objective

The modularity of hydraulic components gives rise to the option of taking the generator out of the nacelle. This would increase the distance between the hydraulic pump and the hydraulic motor. But how feasible is this concept and what are its limitations from an operational point of view? The further the hydraulic motor is placed from the pump, the greater the amount of oil in the system, the greater the friction losses in the pipelines and the lower the hydraulic stiffness of the transmission system. Internal leakages in the hydraulic drive components translate to power losses. A reduction in power transmission efficiency means the damping of power transients increases. It

is therefore not necessarily an unfavorable aspect for the dynamic performance of the turbine.

For the design of a fluid power transmission system for large wind turbines, the influence of these parameters on the performance must be known. Hence the aim of the matter in this chapter is to:

1. derive the limits of stability of the hydraulic drive train (including rotor inertia and torque).
2. analyze the influence of three characteristic power transmission parameters on the dynamic behavior of a horizontal axis wind turbine.
3. experimentally analyze the impact of pressure control on dynamics using variable displacement motors.

5.1.2 Approach

For the purpose of consistency the properties of the fictitious NREL 5MW offshore wind turbine [38] rotor are used for the rotor simulation in this chapter, both on 5MW scale (simulation only) and on 1MW scale (simulation and experimentation).

The chapter is essentially divided in three parts. The first part consists of a stability analysis using a 2nd order transmission system model as defined in 4.4.

The second part is a parameter sensitivity study. For several predefined atmospheric conditions (load cases), the parameters that are being manipulated are

1. the length of the high pressure line (the oil volume),
2. the volumetric efficiency of the hydraulic motor and
3. the mass moment of inertia of the rotor.

The results of time domain simulations are compared to analyze the effect of the different parameters. Although the transmission concept that was selected in section 3.7.2 has two circuits, the focus in this chapter is on a single circuit transmission only. To perform the parameter study, the system should be as simple as possible to avoid the contamination of results by additional complexities. The simulated transmission system consists of a low speed, fixed displacement radial pump (directly coupled to the rotor), a fluid transmission line and a variable displacement hydraulic motor coupled to a fixed-speed synchronous generator.

The third part describes the experiments which were conducted to analyze the behavior of a real fluid power transmission system and the impact of pressure control on the drive train response. As mentioned in section 2.3, a hydraulic pump for a

5MW turbine is not yet commercially available at the time of this writing. Hence, testing at 5MW scale was not a feasible option. However, there was an opportunity in summer 2011 to conduct tests with a 1MW class hydraulic transmission system for wind turbines which incorporated state-of-the-art hydraulic drives. The experiments described in section 5.4 were conducted with an oil based hydraulic transmission that essentially functions as a single circuit. The experimental setup as shown in figure 5.9 has multiple pumps, motors and valves. To model the effective performance of this system, the pumps and motors are lumped together and modeled as a single pump and a single motor.

5.1.3 Assumptions & Conditions

- The wind speed is kept below rated wind speed to exclude the effect of blade pitching.
- The effect of the different configurations of the hydraulic transmission system on the total mass of the nacelle is not taken into account (same structure and top mass is used)
- The diameter and number of hydraulic lines were selected in order to have laminar flow in the hydraulic transmission
- The pipe walls are assumed to be rigid (effect of flexible pipelines is taken into account into the effective bulk modulus of the fluid)
- Thermodynamic effects are assumed negligible
- Properties of the hydraulic fluid are assumed constant

5.2 Stability Analysis of the Linear Second Order System Model

5.2.1 Linearized model of Rotor & Transmission

Aerodynamic torque linearization

The method described here for the simulation of the rotor is derived from [64]. The method for the simulation of the fluid power circuit is presented in [72]. As is observed in section 4.2, the equations for the total torque and thrust are highly non-linear due to the wind turbine aerodynamics. For a fixed pitch operation, the aerodynamic torque coefficient C_T of a fixed-pitch wind turbine is a function of the tip-speed-ratio

λ only. Hence, the linearization of the aerodynamic torque around an arbitrary operating point $(\bar{\omega}_{rotor}, \bar{U})$ is done using:

$$\hat{\tau}_{aero} = -B_r(\bar{\omega}_{rotor}, \bar{U}) \hat{\omega}_{rotor} + K_{r,U}(\bar{\omega}_{rotor}, \bar{U}) \hat{U} \quad (5.1)$$

where,

$$B_r(\bar{\omega}_{rotor}, \bar{U}) = - \left. \frac{\partial \tau_{aero}}{\partial \omega_{rotor}} \right|_{(\bar{\omega}_{rotor}, \bar{U})} = - \frac{\tau_{aero}(\bar{\lambda}, \bar{U})}{\bar{\omega}_{rotor}} \left. \frac{\partial C_\tau / \partial \lambda}{C_\tau / \lambda} \right|_{(\bar{\omega}_{rotor}, \bar{U})} \quad (5.2)$$

$$K_{r,U}(\bar{\omega}_{rotor}, \bar{U}) = \left. \frac{\partial \tau_{aero}}{\partial U} \right|_{(\bar{\omega}_{rotor}, \bar{U})} = \frac{\tau_{aero}(\bar{\lambda}, \bar{U})}{\bar{U}} \left(2 - \left. \frac{\partial C_\tau / \partial \lambda}{C_\tau / \lambda} \right|_{(\bar{\omega}_{rotor}, \bar{U})} \right) \quad (5.3)$$

Note that the bars ($\bar{\cdot}$) and hats ($\hat{\cdot}$) over the variables indicate the steady-state value and the variation with respect to the steady state value. Hence $\bar{\lambda} = R \bar{\omega}_{rotor} / \bar{U}$ is the tip speed ratio at the operating point.

Since the term $B_r(\bar{\omega}_{rotor}, \bar{U})$ is multiplied with the rotation speed it is essentially a damping coefficient which signifies the speed feedback of the rotor. In correspondence with the slope of the $C_\tau - \lambda$ -curve in figure 4.10(a), the value of this term is positive above $\lambda_{C_{\tau,max}}$ and negative below $\lambda_{C_{\tau,max}}$.

The term $K_{r,U}(\bar{\omega}_{rotor}, \bar{U})$ represents the gain between the wind speed and the aerodynamic torque. Under normal operating conditions this gain is positive. At low values of λ , i.e. when the turbine stalls, it becomes negative.

State-Space Representation of Rotor & Transmission

Combining the linearized aerodynamic torque as expressed in equation 5.1 with system equation 4.102 yields the linearized system equation:

$$J_t \dot{\omega}_{rotor} = \tau_{aero} - \tau_p \quad (5.4)$$

$$= \tau_{aero} - [V_p \Delta p_p + B_p \omega_{rotor} + C_f V_p \Delta p_p] \quad (5.5)$$

$$= K_{r,U}(\bar{\omega}_{rotor}, \bar{U}) \hat{U} - [B_r(\bar{\omega}_{rotor}, \bar{U}) + B_p] \omega_{rotor} - V_p (1 + C_f) \Delta p_p \quad (5.6)$$

The second equation of the hydrostatic transmission, including the pump, hose and hydraulic motor is developed based on the flow continuity equation for the high pressure line. The displacement of the motor V_m is controlled by input parameter e .

Leakages of the pump and motor are included so that:

$$C_H \dot{\Delta p_p} = V_p \omega_{rotor} - C_{v,p} \Delta p_p - C_{v,m} \Delta p_m - V_m \omega_m e \quad (5.7)$$

$$= V_p (1 + R_H C_{v,m}) \omega_{rotor} - (C_{v,p} + C_{v,m} + C_{v,p} C_{v,m} R_H) \Delta p_p \dots \quad (5.8)$$

$$- V_m \omega_m e \quad (5.9)$$

The linear dynamic equations 5.6 and 5.9 are rewritten in state-space form:

$$\dot{\mathbf{x}} = \mathbf{A} \mathbf{x} + \mathbf{B} \mathbf{u} \quad (5.10)$$

$$\mathbf{y} = \mathbf{C} \mathbf{x} \quad (5.11)$$

Here, \mathbf{x} is the state vector, \mathbf{u} is the input vector and \mathbf{y} is the output vector. For the hydraulic transmission these vectors are then defined as:

$$\mathbf{x} = \begin{bmatrix} \dot{\theta} \\ \Delta p_p \end{bmatrix}, \quad \mathbf{u} = \begin{bmatrix} \hat{U} \\ e \end{bmatrix}, \quad \mathbf{y} = \begin{bmatrix} \dot{\theta} \\ \Delta p_p \\ \Delta p_m \end{bmatrix} \quad (5.12)$$

The matrices \mathbf{A} , \mathbf{B} , \mathbf{C} and \mathbf{D} of the state-system described in equations 4.109 and 4.110 become:

$$\mathbf{A}(\bar{\omega}_{rotor}, \bar{U}) = \begin{bmatrix} -\frac{B_r(\bar{\omega}_{rotor}, \bar{U}) + B_p}{\frac{J_r}{V_p(1+C_{v,m}R_H)}} & -\frac{V_p(1+C_f)}{\frac{J_r}{(C_{v,p}+C_{v,m}+C_{v,p}C_{v,m}R_H)}} \\ \frac{K_r U(\bar{\omega}_{rotor}, \bar{U})}{C_H} & -\frac{V_m \omega_m}{C_H} \end{bmatrix} \quad (5.13)$$

$$\mathbf{B}(\bar{\omega}_{rotor}, \bar{U}) = \begin{bmatrix} \frac{K_r U(\bar{\omega}_{rotor}, \bar{U})}{J_r} & 0 \\ 0 & -\frac{V_m \omega_m}{C_H} \end{bmatrix} \quad (5.14)$$

$$\mathbf{C} = \begin{bmatrix} 1 & 0 \\ 0 & 1 \\ -V_p R_H & 1 + C_{v,p} R_H \end{bmatrix} \quad (5.15)$$

With a linear mathematical model of this second-order system, the dynamic behavior is characterized through the eigenvalues of the matrix \mathbf{A} .

Characteristic equation

The system of equation is simplified by using B_{eq} and $C_{v,eq}$ to represent the equivalent damping coefficient and the equivalent volumetric loss coefficient respectively.

$$B_{eq} = B_r(\bar{\omega}_{rotor}, \bar{U}) + B_p \quad (5.16)$$

$$C_{v,eq} = C_{v,p} + C_{v,m} + C_{v,p} C_{v,m} R_H \quad (5.17)$$

The characteristic system equation is found by setting the determinant of $A - \lambda I$ equal to zero. The term λ here represents the eigenvalues of matrix A and is not to be confused with the tip speed ratio.

$$\lambda^2 + \left[\frac{B_{eq}(\bar{\omega}_{rotor}, \bar{U})}{J_r} + \frac{C_{v,eq}}{C_H} \right] \lambda + \dots \quad (5.18)$$

$$\left[\frac{B_{eq}(\bar{\omega}_{rotor}, \bar{U})}{C_H J_r} + \frac{V_p^2 (1 + C_f) (1 + C_{v,m} R_H)}{C_H J_r} \right] = 0 \quad (5.19)$$

Natural frequencies

The undamped natural frequencies are determined by the magnitude of each pair of complex conjugated eigenvalues of matrix A . The resulting hydraulic natural frequency ω for the proposed second order system is then given by:

$$\omega_n(\bar{\omega}_{rotor}, \bar{U}) = \sqrt{\frac{V_p^2}{C_H J_r}} K_i(\bar{\omega}_{rotor}, \bar{U}) \quad (5.20)$$

with

$$K_i(\bar{\omega}_{rotor}, \bar{U}) = \sqrt{(1 + C_f) (1 + C_{v,m} R_H) + \frac{B_{eq}(\bar{\omega}_{rotor}, \bar{U}) C_{v,eq}}{V_p^2}} \quad (5.21)$$

Damping Ratios

Damping ratios are obtained from the ratio of the absolute value of the real part and the magnitude of each pair of complex conjugated eigenvalues of matrix A .

$$\zeta(\bar{\omega}_{rotor}, \bar{U}) = \left[\frac{B_{eq}(\bar{\omega}_{rotor}, \bar{U})}{2 V_p} \sqrt{\frac{C_H}{J_r}} + \frac{C_{v,eq}}{2 V_p} \sqrt{\frac{J_r}{C_H}} \right] \frac{1}{K_i(\bar{\omega}_{rotor}, \bar{U})} \quad (5.22)$$

5.2.2 Conditions for (In)stability

According to [40], for the linearized model of the rotor and drive train:

...it is then possible to vary the gains and rapidly calculate various measures of performance which help to evaluate the performance of the controller with those gain settings. Useful measures of performance include:

- *gain and phase margins, to indicate how close the system is to instability;*
- *the crossover frequency (at which the open-loop gain crosses unity), as a measure of the responsiveness of the controller;*
- *the positions of the closed-loop poles of the system, which indicate how well various resonances will be damped;*
- *step responses, illustrating how, for example, the pitch angle and tower motion respond to a step change in wind speed;*
- *frequency responses, showing, for example, how much the pitch responds at critical frequencies such as the blade passing frequency or the drive train resonant frequency, or how much the tower will be excited by the wind.*

The stability of the rotor and drive train combination is analyzed using the state-space model which is derived from the quasi-static rotor model and the second order transmission system model. The stability of this system of equations is essentially dependent on the $C_\tau - \lambda$ curve of the rotor (see figure 4.10(a)), the rotor mass moment of inertia and the stiffness of the hydraulic circuit.

Note that a distinction is made between static and dynamic stability. Static stability is the ability of the system to return to a stable (steady state) condition after being subjected to a perturbation. Dynamic stability is the ability of the system to operate within certain limits under continuously changing (transient state) conditions.

As long as the operating point is on the negative slope of the $C_\tau - \lambda$ curve, the rotor response is statically stable. There where the slope is positive, the system response is unstable. Once the system becomes unstable, the rotor will stall.

From equation 4.8 it is apparent that the value of λ is lower than $\lambda_{C_{\tau,max}}$ when:

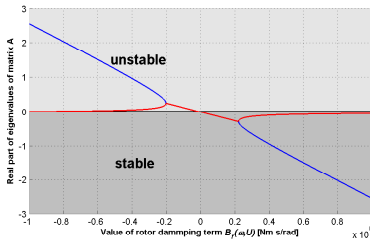
- the rotation speed ω drops sufficiently with respect to the wind speed.
- the wind speed U_∞ increases sufficiently fast with respect to the rotation speed.

For the state-space system to be dynamically stable, the real part of the eigenvalues of matrix A (equation 5.13) must be negative. The only term in matrix A that can make the real part of its eigenvalues positive is $B_r(\bar{\omega}_{rotor}, \bar{U})$. Regarding equation 5.22, this happens when the aerodynamic torque and rotor speed both either increase or decrease, i.e. when the wind speed increases or decreases.

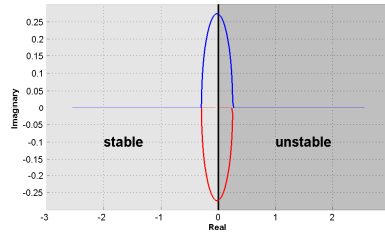
The drive train properties make it possible that during operation, the system is perturbed to the extent that it ventures into a region where it is unstable but still able to recover.

Example: Stability of a 5MW System

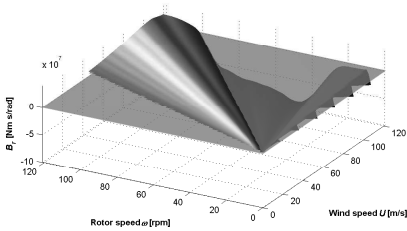
To evaluate the stability of the state-space model of the rotor-drive train combination, the values listed in table 5.1 are used for the respective parameters. The wind speed U and rotation speed ω are varied to find conditions under which the value of $B_r(\bar{\omega}_{rotor}, \bar{U})$ becomes sufficiently negative to cause instability. Figure 5.2 shows the results of this parameter study on stability. Figure 5.2(a) reveals the value of B_r below which the real parts of the eigenvalues of A are positive.



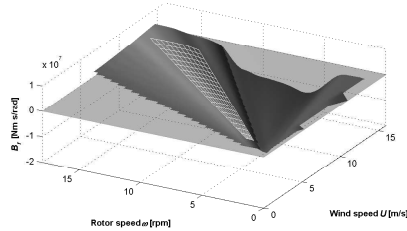
(a) Finding the critical value of B_r



(b) Root locus plot for the values of matrix A (equation 5.13)



(c) The value of B_r as function of U and ω



(d) Figure 5.2(c) zoomed in, showing the design window

Figure 5.2: Stability analysis plots

This value of B_r thus sets the limit for the stability of the state-space system. Figure 5.2(c) shows for which combination of U and ω this limit is transgressed. The zero-crossing is the rotor stability boundary. The lower plane is the rotor and drive train stability boundary. So, if a wind gust occurs and the instantaneous value of B_r does not fall below the lower plane boundary, the system remains stable. For the system modeled here, instability occurs when the instantaneous wind speed is over 100m/s.

Figure 5.2(d) is the zoomed-in version of figure 5.2(c). It shows the design win-

dow, which is defined here as the range of steady-state operational conditions for which the system is designed. For the rotor this is for values of the tip speed ratio between 6.5 and 8.5.

Within the design window, i.e. the range of expected operational conditions, the system is and stable. The unstable condition will only occur if the operator/controller forces it so, for example in the case of an emergency shutdown. Other instabilities that may occur due to interference are assumed to be eliminated by the controller.

5.3 Parameter Sensitivity Analysis for a 5MW Wind Turbine Drive Train

5.3.1 Simulation Setup

The parameter sensitivity study is carried out using a Matlab model similar to the one derived in section 5.2. The main difference of this model is that it also includes uni-directional pipeline flow dynamics, a detailed description of which is given in [59]. The modeling of the pipeline dynamics is considered outside the scope of this dissertation. However for the simulations discussed in this section and in section 7.4, a linear dynamic model of a rigid uniform fluid transmission line is used. This pipeline model is documented in [73]. The inputs for the model are the volumetric flow rate at the ends (inflow positive), the outputs are pressures at the ends and mode shapes of the pressure.

In order to obtain a realistic response of the hydrostatic transmission, accurate simulations of the aerodynamic rotor and wind conditions are required. The numerical model created in MATLAB-Simulink is converted to a Dynamic Link Library (DLL) which is implemented as an external controller for the model of the NREL 5MW reference turbine in the commercial software package GLGH Bladed [74]¹. The multibody dynamics software package “Bladed” from energy consultancy GL Garrad Hassan is the industry standard integrated software package for the design and certification of onshore and offshore turbines [74].

The overall dynamics of the assembled hydraulic transmission model without control (pump + hydraulic line + hydraulic motor + variable displacement actuator)

¹All design calculations are done in Matlab. The properties of the system are defined in a Matlab file. These are loaded into a Simulink model of the drive train. The Simulink model of the drive train is incorporated in a Simulink controller. This controller is compiled to yield a .dll file which is loaded as external controller in Bladed.

are represented through the following linear state-space model:

$$\begin{bmatrix} \dot{\mathbf{x}} \\ \dot{e}_m \end{bmatrix} = \begin{bmatrix} \mathbf{A} - \frac{C_{v,p}}{n_{lines}} \mathbf{b}_1 \mathbf{c}_1^T + \frac{C_{v,m}}{n_{lines}} \mathbf{b}_2 \mathbf{c}_2^T & \frac{V_m \omega_m}{n_{lines}} \mathbf{b}_2 \\ 0 & -\frac{1}{T_{ctrl}} \end{bmatrix} \begin{bmatrix} \mathbf{x} \\ e_m \end{bmatrix} + \begin{bmatrix} \frac{V_p}{n_{lines}} \mathbf{b}_1 & 0 \\ 0 & \frac{1}{T_{ctrl}} \end{bmatrix} \begin{bmatrix} \omega_r \\ e_{demand} \end{bmatrix} \quad (5.23)$$

Where the following outputs are defined:

$$\begin{bmatrix} \tau_{pump} \\ \Delta p_p \end{bmatrix} = \begin{bmatrix} V_p (1 + C_{f,p}) \mathbf{c}_1^T & 0 \\ \mathbf{c}_1^T & 0 \end{bmatrix} \begin{bmatrix} \mathbf{x} \\ e_m \end{bmatrix} + \begin{bmatrix} B_p & 0 \\ 0 & 0 \end{bmatrix} \begin{bmatrix} \omega_r \\ e_{demand} \end{bmatrix} \quad (5.24)$$

The fluid power transmission is designed based on the same operational parameters of the reference rotor. Quasi-static models are used to represent the behavior of the hydraulic pump and motor. A modal method is used for time domain modeling of the pressure transients of hydraulic lines. The dynamic interaction between the different subsystems of the complete model is observed in the block diagram of figure 5.3. Note that the hydraulic transmission model described in this section, together with the load and pitch controllers, are implemented in MATLAB-Simulink and then compiled into a discrete time Dynamic Link Library file. This DLL file is used by the external controller interface of GH Bladed and called with a timestep of 0.01 ms. The different output parameters of the hydraulic transmission are also available through the external controller interface of GH Bladed.

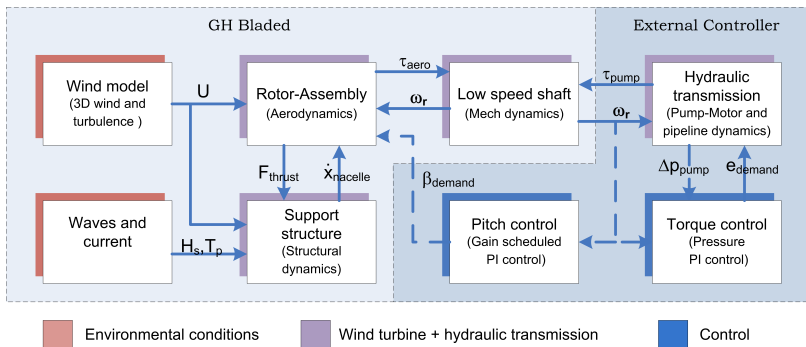


Figure 5.3: Subsystem block diagram of the wind turbine with hydraulic transmission

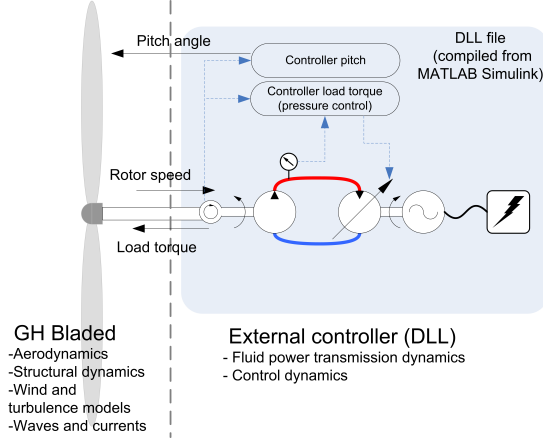


Figure 5.4: GH Bladed interface with the external controller

5.3.2 PI Control strategy for variable speed

The control strategy is based on a PI pressure control of the high-pressure line by adjusting the motor displacement and thus the flow at the hydraulic motor side. In order to avoid wind speed estimations, reference values for the pressure are taken from the corresponding steady-state values for different rotational speeds of the rotor. The equations for the Proportional-Integral control are:

$$e_{ctrl} = K_P (\Delta p_{ref} - \Delta p_p) + K_I \int_0^t (\Delta p_{ref} - \Delta p_p) dt \quad (5.25)$$

$$= K_P (\Delta p_{ref} - \Delta p_p) + e_I \quad (5.26)$$

$$\dot{e}_I = K_I (\Delta p_{ref} - \Delta p_p) \quad (5.27)$$

5.3.3 Reference Properties and Steady-state Operation

To demonstrate the implementation of the proposed model and controller, the rotor of the NREL offshore 5 MW reference turbine is coupled to a fluid power transmission with a fixed-speed generator. The same rotor specifications are used in order to establish a reference when comparing the dynamic behavior. The properties of the hydraulic pump are derived from the Häggglunds hydraulic motors [11]. The specific values applied in the model are listed in table 5.1. The diameter of the hydraulic lines was selected in order to have laminar flow in the hydraulic transmission.

Description	Symbol	Unit	5MW
Rotor mass moment of inertia	J_{rotor}	[kg m ²]	3.88e7
Rotor diameter	D_{rotor}	[m]	126
Rotor shaft viscous damping coefficient	B_r	[Nm s]	3500
Nominal speed of rotor-pump assembly	n_p	[rpm]	12.1
Pump volumetric displacement	V_p	[L/rev]	1400
Hydraulic motor volumetric displacement	V_m	[L/rev]	1.2
Nominal pressure	p_{nom}	[Pa]	350e5
Nominal volumetric efficiency of hydraulic motor	η_{vol}	[-]	0.90
Nominal volumetric efficiency of hydraulic motor	η_{vol}	[-]	0.96
Hydraulic motor nominal speed	n_m	[rpm]	1500
Pump laminar volumetric leakage coefficient	$C_{v,p}$	[m ³ /s/Pa]	9.1e-11
Motor laminar volumetric leakage coefficient	$C_{v,m}$	[m ³ /s/Pa]	5.71e-10
Pump & motor dry friction coefficient	C_f	[-]	0.02
Pump viscous damping coefficient	B_p	[Nm s]	50e3
Motor viscous damping coefficient	B_m	[Nm s]	3.5
Dynamic viscosity of fluid	μ	[m ² /s]	40.0e-6
Effective bulk modulus of fluid	E_{fluid}	[Pa]	1.0e9

Table 5.1: Reference values for a 5MW hydrostatic wind turbine transmission system

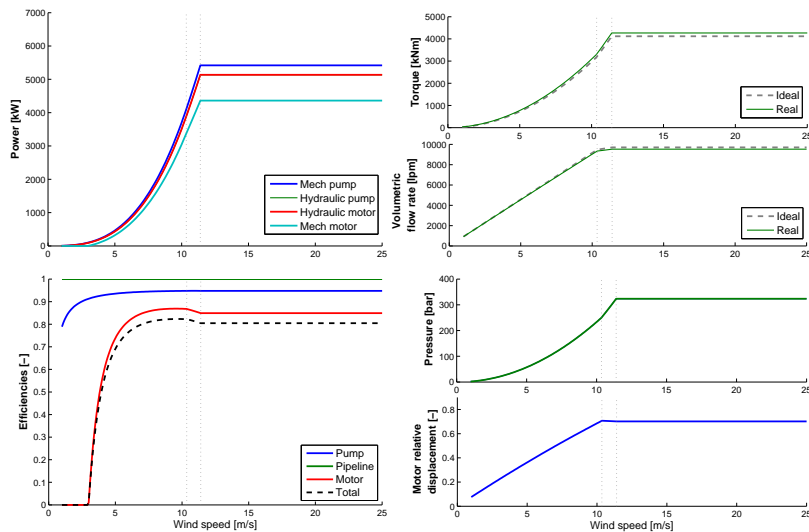


Figure 5.5: Steady-state operation for operational wind speeds

5.3.4 Results for Variations from Default Properties

Variation 1: Length of Oil Line

This parameter is directly associated to the amount of oil present in the system. When more oil is used, the effective stiffness is reduced due to compressibility of hydraulic fluids, and the fluid inertia is increased. The 10m and 100m line correspond to the nacelle and tower based solution respectively. Depending on the type of configuration this effect might be of importance as shown in figure 5.6(b),5.6(c).

variation		1	2	3	4
rotor inertia	J_{rotor}	3.88e7kg m ²			
pressure line length	L_{hp}	10m	20m	50m	100m
motor volumetric efficiency	η_v	90%			

Table 5.2: Variation from the reference values in table 5.1 for the length of the oil line

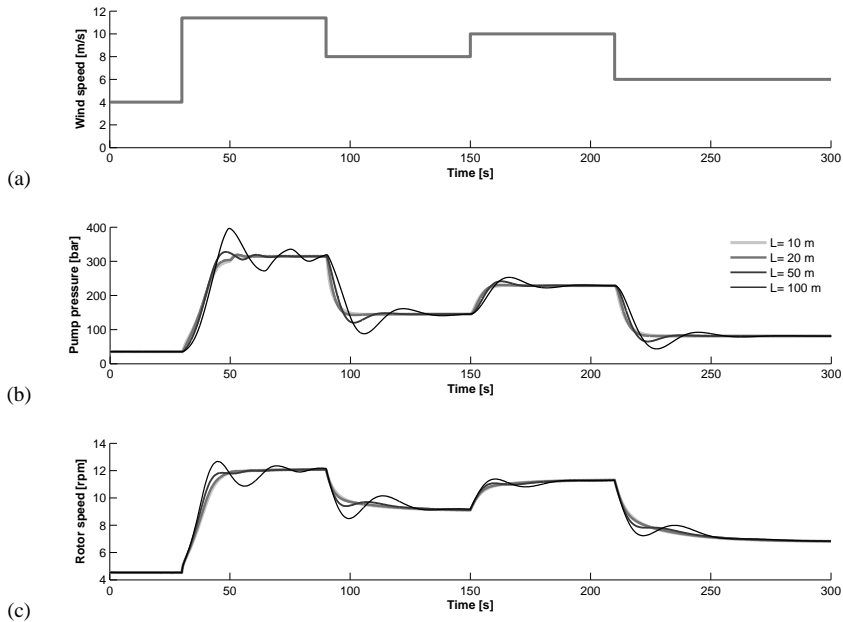


Figure 5.6: Transient response to a series of wind speed steps for different pipeline lengths; $\eta_{vol,m} = 90\%$

Pressure fluctuations are relatively high for the 100m pipeline, with overshoots from 10 to 40% with respect to the reference; the 50m shows 4 to 20% difference while the 10m and 20m only shows fluctuations from 1 to 2%.

Variation 2: Volumetric efficiency of the hydraulic motor

One of the main concerns of hydraulic transmissions for wind turbine is the efficiency of the variable displacement hydraulic motor(s), especially at partial load operation. However the oil leakages, which depend on the pressure difference across the unit, provide damping in the pressure fluctuations as shown in figures 5.7(a) and 5.7(b).

variation		1	2	3	4
rotor inertia	J_{rotor}	3.88e7 kg m ²			
pressure line length	L_{hp}	100m			
motor volumetric efficiency	η_v	60%	80%	90%	95%

Table 5.3: Variation from the reference values in table 5.1 for the volumetric efficiency of the hydraulic motor

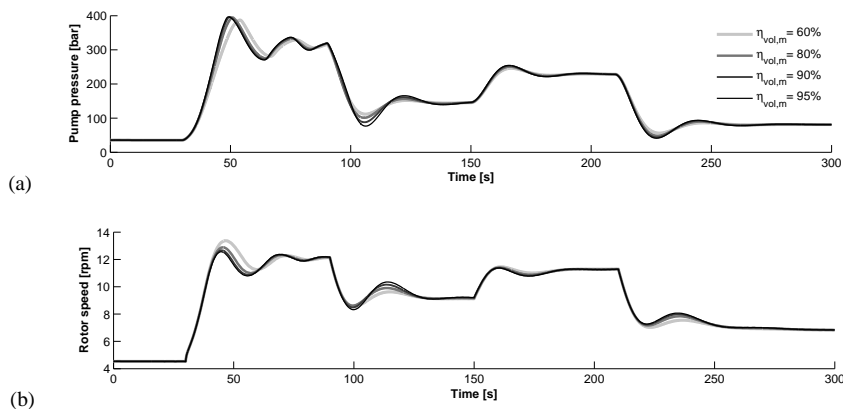


Figure 5.7: Transient response to a series of wind steps for different motor volumetric efficiencies lengths; $L = 100m$

The results of variation 1 show that the 100m long line yields the highest pressure overshoots. To show the effect of the volumetric efficiency on damping, this length is also used here.

As is observed in figure 5.6, the effect of the volumetric efficiency of the motor on the damping characteristic is not significant. When the volumetric efficiency of the motor is reduced from 95 to 60%, the maximum overshoot of the pressure is reduced from 50% to 30%.

Variation 3: Rotor mass moment of inertia

variation		1	2	3
rotor inertia	J_{rotor}	3.5e6kg m ²	3.5e7kg m ²	3.5e8kg m ²
pressure line length	L_{hp}	60m (middle)		
motor volumetric efficiency	η_v	90% (middle)		

Table 5.4: Variations from the reference value in table 5.1 for rotor mass moment of inertia

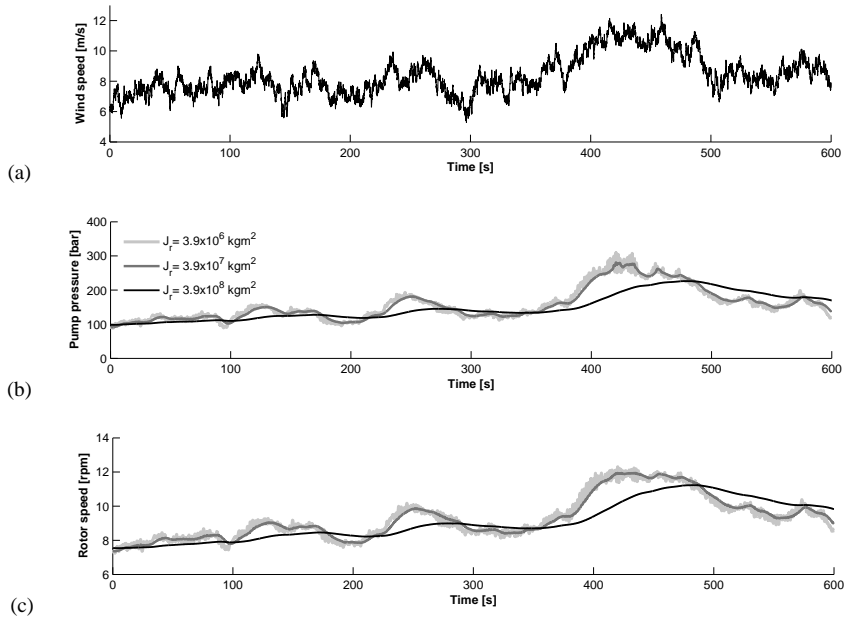


Figure 5.8: Transient response to dynamic wind speed for different rotor mass moments of inertia; $L = 10\text{m}$, $\eta_{vol,m} = 90\%$

The different values of the mass moment of inertia in table 5.4 account for a rotor which is effectively ten times lighter or heavier with respect to the reference turbine using the same rotor geometry. If the comparison is made in terms of rotor diameter, the inertias correspond to those of a 80m-2MW, 63m-5MW (reference case) and 200m-12.5MW turbines. However this approach can not be compared directly in the results, since each rotor would have different operating rotational speeds.

A dynamic input simulating a hub height mean wind speed of 8 m/s and 17.67% turbulence intensity is used to observe the response of the model in figure 5.8. The rotor mass moment of inertia has a direct influence in the time response of the system. The results show that larger inertias lead to lower fluctuations of pressure and rotational speed.

5.4 Experiments with a 1MW Hydrostatic Transmission System

5.4.1 Experimental Setup

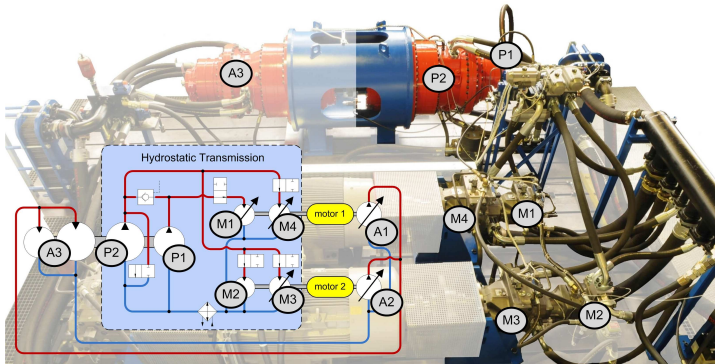


Figure 5.9: Overview of the test facility at IFAS: “P” is pump, “M” is hydraulic motor. “A” refers to “Antriebe”, the hydraulic drive system components used to recycle energy and simulate the behavior of the aerodynamic rotor [*Image courtesy of IFAS*]

In the scope of a research project funded by the Federal Ministry for the Environment, Nature Conservation and Nuclear Safety of Germany, IFAS (the Institute for Fluid Power Drives and Control of the University of Aachen) has developed a hydrostatic transmission test bench for wind turbines of the 1-MW power class. Its purpose

is to study the feasibility of replacing the commonly used gearbox and the frequency converter [75]. An overview of the experimental setup is given in figure 5.9.

The main components of the hydrostatic transmission are the radial piston pumps directly connected to the turbine shaft and the axial piston motors with variable volumetric displacement. The specifications are listed in table C.1 of appendix C. The test bench consists of two hydraulic circuits:

1. the drive system that simulates the behavior of the rotor,
2. the hydrostatic transmission system as part of a wind turbine drive train.

The electric motors are connected to both circuits. The pumps of rotor simulating drive system are thus driven by these motors and by the hydraulic motors of the drive train. The use of electricity is minimized in this way.

By switching on and off different combinations of pumps and motors and varying the volumetric displacement of motors 1, 3 and 4, the drive train can be adapted to the current wind situation optimizing the power output especially in partial load. The controls configure the fluid power drive train such that for every wind speed:

- Control valves engage the optimal combination of pumps and motors,
- The bent axis or swash plates of the motors are set on the desired displacement.

More information on properties of this test facility is given in appendix C and in [25].

5.4.2 Transmission Input: Fixed-Speed Rotor Simulation

Application of a Scaled Version of the NREL rotor

Since there is no accurate model of a 1MW-class WT freely available (at the time of these experiments), the approach is to convert data from simulation runs in GH Bladed with the NREL 5MW system (see section 3.1.5) to those of a 1MW system using simple relations. Even if the blades are scaled exactly, maintaining the airfoils, the chord distribution and other design ratios, the aerodynamics change.

The method applied here for scaling down the rotor from a 63m to a 25m radius does not account for influence from:

- The rotor mass moment of inertia: the control settings in GH Bladed have been adapted to have the rotor running at fixed speed. This reduces the influence of the mass moment of inertia on the scaling of the Bladed results.
- Dynamic stall: local changes in the angle of attack of the effective airspeed.

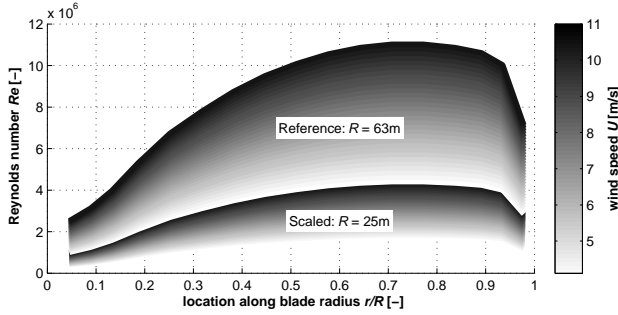


Figure 5.10: Effect on the Reynolds number of scaling the rotor radius from 63m to 25m

- Dynamic inflow: local changes in effective airspeed experienced by the blades. Since the rotation speed of the 50m rotor is 126/50 times higher than the 126m rotor, local effects due to dynamic inflow change.
- The Reynolds number Re decreases for the same wind conditions. As figure 5.10 shows, the values of Re remain of the same order of magnitude ($> 10^6$).

However, the preciseness of the rotor simulation are of lesser concern and it is deemed sufficiently accurate for application here.

Matching Transmission & Rotor Operational Envelopes

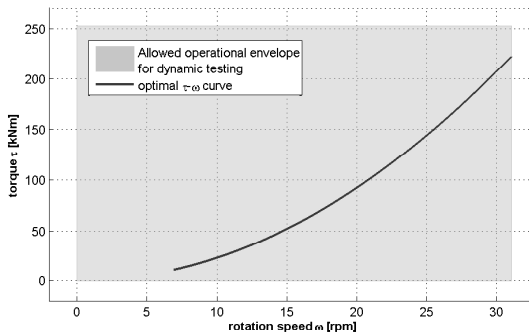


Figure 5.11: Results of scaling the rotor to fit the drive train envelope limits

The nominal line pressure for dynamic loads on the hydrostatic transmission is set at 220bar. This translates directly to a nominal torque of around 230kNm. The maximum possible speed is approximately 31 rpm. These two conditions are the limits for the operational range of the rotor simulation.

When scaling down the rotor properties of the NREL turbine to match the transmission capability, the relation between power coefficient C_P and tip speed ratio λ stays the same. The maximum allowable rotor diameter is found by setting the torque and speed limits as rated power conditions of the wind turbine rotor. The resulting curve for the optimal torque versus rotation speed is displayed in figure 5.11.

A comparison between the rotor properties of the original NREL turbine and the version adapted to match the hydrostatic transmission is given in table 5.5.

Description	Symbol	Original	Adapted
Power rating at low speed shaft	$P_{rated,ls}$	5,297kW	1,000kW
Rotor radius	R	63m	25m
max. rotational speed	ω	12.1rpm	30.5rpm
No. of blades	B	3	
optimal tip speed ratio	λ_{opt}	7.55	
max. power coefficient	$C_{P,max}$	0.48	
rated wind speed	v_{rated}	11.4m/s	

Table 5.5: Comparison of original NREL 5MW and adapted 1MW rotor properties [38]

Input from Wind Turbine Simulation Software GH Bladed

A drawback of using the software package GH Bladed to create the transmission input was that the software was not suited for interactive use, i.e. hardware-in-the-loop. The braking torque of the drive train thus cannot be fed back into the program. This creates an unrealistic coupling between the simulated input and the transmission response. To make the coupling more realistic, the rotor control settings are set to fixed speed operation. This fixed speed is predetermined using the optimal tip speed ratio λ_{opt} , where the wind speed is the average taken from the wind file corresponding to the load case.

To run a simulation in Bladed a wind file is required. These files are also created in Bladed. The nature of a wind file is determined by a number of user picked settings, such as the mean wind speed, the turbulence intensity, the turbulence seed, the yaw misalignment angle, the inclusion of tower shadow and how this is modeled and the type of wind shear profile. An overview of the process to create the test bench input

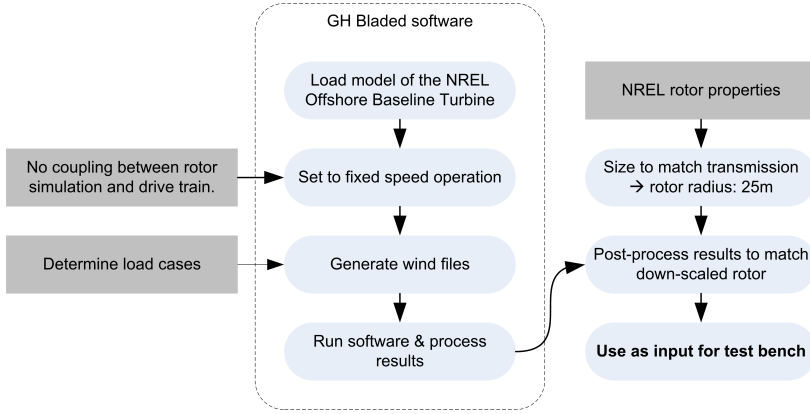


Figure 5.12: Flow chart for acquisition of drive train inputs for GH Bladed

is given in figure 5.12 For more information on how this is achieved, see the Bladed manual. The output parameters of interest are the torque and angular velocity of the low speed shaft versus time.

Rotor Input Scaling: Adaptation of GH Bladed Results to a 50m Rotor

The results from Bladed are scaled down to create the input for the transmission. They have to be translated from results of a 126m to a 50m rotor diameter. Only steady state relations are considered here, maintaining the same tip speed v_{tip} and power coefficient C_p . From equations 4.8 and 4.16, the following translations for speed and torque are derived:

$$\omega_2 = \omega_1 \frac{R_1}{R_2} \quad (5.28)$$

$$\tau_2 = \tau_1 \left(\frac{R_2}{R_1} \right)^3 \quad (5.29)$$

The standard deviation of the torque with respect to the mean value is the same for both the original and the scaled rotor.

5.4.3 Drive Train Control Configurations

In order to demonstrate the effect of pressure control, the drive train was set to operate in two different manners:

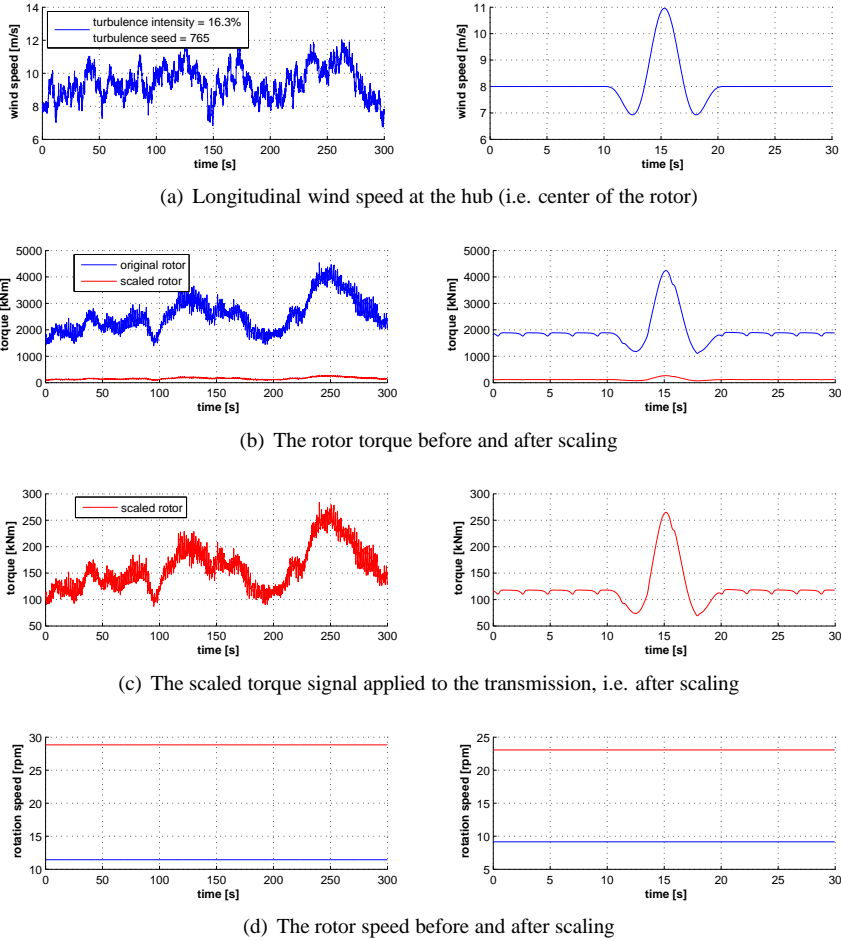


Figure 5.13: Bladed results for fixed speed simulation of NREL Offshore Baseline Turbine for wind speed with turbulence intensity 16.3% and turbulence seed 765 (left) and an extreme gust (right) and the results after scaling

1. Fixed transmission ratio: the volumetric displacement of the motors remains constant. No form of control is applied to the hydrostatic transmission, which thus acts similarly to a common wind turbine gearbox. The fixed speed of the low speed and the high speed shafts and the fixed transmission ratio mean that

a change in torque directly induces a change in pressure.

2. Variable transmission ratio with pressure control: the volumetric displacement of the motors is controlled. A lookup table for the ideal relation between torque (pressure) and rotor speed is used as reference. The variable transmission ratio allows the controller to manage the pressure difference Δp (and the change in Δp) over time in the system.

The basic functionality of both control configurations is shown in figure 5.14.

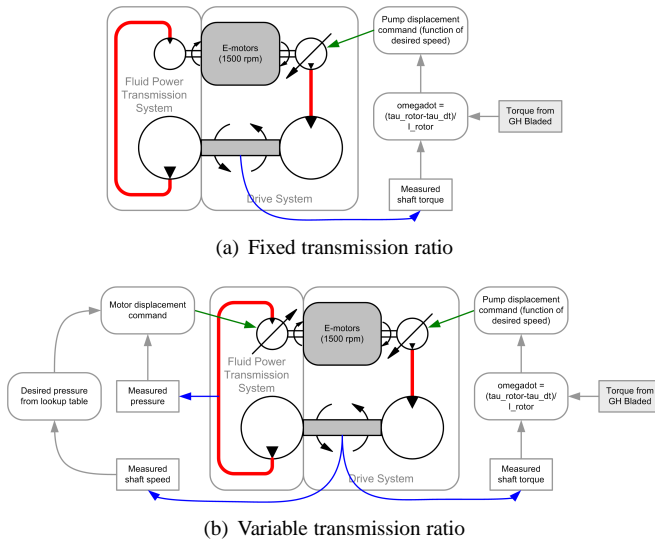


Figure 5.14: The basic functionality of the configurations and control of the experimental drive train

5.4.4 Overview of Consulted Loads Cases

The transmission response to dynamic loading and the effects of the control strategy are demonstrated using three different load cases shown in figure 5.15. Load Case A is a simple torque step from 100kNm to 150kNm. This is not a realistic scenario, but it serves well to reveal the dynamic properties of the system. Load Case B is the simulated aerodynamic torque resulting from an extreme wind gust. Load Case C is the simulated aerodynamic torque resulting from turbulent wind loads.

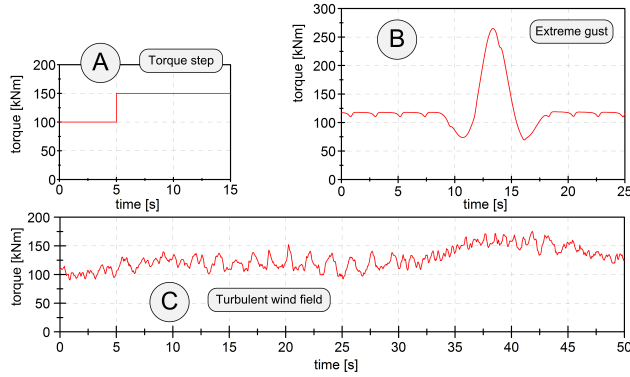


Figure 5.15: Simulated aerodynamic torque applied in the experiments

5.4.5 Response to Torque Step on Rotor Shaft including Rotor Inertia

In the figures 5.16, the measure response is plotted together with two forms of simulated response. By identifying a number of key points in the response, the essential dynamic properties of the system were derived. They are listed in table 5.6. These values are applied to simulate the drive train as a second order system, using the equations given in section 4.4. The simulated response is defined in two ways:

1. with the values of C_H and R_H are derived from the specific measured response step data (black dots in one plot).
2. with fixed values of C_H and R_H , which are taken to be $3.93e-11$ and $3.50e10$ respectively, are used in all cases. These values are most representative, since the responses where these values were measured have the least deviation of rotational speed, i.e. additional damping.

The results show the likening of the measured response to the response of a second order model of the drive train.

5.4.6 Effect of Torque Control

On the Response to a Step Input

The measurement result with an applied torque step is shown in figure 5.17. The two upper diagrams present the behavior of the hydrostatic transmission with constant

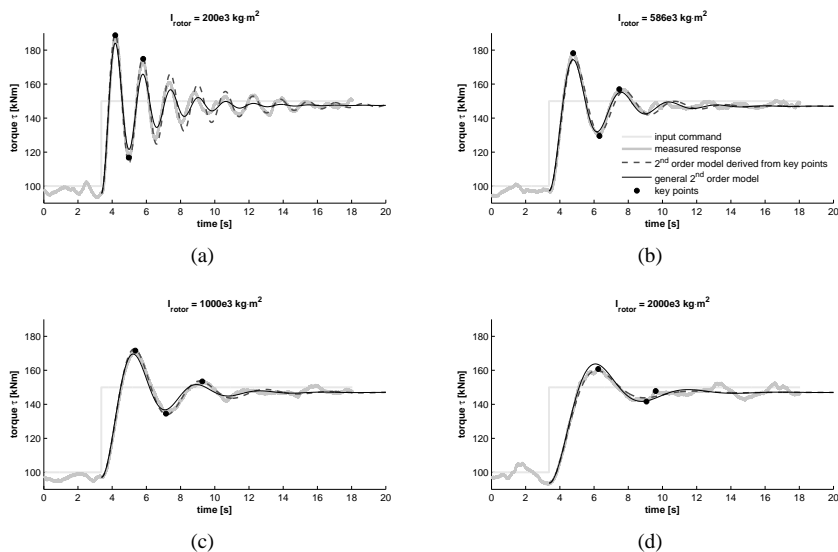


Figure 5.16: Torque step responses for different simulated rotor mass moments of inertia

Description	Symbol	Units	Values			
Rotor moment of inertia	J_r	[kg·m/s]	2e5	5.86e5	10e5	20e5
Natural frequency	ω_n	[Hz]	0.62	0.35	0.27	0.21
Damping ratio	ζ	[-]	0.07	0.18	0.22	0.41
Rise time	t_{rise}	[s]	0.46	0.83	1.08	1.38
Peak time	t_{peak}	[s]	0.68	1.19	1.74	2.41
Settling time	t_{settle}	[s]	18.1	11.9	12.8	8.6
Maximum overshoot	PO_{max}	[%]	0.82	0.62	0.48	0.28
Hydraulic resistance	R_H	[Pa·s/m ³]	5.44e10	3.24e10	3.50e10	2.73e10
Hydraulic capacitance	C_H	[m ³ /Pa]	3.61e-11	3.98e-11	3.93e-11	3.61e-11

Table 5.6: Response data for the torque step input from 100kNm to 150kNm at approximately 15.7rpm constant speed, for different mass moments of inertia

motor displacement. On the left side the applied torque step and the resulting load torque measured for three different inertias of the turbine are plotted. After the torque step occurs, the measured torque on the test bench also rises and oscillates to the new value. With an increased inertia of the turbine the resonant frequency of the drive train is decreasing [76]. The diagram on the right presents the effect on the rotation speed of the turbine. Due to a rising pressure in the transmission the leakage is increased leading to a slightly increasing rotation speed of the turbine. The higher the turbine inertia is set, the more energy is stored in the flywheel with the slight change of speed. The plots in the second half of the diagram display the same measurement as before, but with a torque controlled transmission. In this case the torque step leads to higher applied torque than braked by the transmission and consequently a rising rotation speed. The load torque on the test bench rises proportional to the rotation speed until the equilibrium of torque is set again.

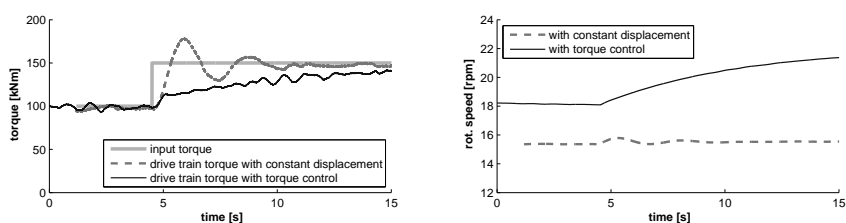


Figure 5.17: Measurement results for a torque step

On the Response to an Extreme Gust

With a constant motor displacement there is only a short delay between applied and measured torque. The rotation speed can only rise slightly and therefore the peak power delivered by the wind has to be transferred by the transmission. Due to the elasticity of the hydraulic drive train the measured torque on the test bench is even higher than the one applied on the inertia. In figure 5.18 the results of the gust response with and without a torque controlled transmission is presented. In this case the turbine can speed up about 2 rpm and thereby store most of the peak energy of the gust. The maximum torque measured on the test bench is 120kNm lower than the applied load. When this torque is going down again, rotation speed decreases also extracting stored energy in the flywheel and going back to constant operation.

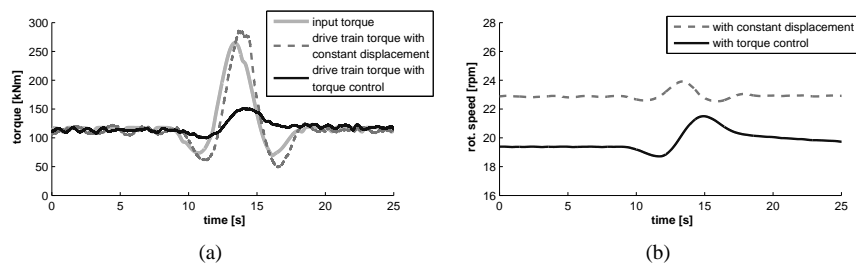


Figure 5.18: Measurement results for a wind gust

On the Response to Turbulent Wind Loads

Figure 5.19 shows the measured torque and the behavior of the rotation speed for the two different control strategies. When the motor displacement is set to constant, the measured torque follows the applied torque only smoothing torque peaks with a short delay. When the torque controller is activated, the power output is significantly smoother. The high pressure surge of the uncontrolled response is undesirable. When more efficient drives are used the damping of the system will be even less. To avoid large pressure fluctuations when operating below rated conditions, a controlled valve can be used. The maximum pressure is already limited by a pressure relief valve. A solution here would be to have a valve that limits the rate of pressure increase.

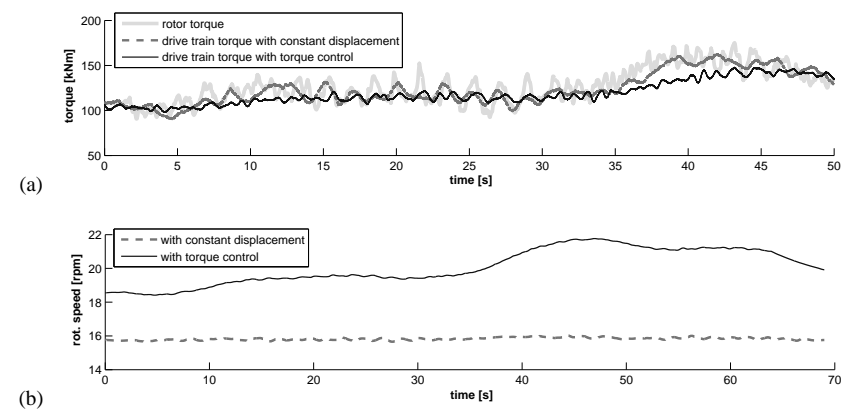


Figure 5.19: Measurement results for realistic wind loads

5.5 Conclusion

On the General Stability Analysis

From the theoretical description of the rotor and drive train system it is found that its response is stable within the design window.

On the Parameter Sensitivity Analysis for a 5MW Wind Turbine Drive Train

The inherent damping characteristics of the hydraulic drives are mostly associated to the leakage losses and the effective hydraulic capacitance. Although low natural frequencies of the hydraulic transmission could be present in the (1p and 3p) operational frequencies of the rotor, the proposed model shows a very well damped response of the rotor speed. Pressure variations due to harmonic inputs of the motor setting are significant at low frequencies and should be avoided by means of a well-designed controller. Special attention should be given for over damped systems in order to avoid a sluggish response.

For the reference case the combinations of length of the hydraulic line and efficiency of the hydraulic transmission are given for the require variable speed operation. It is seen that some damping in the system is introduced due to the oil leakages in the hydraulic drives, given or represented by the volumetric efficiency. In this regard although a lower efficiency represents a less favorable condition in terms of power production, it becomes an advantage for the dynamic performance resulting in lower pressure fluctuations. The amount of oil in the system has a significant influence in the stiffness of the transmission and therefore in the pressure transients; the main reason is that the high fluid inertia of the system is able to produce large pressure peaks (water hammer effects) whenever there are sudden variations of volumetric flow. Including an accumulator in the high pressure line, might reduce the pressure pulsations. On the other hand, the rotor mass moment of inertia has an important influence in the time response of pressure and rotational speed, leading to a slower but smoother response of the system.

In general a tower base solution with long pipelines is prone to higher pressure fluctuations with a clear effect on the controllability. The compressibility of the hydraulic fluid and the length of the high pressure line determine the hydraulic stiffness. If the stiffness becomes to low, the response becomes sluggish and large pressure overshoots occur. This effect is mitigated using pressure control, as was demonstrated by the experiments shown in section 5.4.6. Hence the idea of having a 5MW class wind turbine with the pump in the nacelle and the hydraulic motor at the base of the tower is still regarded as feasible.

Low volumetric efficiency of the hydraulic transmission provides a small pressure

fluctuation damping however its influence is minor and unlikely to be advantageous when compared to the loss in power production.

On the Experiments with 1MW-Class Transmission System

The hydrostatic transmission was subjected to two main types of input load:

1. Simple disturbances in the form of step inputs. Although these inputs are not realistic, they clearly reveal information on the response of the system in the form of the natural frequency and damping ratio.
2. Simulated aerodynamic torque, resulting from wind gusts and turbulent wind loads. These experiments were conducted using input from GH Bladed which was scaled from a rotor with a 63m radius to one with a 25m radius. This conversion is an engineering trick which neglects several aerodynamic scaling effects. However, for the purpose of the experiments it suffices. Initially the test were conducted using fixed speed operation. This omits two problems with translating the GH Bladed results to the input for the transmission:
 - (a) The missing coupling between rotor and drive train responses.
 - (b) The influence of the mass moment of inertia on the acceleration of the low speed shaft.

Measurements were made using both static and dynamic transmission (constant and variable motor volumetric displacement).

From the conducted experiments, it is observed that torque impulses applied to the drive train are quickly dampened, leading to a smoothened electrical power output. Apart from mapping the dynamic response characteristics, the measurements were also used to validate simulation models of the test bench.

It was observed that for real-life application of fluid power transmission in large wind turbines the following issues require special attention:

- Other natural frequencies: the natural frequency of the bed-plate of the test bench was measured to be around 27rpm. During the runs with $U_{mean} = 10\text{m/s}$ the average speed of the rotor was around 28.84rpm. Being so close to the natural frequency of the bed-plate led to an increase in noise. For same rotor torque at higher rotation speed the noise level dropped again. What this demonstrates is that knowing your environment is crucial in the design of a transmission.
- Oil temperature: under heavy loading (see turbulent wind case), the temperature of oil & components quickly rose to level out at approximately 60°C. This is well above the optimal temperature of around 45°C. Due to the amount of steel in the pump, the housing cools very slowly.

Passive Torque Control for Variable Speed Wind Turbines using Fluid Power Technology

6.1 Introduction

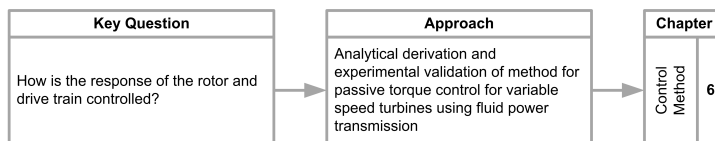


Figure 6.1: Flowchart for the objective and approach of this chapter

As mentioned in section 3.6, there are several ways to control the rotation speed and torque of the rotor and the hydrostatic drive train of the DOT. Both wind power and hydraulic power are essentially fluid flows. Hence, the same mathematical relations hold for both.

Already at an early stage of the research for this dissertation it was found that in theory it is possible to configure the fluid power transmission system in such a way that no form of active control is required for the drive train. The term active control here refers to the general manipulation of drive train properties or settings during operation. Hence, the method where no active control is required is referred to as passive control. Passive control is thus an inherent property of the system. The transmission components that enable this passive control are a nozzle and a pressure relief valve.

In figure 3.10 a simplified hydraulic diagram of the DOT concept of figure 3.13(c) is shown. The water pump is connected to a nozzle with constant cross-section through a high pressure line (pipe or hose) in an open-loop system. For the purpose of simplicity, the oil circuit is omitted here. The flow generated by the water pump eventually exits the hydraulic system through the nozzle, which in turn pressurizes the system in the required way for the rotor and hydraulic power transmission system to operate in stable conditions independently of the wind speed. By correctly sizing of the components between the rotor and the pressurized fluid jet at the exit of the nozzle, the wind turbine operates stable without any active control. Different “tuning” of the operational characteristics is possible by merely adjusting the size of the nozzle.

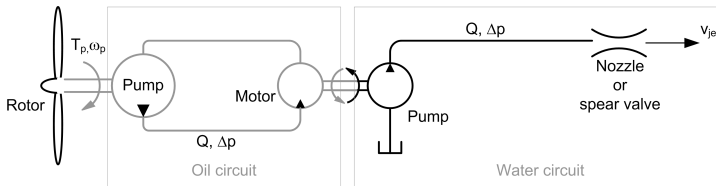


Figure 6.2: Hydraulic diagram of the double circuit as described in section 3.7.1; only the second part of the circuit is considered in this chapter

The objective of the research presented in this chapter is to prove that using fluid power technology, a wind turbine rotor is passively operated with variable speed at (or near) maximum efficiency for its allowable range of wind speeds.

The theoretical framework presented in chapter 4 is used to describe the hydraulic passive torque control concept. The proper dimensioning of the nozzle diameter is proposed by matching the static characteristics of the aerodynamic rotor with those of the hydraulic components.

To demonstrate the application of this idea of passive control, wind tunnel experiments (see figure 6.3) were conducted using a 1.8m diameter rotor with fixed blade pitch angle. The rotor was directly coupled to a water-hydraulic pump and different nozzle diameters were tested under a range of wind speeds, resulting in different operational characteristics of the rotor. The hydraulic braking and torque limitation were also tested and proven for the functionality of the concept.

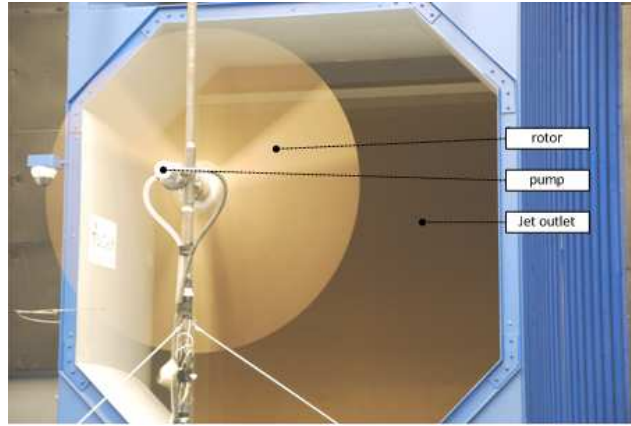


Figure 6.3: The experimental setup in the wind tunnel of the Open Jet Facility (OJF) of the Delft University of Technology

6.2 Passive Operation

6.2.1 Description of Principle

Torque balance at the rotor shaft

The angular acceleration of the rotor is determined by the balance between rotor torque τ_{rotor} and drive train torque τ_{pump} and the mass moment of inertia J_t of the rotor-pump assembly (see equation 4.1). When the rotor is operating at steady state, i.e. with constant rotation speed at constant wind speed ($\dot{\omega} = 0$), the equation 4.1 becomes:

$$\tau_{rotor} = \tau_p \quad (6.1)$$

The rotor torque coefficient C_τ is a function of the tip speed ratio λ , see figure 4.10(a).

Regard equation 4.14. The air density ρ_{air} is assumed constant here. Hence for a constant λ , τ_{rotor} is directly proportional to U_∞^2 . The aerodynamic torque as a function of the rotor speed is obtained by combining equations, 4.14, 4.17, 4.8 and 4.18:

$$\tau_{rotor} = \frac{C_p}{\lambda^3} \cdot \frac{1}{2} \cdot \rho_{air} \cdot \pi R^5 \cdot \omega^2 \quad (6.2)$$

$$= K_1 \cdot \omega^2 \quad (6.3)$$

Regard equation 4.41. The counter torque produced by the pump with fixed volumetric displacement V_g is essentially a function of pressure. The mechanical efficiency η_{mec} of the pump is a nonlinear parameter. As shown in figure 4.15(a), the value of η_{mec} is relatively constant over a wide range of operation. For simplicity, it is assumed constant here.

The flow Q produced by the pump is essentially a function of the rotor speed, see equation 4.35. The torque at the rotor is thus determined by the pressure difference Δp over the pump. The pressure difference Δp over the pump is predominantly determined by the outlet diameter of the nozzle at the end of the high pressure line.

The torque transmitted by the pump is derived from equations 4.46, 4.41 in combination with the nozzle equation 6.9 yield:

$$\tau_p = \left(\frac{\eta_{vol}^2}{\eta_{mec} \cdot C_d^2} \right) \cdot \frac{1}{2} \cdot \rho_{hyd} \cdot \frac{V_p^3}{A_{nozzle}^2} \cdot \omega^2 \quad (6.4)$$

$$= K_2 \cdot \omega^2 \quad (6.5)$$

Equation 6.5 shows that the pump-nozzle torque is described as a quadratic function of the rotor speed, which is the same relationship for the optimal aerodynamic performance given by equation 6.2. Hence, given the aerodynamic performance of the turbine, it is possible to closely match both curves by proper dimensioning of components by letting $K_1 = K_2$.

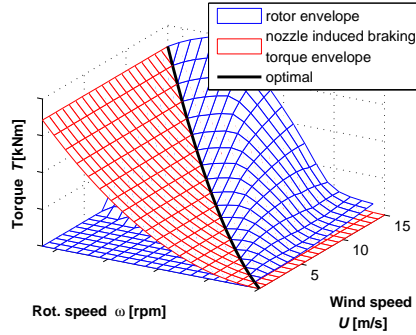


Figure 6.4: 3D torque curves of a conventional wind turbine

The resulting steady state performance envelope of the rotor and drive train should look like figure 6.4. Here the red area is the envelope of the counter torque produced by the pump, which is a function of the rotation speed only. It is directly proportional to the rotation speed squared. The blue area is the rotor torque envelope, which

is a function of the tip speed ratio, i.e. both rotation speed and wind speed. The intersection between the red and blue areas marks the region where the system will operate. If the nozzle is dimensioned optimally (as is the case here), this intersection will correspond to the line of optimal performance of the rotor in figure 4.10(c).

6.2.2 Dimensioning of the Constant Area Nozzle

Euler/Bernoulli's Equation for Dynamic Pressure

The function of the nozzle is to create a load resistance which allows to convert the hydraulic energy in the form of pressure (or equivalent head) into kinetic energy in the form of a high speed water jet. Consider a steady, inviscid, incompressible, laminar,

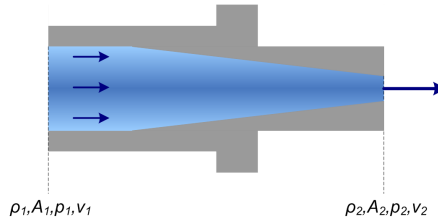


Figure 6.5: Diagram of the cross sectional view of the flow through the nozzle

unidirectional, one-dimensional flow through a conduit with constant diameter. At the end of the conduit is a nozzle, see figure 6.2.2. The static pressure in the conduit and at the nozzle outlet are p_1 and p_2 respectively, v_1 and v_2 are the related flow speeds. The relation between change in pressure and velocity for an inviscid flow is given by the Euler equation:

$$dp = -\rho v dv \quad (6.6)$$

Assuming incompressible flow, p_1 and v_1 at cross section 1 are related to p_2 and v_2 cross section 2 by:

$$\int_{p_1}^{p_2} dp = -\rho \int_{v_1}^{v_2} v dv \quad (6.7)$$

This results in Bernoulli's equation:

$$p_1 - p_2 = \frac{1}{2} \rho (v_1^2 - v_2^2) \quad (6.8)$$

The static relationship which describes the pressure drop as a function of the volumetric flow is derived from the Bernoulli's energy equation for an inviscid, incompressible, one-dimensional flow with constant density ρ . This relation is not linear and considers that the conduit cross sectional area is relatively larger than the orifice or nozzle area $A_{nozzle}/A_{conduit} \ll 1$.

$$\Delta p = \frac{\rho}{2} \cdot \left(\frac{1}{C_d \cdot A_{nozzle}} \right)^2 \cdot Q \cdot |Q| \quad (6.9)$$

Here, C_d is a discharge coefficient which considers pressure losses depending on the geometry and Reynolds number. The discharge coefficients are obtained experimentally.

The Continuity Equation

The speed v_2 of the flow out of the nozzle is calculated using the continuity equation. The physical principle of conservation of mass is that mass can be neither created nor destroyed. The mass flow m on either side of the nozzle outlet is thus in equilibrium.

$$m_1 = m_2 \quad (6.10)$$

$$\rho_1 Q_1 = \rho_2 Q_2 \quad (6.11)$$

Assuming incompressible fluid: $\rho_1 = \rho_2$, equation 6.11 becomes:

$$Q_1 = Q_2 = Q = A_1 v_1 = A_2 v_2 \quad (6.12)$$

$$v_1 = \frac{Q}{A_1} \quad v_2 = \frac{Q}{A_2} \quad (6.13)$$

Optimal Nozzle Area

By combining equations 6.8 and 6.13, it is found that the outlet area of the nozzle and the flow out of the pump determine the pressure in the line. The difference in static pressure inside and outside the conduit is expressed as:

$$\Delta p = \frac{1}{2} \rho Q^2 \left(\frac{1}{A_2^2} - \frac{1}{A_1^2} \right) \quad (6.14)$$

The optimal area of the nozzle outlet is calculated by combining equations 4.1, 4.8, 4.14, 4.41, 4.35 and 6.14 and setting the angular acceleration $\omega = 0$.

These equations are made more accurate by including the known losses throughout the transmission. The optimum power extraction corresponds to $C_{P,max}$, which

occurs at the optimal tip speed ratio λ_{opt} . This results in expression 6.16 for the optimal nozzle outlet area A_2 .

$$A_{nozzle}^2 = \frac{\eta_{vol}^2}{\eta_{mec} \cdot C_d^2} \cdot \frac{\rho_{hyd}}{\rho_{air}} \cdot \frac{\lambda^3 \cdot V_p^3}{C_p \cdot \pi R^5} \quad (6.15)$$

$$A_{nozzle} = \sqrt{\frac{\rho_{hyd}}{\rho_{air}} \frac{V_g^3 \lambda_{opt}^3 \eta_{vol}^2}{C_{p,max} \eta_{mec} \pi R^5} \left(1 - \frac{A_2^2}{A_1^2}\right)} \quad (6.16)$$

In reality the values for mechanical and volumetric efficiency will vary slightly depending on the operational conditions. For dimensioning the nozzle however they may be assumed constant. Hence, each term in equation 6.16 is a constant. Typically $A_2^2 \ll A_1^2$, which allows for a simplification of the equation. Since the nozzle outlet is typically circular, its dimension is hence forth given through its diameter.

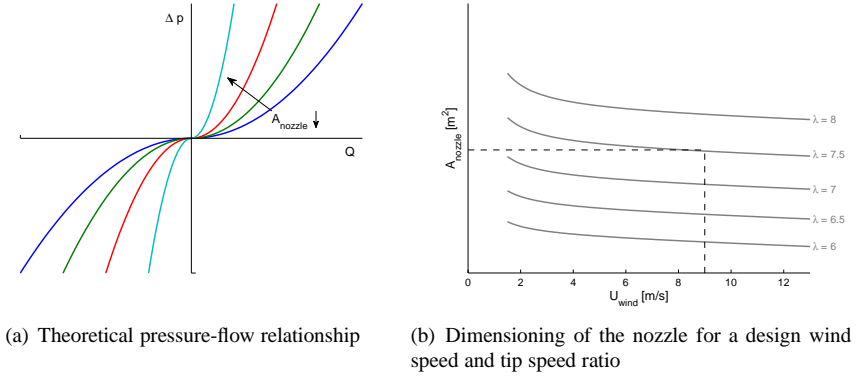


Figure 6.6: Graphs for the dimensioning of a constant area nozzle

A constant value of the nozzle area is selected for a design wind speed and tip speed ratio. For lower wind speeds, this will result in a lower tip speed ratio and for higher wind speeds the tip speed ratio will increase. From figure 6.6(b) it is observed that for a given rotor and fluid power transmission system, the nozzle area optimized for a chosen wind speed of 9 m/s and tip speed ratio of $\lambda = 7.5$, with variations of the tip speed ratio between $\lambda = 7.2$ for low wind speeds and $\lambda = 7.6$ for higher wind speeds.

6.2.3 Performance evaluation

When a design wind speed and nozzle has been selected, the resulting torque-speed curve of the rotor closely matches that of the hydraulic system, as shown in figure 6.7(a). Results are also shown for nozzles with $\pm 10\%$ variation from the design nozzle diameter. The power-speed curves of the system are given in 6.7(b).

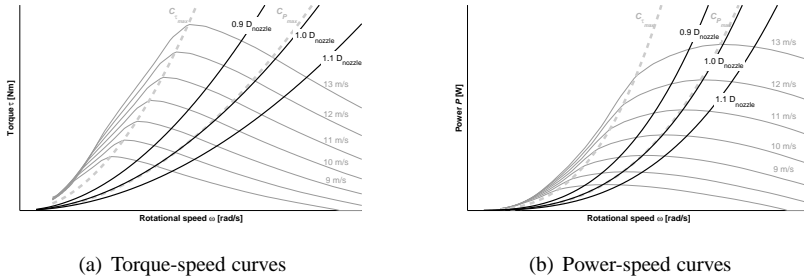


Figure 6.7: Operational curves for the design nozzle diameter with $\pm 10\%$

The total efficiency of the system is given by both the aerodynamic performance and the hydraulic transmission efficiency (pump and nozzle). Aerodynamic performance, as mentioned in section 4.2, is characterized through the power coefficient C_P , while the hydraulic transmission efficiency includes the discharge coefficient C_d of the nozzle, together with the both the overall efficiency (mechanical and volumetric) of the hydraulic drive. An example of the operating performance for different nozzle diameters is shown in figure 6.8.

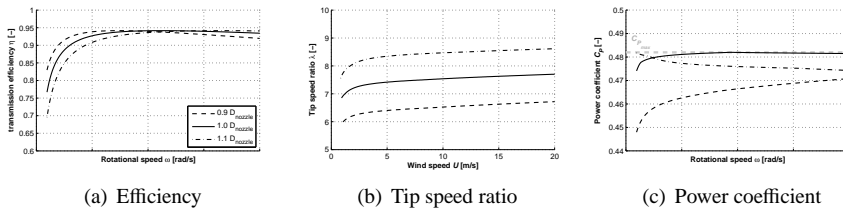


Figure 6.8: Performance of the rotor and hydraulic transmission (pump & nozzle)

Regarding stability, the turbine operation will be stable as long as the torque-speed curve of the combined pump-nozzle matches the envelope curves of the rotor where it has a negative slope ($dT/d\omega < 0$). If the wind speed increases, the rotor will exert a higher torque than the pump-nozzle torque and the rotor speed will increase.

Increasing the rotor speed will also decrease the aerodynamic torque for the given wind speed and increase the pump-nozzle torque, leading to a point where a new equilibrium is reached. On the other hand, the turbine operation will be unstable in the region where the slope of the rotor torque curve is positive ($dT/d\omega > 0$). Following the same reasoning, if the wind speed increases, the rotor will exert less torque than the pump-nozzle, therefore the rotor will stall and eventually stop. Therefore it is important to correctly size the nozzle in order to operate in the stable region of the rotor (see figure 4.10(a)).

6.3 Validation through Wind Tunnel Experiments

6.3.1 Overview of the Experimental Setup

Experiments for the validation of the passive control method were conducted at the Open Jet Facility (OJF) of the Delft University of Technology. The hydraulic diagram in figure 6.9 identifies the essential components of the experimental setup. Most of these components are identified in figure 6.3.1. The rotor diameter is 1.8m.

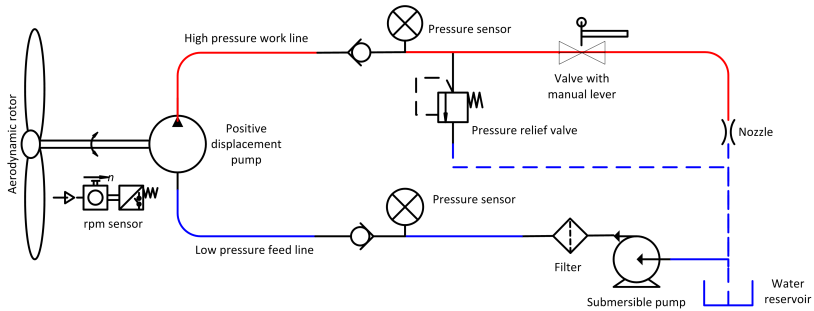


Figure 6.9: Hydraulic diagram of the experimental setup

The pump volumetric displacement is 12.5cc. Several nozzles were used, the cross-sectional diameter of their outlets ranging from 1.24mm to 2.07mm. More details on the experimental setup and how the measurements were interpreted are found in appendix D.

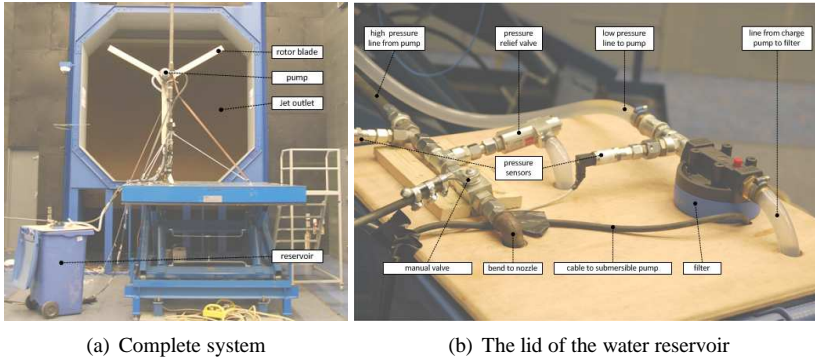


Figure 6.10: Pictures of the experimental setup

6.3.2 Experimental Results

Distinguishing between Steady State and Transient Results

Steady state measurements were done by going from one steady wind speed to the next. The result from one measuring sequence versus time is shown in figure 6.11. In this case $D_{nozzle} = 1.32\text{mm}$. This nozzle diameter proved to yield a braking torque that resulted in rotor operation around $C_{P,max}$, see figure 6.13(b).

A “steady-state” point was logged when the measured air speed out of the OJF remained constant, with a slight variation (turbulence intensity $\approx 0.23\%$), for a few seconds. A “transient” here refers to the transition between steady state points, as is indicated in figure 6.12.

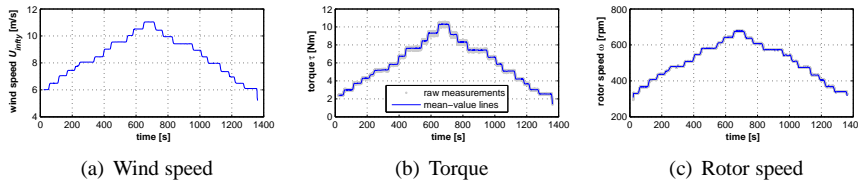


Figure 6.11: Time series for one continuous run of measurements; horizontal lines indicate results for steady state conditions

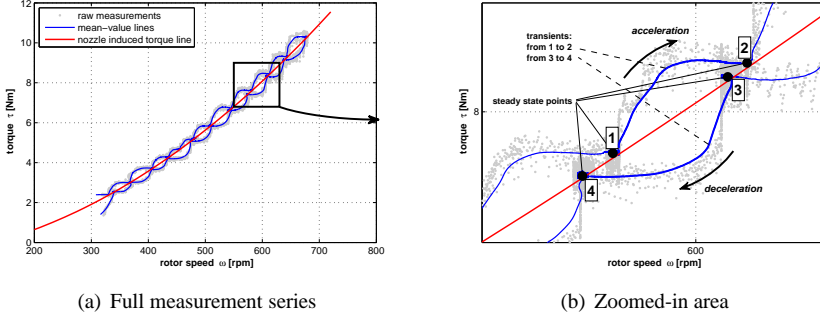


Figure 6.12: Steady-state and transients explained for the torque-speed curve, corresponding to the time series in figure 6.11 for $D_{nozzle} = 1.32\text{mm}$

Steady State Results

The measured steady state points are shown in figures 6.13(a) and 6.13(b). As seen in

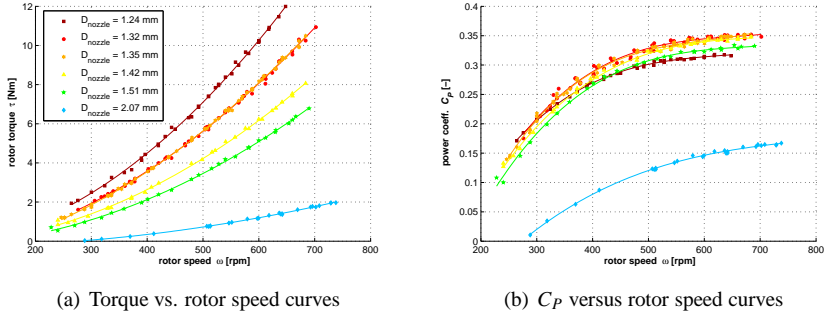


Figure 6.13: Steady-state results of the OJF measurements

figure 6.13(b), the nozzle diameter $D_{nozzle} = 1.32\text{mm}$ proved to yield a braking torque that resulted in rotor operation with the highest C_P . Under ideal circumstances, assuming incompressible flow and an ideal pump, the steady-state value of C_P in figure 6.13(b) would be constant throughout the displayed range of rotational speeds. Above 500rpm the calculated values of C_P still increase, but only marginally. However, for decreasing wind speed and rotational speed, the measurements and related trend lines in the figure show a deviation from this expected constant value that is increasingly severe. Two causes are attributed to this phenomenon:

1. The internal friction in the cylinders of the water pump has a significant effect on effective braking torque at low rotational speeds ($\omega < 500\text{rpm}$). This is seen in the relatively high value of the required start-up torque of 4Nm for the Danfoss PAH12.5 pump.
2. The Reynolds number at low wind speeds is small enough for viscous friction to play a significant role. The effect of this phenomenon is minimal for large wind turbines simply because of the greater rotor diameter. This is also noted in [77].

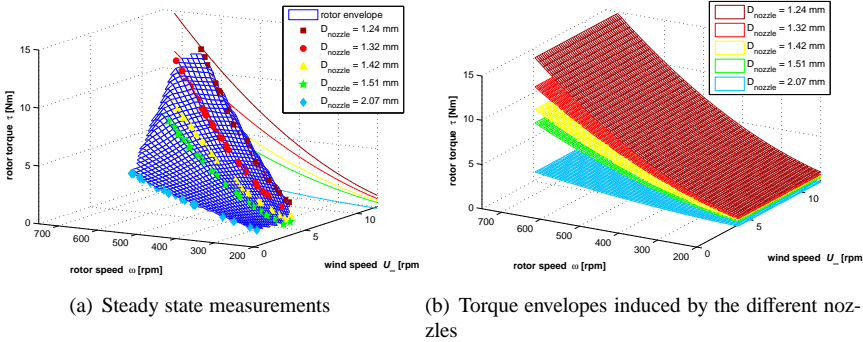


Figure 6.14: The 3D representation of the steady state results for multiple nozzle diameters

Transient Results

For the presentation of the transient results, the case where $D_{nozzle} = 1.32\text{mm}$ is taken. The results in figure 6.15 show the operation of the rotor around the intersection between the rotor envelope and the transmission envelope. The data around the intersection displays a pattern of bends. These are explained by the experimentation sequence. After start-up, the wind speed was increased from point to point until a certain maximum (10-12m/s) and again decreased along the same points, to yield multiple “steady state” measurements for the same wind speed. The data in between the “steady state” points forms the bends. The bend above the intersection indicates the torque and speed transition to a higher wind speed. The lower bends result from a decrease in wind speed.

This shows that for a change in wind speed, the torque always balances along the intersection of envelopes.

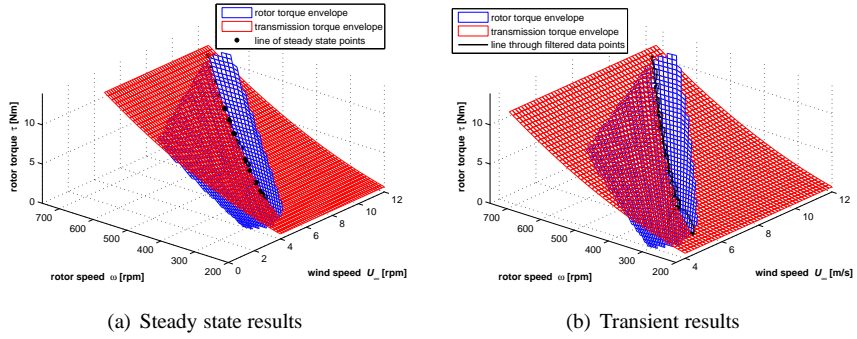


Figure 6.15: The measured transient response mapped onto the operational envelope determined from steady state measurements for different nozzle diameters

Limiting Braking Torque through the Pressure Relief Valve

For the purpose of general safety, every hydraulic circuit should have one or more pressure relief valves (see figure 2.6). These valves are set to open when the pressure p reaches a predetermined threshold p_{lim} .

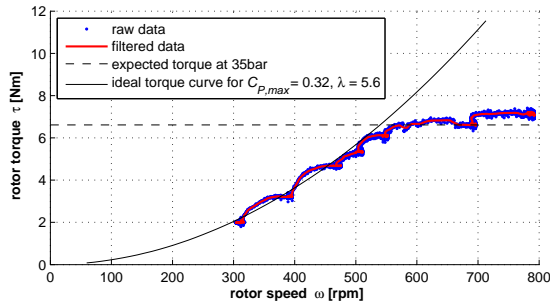


Figure 6.16: Results for when the pressure relief valve was adjusted to open at around 35 bar

To demonstrate its effect on the braking torque, the pressure relief valve was adjusted to open at around 35bar. The result for the system's performance is shown in figure 6.16. The significance of this demonstration is that such a simple and highly reliable component is able to limit the pressure (i.e. torque) to a preset maximum.

The effect of the pressure relief valve is thus that it sets the limit for the maxi-

imum torque. For a conventional drive train, the maximum torque is set by the power electronics.

At high wind speeds, overspeed of the rotor due to the surplus of aerodynamic torque over the drive train torque is prevented through pitch control, i.e. manipulating the pitch angle of the rotor blades.

Thus, by setting the activation pressure of the relief valve correctly, the torque envelope of the hydrostatic drive train can be rendered the same as for an electrically controlled drive train, but with more simple and far less expensive components.

Emergency Shutdown Function: Hydraulic Braking Results

One has to be able to shut down a wind turbine at any moment in time. The requirements for an emergency stop are given in the IEC 61400-1 standard. Three independent ways to stop a wind turbine from rotating are:

1. pitching the blades so no less aerodynamic torque is produced.
2. yawing the rotor out of the wind.
3. increasing the transmission torque.

For a hydraulic transmission system, solution 3 is achieved by means of a (slowly closing) valve. When the valve closes, the flow is choked and the pressure in the system builds up, essentially in the same way as the nozzle induces pressure. The required rotor torque thus increases and the rotor slows down.

Looking at the C_τ curve in figure 4.10(a), the point of operation thus moves from the point in line with $C_{P,max}$ to the left up to the point $C_{\tau,max}$. This point marks the border between stable and unstable operation. To the left of this point, $C_{\tau,max}$ value drops rapidly; the torque that is required from the rotor by the transmission cannot be matched and the rotor will slow to a stop.

The experiments with hydraulic braking were done using a manually operated valve (indicated in figures 6.9 and 6.10(b)). The initial condition is steady state operation, meaning constant rotor speed and torque and constant wind speed.

The measurement results in figure 6.17 show how the pressure (and thus torque) gradually builds up and the rotor speed slows down as the manual valve is slowly closed. Once the threshold corresponding to $C_{\tau,max}$ is reached the rotor rapidly comes to a halt.

The hydraulic braking can be done at any point along the high pressure line(s) of the fluid power transmission. Thus, for a DOT wind farm, the control valve responsible for the braking could be placed at the generator station. Although many configurations are possible, the simplest is to have a second relief valve with a much

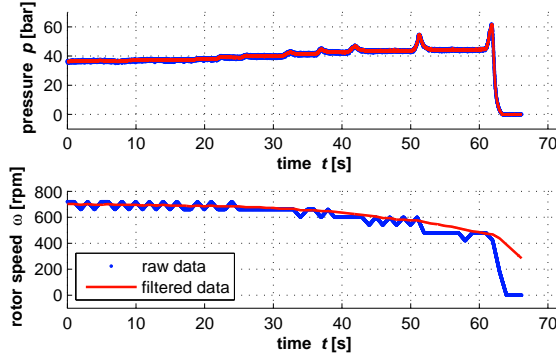


Figure 6.17: HydraulicBraking: the results from gradually closing the manual valve located before the nozzle (indicated in figures 6.9 and 6.10(b))

higher threshold pressure upstream of the shutting valve and the torque limiting pressure relief valve down stream, see figure 6.18.

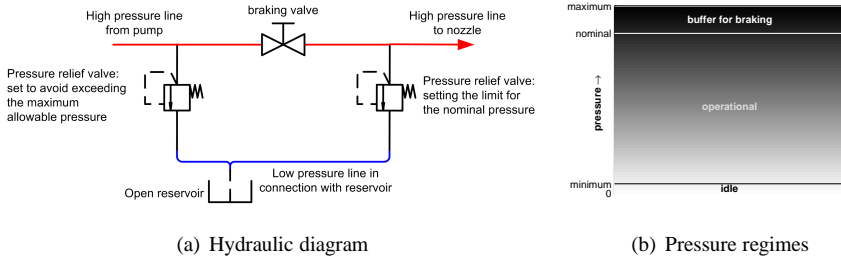


Figure 6.18: The proposed braking & relief valve configuration for passive control

In contrast to a mechanical brake, a hydraulic brake is continuously operable, because it loses heat through the hydraulic fluid.

6.3.3 Simulation versus Measured Results

Figure 6.13(a) shows that the optimal D_{nozzle} , i.e. the one yielding the highest values for C_P is around 1.32mm. The manner in which C_P is derived from the measurement results does not account for the volumetric and mechanical efficiencies of the pump and the bearing friction of the rotor shaft. Hence this C_P is effectively the power

rotor radius R	0.9m	measured
optimal tip speed ratio λ	5.6	measured
maximum rotor power coefficient $C_{P,max}$	0.32	measured
air density ρ_{air}	1.210kg/m ³	measured
water density $\rho_{tapwater}$	979.0kg/m ³	assumed
pump volumetric displacement V_g	12.5/(2 π) $\times 10^{-6}$ m ³ /rad	from folder

Table 6.1: Values required to calculate the optimal nozzle diameter

coefficient at the pump. Since this is the C_P that is used, the term $\frac{\eta_{vol}^2}{C_{P,max} \eta_{mec}}$ in equation 6.16 is replaced by $\frac{1}{C_{P,max}}$. The term A_2^2/A_1^2 is assumed to be negligibly small. Equation 6.16 then becomes:

$$A_{nozzle} = \sqrt{\frac{\rho_{hyd}}{\rho_{air}} \frac{V_g^3 \lambda_{opt}^3}{C_{P,max} \pi R^5}} \quad (6.17)$$

Table 6.1 lists the properties required to calculate the optimal nozzle diameter. For these values the nozzle diameter is calculated to be $D_{nozzle} = 1.32$ mm. The simulated ideal ($C_P = C_{P,max}$) and measured results for this nozzle diameter are plotted in figure 6.19.

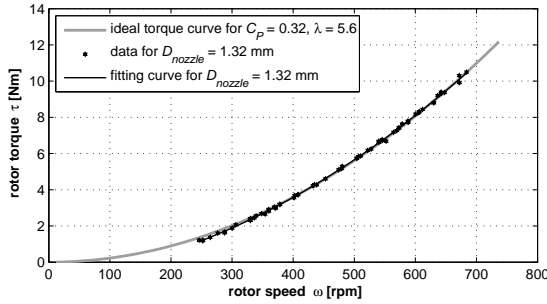


Figure 6.19: Comparison of simulated and measured torque curve for a nozzle diameter $D_{nozzle} = 1.32$ mm

In this figure and slightly more pronounced in figure 6.7 the torque curve deviates slightly from the ideal line ($C_P = C_{P,max}$) due to changes in efficiencies throughout the operational envelope. The point where the two curves cross is the design point. By making small changes to the nozzle diameter this design point is shifted up or down

the ideal torque curve. The design point thus translates to a specific wind speed. The selection of this design wind speed depends on the local wind climate. The design wind speed should be that at which the annual energy production is maximum.

6.4 Conclusion

6.4.1 Concept of Passive Torque Control

If a wind turbine rotor is connected to a fixed displacement hydraulic pump which is connected via a high pressure line with a pressure relief valve to a nozzle with fixed cross-section, the torque and speed of the rotor are passively controlled. By sizing the nozzle correctly, the rotor will operate at (or near) maximum efficiency for its allowable range of wind speeds. The setting of the pressure relief valve determines the maximum torque and thus the rated wind speed. During experiments, the rotor was brought to a full stop by cutting of the flow with a control valve.

The presented concept of passive control for variable speed rotors using fluid power technology works as predicted. The torque envelope of a conventional variable speed wind turbine drive train can be achieved for hydrostatic transmission through solely passive control.

The activation pressure of the relief valve effectively determines the rated wind speed. The cross-sectional area of the nozzle determines the envelope below rated wind speed. Shutting down the wind turbine is done by increasing the pressure using a braking valve.

6.4.2 Passive Control for $U_\infty > U_{rated}$

When variable speed wind turbines approach a nominal point of operation (U_{rated}), the blades are pitched to limit the rotational speed and torque. In the case of hydrostatic transmission, the torque can be limited simply by an overpressure (safety) valve. Once a threshold is reached, the valve opens and the pressure ceases to increase. However, limiting the torque results in a spin-up of the rotor if the rotor speed is not controlled. Hence a form of blade pitch control is needed.

6.4.3 Forced Shutdown Control Options

In the case of extreme wind speeds, maintenance or system malfunctioning a wind turbine is shut down. In the case of hydrostatic transmission, braking can be done hydraulically by closing off the high pressure line, allowing the torque to build up

until the rotor blades stall. For the sake of redundancy, auxiliary systems are required, such as yawing the rotor out of the wind.

Regarding the emergency shut down function, the relatively large mass moment of inertia of larger rotors will require a gradual shutting down of the flow in order to avoid high pressure peaks.

6.4.4 Proof of Concept: Wind Tunnel Experiments

The experiments showed that:

- The effect of hydraulic losses is minimal at pump rotation speeds greater than 500rpm. The pump used in the experiments was not designed for speed below 500rpm. Its start-up torque makes it unsuited for this type of application outside of a test environment.
- The passive torque control solution is inherently stable for all nozzles used in the experiments.

6.4.5 Design Point

Using the passive control method, the performance of the rotor will be at or near optimum for a wide range of operation. The design challenge is to select at which wind speed operation of the rotor and drive train should be exactly optimal. This wind speed should be the one for which the annual energy production is maximum. What this means is that the design point is set by the local wind climate. Since the nozzle is a modular and relatively simple component, adjustments for a specific site can be made afterwards (when the turbine is already installed). An example of how the design point is found is given in chapter 7.

6.4.6 Drawback of Passive Torque Control: No “Frequency Skipping”

An important consideration is the overlapping of the rotor rotation frequencies with the natural frequencies of the support structure. During the experiments it was observed that around 460 rpm the rotation speed matched a resonance frequency of the support structure. The entire configuration would then shake violently. To prevent this phenomenon from occurring and potentially causing damage, the wind speed corresponding to this rotor speed (which is different for every nozzle diameter) was skipped for “steady state” measurements.

Natural frequencies of one or wind turbine component may lie within the operational frequencies of the rotor. An example of this was encountered during the

experiments described in section 6.3. The support structure resonated when the rotor speed was approximately 460rpm. The mitigating measure was to pass over the wind speed at which this occurred.

A common solution to avoid resonance between the rotor and the wind turbine support structure is so-called frequency skipping. A small bandwidth of rotor rotation frequencies is rapidly transgressed by increasing or lowering the braking torque when this bandwidth is reached. For example, when the wind speed increases, the rotor speed increases. As the rotor speed nears a natural frequency of the foundation, the braking torque is reduced so that the rotor quickly accelerates to a speed beyond this resonance frequency. Here, the braking torque is increased again. In such a case, the wind turbine acts as a fly-wheel. Hence there is little loss of energy throughout the process.

Active manipulation of the braking torque was not possible with the experimental setup. This issue should be taken into account in the design for real-life application.

Preliminary Design of the DOT Fluid Power Transmission System Using the NREL 5MW Rotor

7.1 Introduction

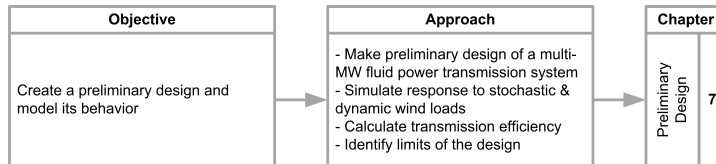


Figure 7.1: Flowchart for the objective and approach of this chapter

7.1.1 Background, Objective & Approach

In chapter 3, the possible configurations of a fluid power transmission system for offshore wind turbines are presented. The chapter concludes with three conceptual designs. The final concept selection (section 3.7.2) has yielded concept 3; the Delft Offshore Turbine (DOT).

In this chapter the DOT conceptual design is worked out in more detail to yield a preliminary design. The scope of the design is from the hydraulic pump coupled to

the low speed shaft and the spear valve of the seawater hydraulic circuit, see figure 7.2.

Of the components which are critical for the power performance the relevant dimensions are given, such as the volumetric displacements of pumps and motors or the length of the high pressure line. The properties of hydraulic equipment are taken from the state-of-the-art industrial off-the-shelf components described in section 2.3. These include drive efficiencies (damping coefficients), pipe inner surface roughness and fluid bulk moduli.

Using techniques described in section 5.3, the performance is simulated to yield the steady state response (power curve, torque-speed curve) and the response to dynamic and stochastic loads. Efficiencies are assumed for individual components and calculated for the system.

The control of the DOT rotor and drive train is done using the passive control method described in chapter 6.

The starting point of the design is the rotor of the NREL 5MW Baseline offshore turbine. The design methodology applied here is explained in section 7.3.1. The simulation results for the power curve and the response of the system to dynamic wind loads are presented in section 7.4. As in chapter 5, the simulated wind conditions vary from unrealistic (step-wise) to more realistic.

7.1.2 Functional Requirements of the Power Transmission System of a Single DOT

The rotor is outside the design scope. However, to evaluate the performance of the rotor and transmission system, the rotor of the NREL 5MW reference turbine rotor is used.

The following functional requirements of the preliminary design of the DOT rotor & transmission system flow down from the ones set in section 3.4.1:

- The harvesting of power from the wind.
- Transmitting harvested power to the generator station.
- Operate at or close to maximum aerodynamic efficiency below rated wind speed.
- Smoothen ripples in the aerodynamic torque.
- Operate with energy efficiency of $> 80\%$ between the rotor shaft and the generator station at nominal conditions.

For the detailed design further specification of the functional requirements is required.

The generator station including the Pelton turbine are also outside the design scope. Pelton turbines typically operate with efficiencies of around 90-92%, from jet to electricity [78].

7.2 Design Considerations for the DOT Fluid Power Transmission System

7.2.1 Cooling of the Oil Circuit

This subsystem functions similarly to a mechanical gearbox. Large torque and low rotation speed are converted to low torque and high rotation speed. The transmission ratio is essentially constant: the effects of speed and pressure on efficiency of this subsystem introduce variations smaller than 5% throughout the operational envelope.

Whether active cooling will be required depends on the efficiencies of the components and the heat transfer of the pipelines. The way a cooling system is typically dimensioned is by estimating the power loss of a system and multiplying this with a safety factor. So, in the case of a 5MW system with 95% transmission efficiency at rated power conditions, the required cooling capacity is 250kW. Long lines allow the heat to dissipate via convection and radiation. A detailed study of the thermodynamics of the system is required to determine whether a cooling system is needed.

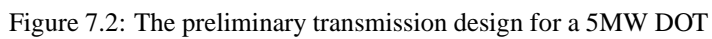
7.2.2 Boosting, Filtering and Cooling of the Seawater Circuit

The seawater hydraulic pump of which the properties have been scaled and extrapolated to reach approximately 5MW power capacity is not self-priming. Thus the pressure needs to be boosted to secure the flow to the pump. The foreseen method to be applied for this is to have an integrated boost and filter system. An electrically driven centrifugal pump sucks in seawater through an initial filter known as a suction screen. The flow then enters a filter system (to be developed) for 100 μ m, after which it reaches the pump.

Cooling is not required in this open system. The seawater pipeline will transfer heat to the surrounding environment. This is similar to the case for offshore power cables.

7.2.3 Startup Torque

The start-up torque of the system depends predominantly on the internal frictions of the main shaft bearing system and the bearings and the cylinders of the pumps and



the motor. If the value of this parameter is sufficiently low, the system need not shut down if $U_{\infty} < U_{cut-in}$ and no blade pitching action is required for start-up. Based on experience with the 1MW facility described in section 5.4.1, the startup torque is low enough that a person is able to rotate the rotor shaft with his bare hands. In contrast, the start-up torque of the water pump described in section 6.3.1 was too high for the rotor to overcome without help. In the experimental setup described in B, the starting torque of the water pump also proved to be a concern. The Hydrowatt R250/250S pump has a start-up torque of 150Nm. This is around 4.5% of its nominal torque.

7.2.4 Control System Properties

The document which provides the definition of the reference turbine [38, p17] knowingly omits the definition of control actions for non-power-production operations such as start-up, normal and emergency shutdown. These actions are also considered to be too detailed for this stage of the DOT design.

The reference rotor has a variable blade-pitch-to-feather configuration. This enables the turbine to shut down by pitching the blades.

The control for power-production operation relies on two independently working systems: the generator torque controller and the full-span rotor-collective blade-pitch controller. For the DOT, the generator torque controller is replaced by the passive torque control provided by the architecture and dimensioning of the fluid power transmission system.

The rotor control system essentially does not conflict with the control of the hydraulic drive train. However, a reconfiguration of the control software is required to match the new operation limits of the system.

Overloading of the fluid power transmission system is prevented by pressure relief valves.

The application of a spear valve allows the operator to make small adjustments to the area of the jet outlet in order to maximize energy yield. If a simple nozzle were to be applied, there is an argument to be made that the system should be designed for maximum annual energy yield. This requires data of the annual wind speed distribution. The way in which the nozzle is modeled indicates that below the design wind speed the value of the tip speed ratio is below the optimum value. Above the design wind speed the value of λ is above the optimum value, until the nominal rotation speed ω_{nom} is reached. Hence, the disadvantage of designing for a wind speed below rated is that the ω_{nom} is reached at a lower wind speed, which then becomes the rated wind speed. In this way the nominal power is reduced. The optimization of the design of the system for maximum annual energy yield is then an exercise with multiple iterative loops.

7.2.5 Local Electric Power Source

For several control functions and safety related functions, sensors and control valves are required. These require an electric power supply. Possible sources of power are:

- A power cable running from the generator platform, along the seawater pipeline, to each turbine.
- Solar panels and storage battery.
- A small wind powered generator system with storage battery, coupled to the oil-hydraulic circuit.

7.3 Dimensioning of the Main Transmission System Components

7.3.1 Method for Dimensioning

The design constraints are based on properties of state-of-the-art off-the-shelf components. The properties that define the design values are (1) the maximum allowable tip speed of the blades of 80m/s, which sets the limit for the rotation speed of the aerodynamic rotor: $\omega_{nom} = 12.1\text{rpm}$, (2) the nominal pressure in the oil and water hydraulic circuits, $p_{c1,nom}$ and $p_{c2,nom}$, (3) the nominal rotation speed of the hydraulic motor $\omega_{m,nom}$.

To design for nominal operating conditions is a straight forward process as described in figure 7.3. The final dimensions are given in table 7.2.

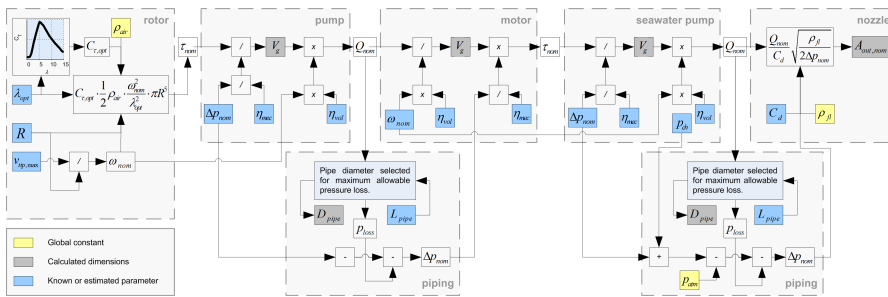


Figure 7.3: Flow chart for dimensioning of the main DOT components

7.3.2 Oil Circuit Components Properties

Oil Hydraulic Pump

All properties of the radial piston pump, except the volumetric displacement, the number of cams and the number of cam rings, are taken from the Häggglunds CBP840 hydraulic motor. Using equation 4.41 the required volumetric displacement V_p is found.

Oil Pipeline

The length of the line between the oil pump and motor is determined according to equation 7.1.

$$L_{pipe} = \frac{1}{2} D_{rotor} + s_{clear} + s_{platform} + s_{sub} \quad (7.1)$$

Here, s_{sub} is the vertical distance under the mean sea level (MSL) where the transformer is located. The distance $s_{platform}$ between the MSL and the platform is normally determined by the maximum 50 year wave height. Its value has been selected with reference to the range (13 - 19m) typically found in the Dutch sector of North Sea [79, 80]. The distance s_{clear} is the clearance gap between the platform and the passing height of the rotor tip.

Given that the nominal flow through from the slow turning pump is known, the selection of the inner diameter of the pipeline determines the pressure loss in the line. A loss of 1% at nominal conditions is considered acceptable here. This translates in an allowable pressure loss of 3.35bar over a distance of 100m. The resulting inner pipeline diameter for a single high pressure line is approximately 15cm. Ensuring minimum pressure loss due to friction whilst minimizing the pipe diameter means that high Reynolds numbers are inevitable for long distance pipelines. Flow in such pipelines will thus be turbulent for the greater part of the operational envelope. The flow speed at nominal operating conditions is 6.55m/s.

Figure 7.4(a) shows the relation between the number of parallel pipelines and the inner pipeline diameter. The lowest value of the efficiency of the pipeline is around 99%, see figure 7.4(b).

Hydraulic Motor

The hydraulic axial-piston motor is modeled as having the same properties as the pump, with a volumetric displacement of around 3.8 liters per revolution. The design nominal rotation speed is 1800rpm.

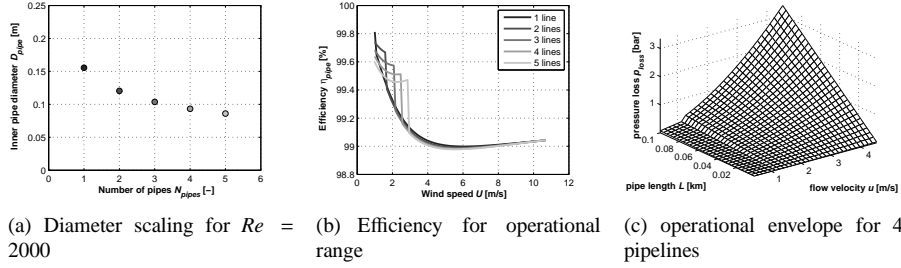


Figure 7.4: Pipeline design figures, corresponding to the results in table 7.2

7.3.3 Seawater Circuit Components Properties

Seawater-Hydraulic Pump

Using equation 4.41 and considering the steady state power losses from the rotor shaft up to this point, the required volumetric displacement V_d of the seawater pump is found. It is assumed here that the input torque of the seawater pump is the same as the output torque of the oil motor: $\tau_p = \tau_m$. The friction losses related to the rotation of the shaft which connects this pump to the oil motor are included in the models of the pump and motor.

Seawater Pipeline

The length of the water pipeline depends on the location of the turbine in the wind farm. As for the high pressure oil line, the design condition is that at nominal operation the maximum energy loss in the pipeline is 1%. This translates to an allowable pressure loss of 4.07bar. The resulting inner diameter for a 1km long pipeline is 18.5cm. At nominal operating conditions the speed of the flow in the line is calculated to be 3.04m/s. Figure 7.5(a) shows the relation between the pipe diameter and the pressure loss for nominal flow conditions and the design point.

Spear Valve

The flow through the high pressure seawater is guided through a spear valve such as pictured in figure 3.11. The choice to have an adjustable nozzle area has two main advantages:

1. It enables the operator to shut off the flow and thereby acting as a hydraulic brake.

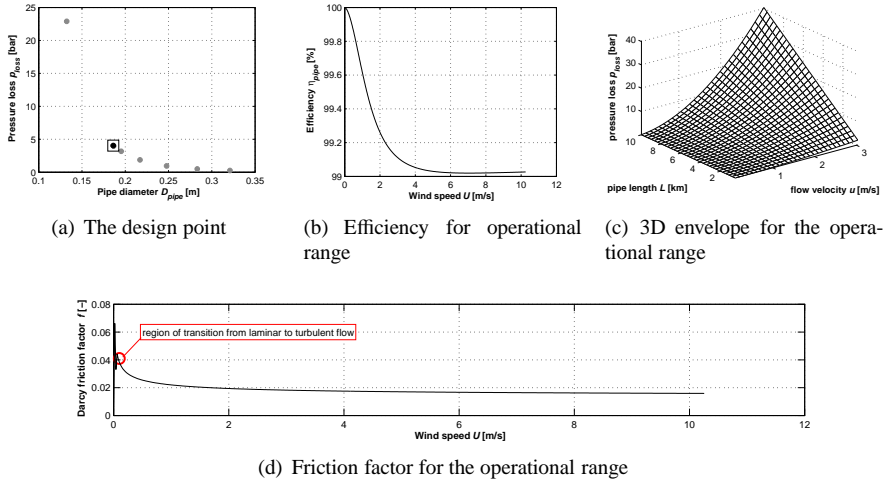


Figure 7.5: Seawater pipeline design figures, corresponding to the results in table 7.2

2. The behavior of the transmission system will change over time. This may be due to for instance wear in the hydraulic systems or changes in aerodynamic performance of the rotor. Being able to adjust the nozzle area enables the operator to optimize the power output for such changes.

The sizing of the optimal nozzle area is explained in detail in section 6.2.2. This is also the size of the nominal outlet area of the spear valve. Other dimensions of the spear valve are not considered as relevant at this stage of the design.

The equivalent nozzle diameter is determined at 19.5mm. The nominal speed of the jet exiting this nozzle is calculated to be 263m/s.

Implications of the Selection of the Nominal Operating Pressure in the Seawater Sub-System

The nominal pressure in the water pipeline determines the nominal speed of the jet exiting the spear valve. As described in section 3.8.3, the DOT concept is to apply a Pelton-type hydro turbine to convert the power in this jet to electricity. Similar to a wind turbine, there is an optimal ratio Λ between the speed of the bucket v_b and the speed of the incoming jet v_{jet} .

$$\Lambda = \frac{v_b}{v_{jet}} \quad (7.2)$$

According to [78], the optimal value of this speed ratio Λ is typically around 0.48. Hence, the nominal jet speed in turn determines the pitch circle diameter (PCD) of the Pelton turbine.

So far the greatest head (highest pressure) found in hydro dams is 1869m ($\approx 180\text{bar}$) [81]. The Pelton runners of its turbines run at a synchronous speed of 428.6rpm (14 poles) and its pitch circle diameter is 3.99m. This is proven technology.

For the DOT system it will be beneficial to work with much higher nominal pressure to improve the compactness of the transmission system. The reference technology for the seawater pump is the Hydrowatt[12] technology, where the nominal operating pressure is 415bar. Therefore this value selected as the nominal pressure of the seawater hydraulic circuit.

The velocity of the jet exiting the seawater line increases with the square root of the pressure. This effectively means that the PCD of the Pelton runner also increases with the square root of the pressure, provided that the nominal rotation speed is maintained. Hence, for a system with 415bar nominal pressure, powering a Pelton runner (and generator) with a nominal speed of 428.6rpm (same as [81]), the PCD is approximately 6m. A larger runner diameter will result in a higher mass moment of inertia, which smoothes the torque delivered to the electricity generator, to which the runner is coupled.

7.3.4 Reduction of Mass

Two factors are dominant for determining the top mass of a wind turbine: the design of the rotor and the configuration of the drive train. The DOT has the same rotor as the NREL 5MW. Based on the calculations presented in appendix A, the DOT has a significantly lower tower top mass than the NREL 5MW turbine. A breakdown of the masses which make up the total nacelle mass is given in table 7.1. The term “unspecified” covers the power electronics. The reduction in mass for the combined drive train parts in the nacelle is 62%. The reduction in mass of the complete nacelle is 66%. The reduction in mass of the rotor-nacelle assembly (tower top) is 45%. Since positive displacement pumps for 5MW wind turbines are not yet commercially available, the margin for error of the estimated mass of such a pump is uncertain.

	Reference	DOT
Drive train components	101,538	39,482
low speed shaft	16,518	16,518
bearing system	5,401	5,401
gearbox	60,940	-
high speed shaft	984	-
mech. brake & couplings	995	-
generator	16,700	-
hydraulic pump	-	17,564
Other components	138,462	42,554
bedplate/mainframe	62,470	18,890
platforms & railings	7,809	2,361
nacelle cover	6,837	3,419
built-in crane	24,256	4,733
cooling system	400	-
yaw system	13,152	13,152
unspecified	23,538	-
Nacelle total mass	240,000	82,037

Table 7.1: Breakdown of masses [kg] of the DOT and the reference turbine

7.4 Power Performance Simulation of a Single DOT

7.4.1 Steady State Response: The Power and Torque Curves

For the reference turbine, the torque still increases with wind speed after the nominal rotation speed of 12.1rpm is reached. Because of the passive control method, the nominal rotation speed of the DOT determines the nominal torque.

The operational envelope of the NREL rotor thus changes slightly for the DOT with respect to the reference turbine. The maximum tip speed is the design value that is maintained for both. The rated wind speed thus becomes 10.3m/s. Hence the rotor of the NREL 5MW turbine is limited to produce maximum power of approximately 4MW. This is shown in figure 7.6(a).

The efficiency of the transmission system from rotor to generator station is broken down in figure 7.6(c) and compared in figure 7.6(d) to that of other drive train technologies as presented in [82]. The efficiencies of these other drive trains are defined as the combined efficiencies of the gearbox (if applicable), the generator, the frequency converter and voltage transformer. These systems are located within one turbine. Losses between turbine and offshore transformer station are not included.

Description	Symbol	Value	Units
Adapted Application of the NREL Rotor			
Maximum blade tip speed	$U_{tip,max}$	80	[m/s]
Nominal rotation speed	ω_{nom}	12.1	[rpm]
Rated wind speed	U_{rated}	10.3	[m/s]
Rated power at the rotor	P_{rated}	4.0	[MW]
Closed Oil-Hydraulic Circuit			
Hydraulic Fluid		HPL46	
Pump volumetric displacement	V_p	579	[l/rev]
Nominal pressure	p	350	[bar]
Total nominal flow	Q	6880	[lpm]
Number of pipes	N_{pipes}	1	
Pipe length	L_{pipe}	100	[m]
Pipe diameter	D_{pipe}	15.2(6)	[cm (inch)]
Nominal flow velocity	U	6.55	[m/s]
Motor volumetric displacement	V_m	3.75	[l/rev]
Motor nominal rotation speed	ω_m	1800	[rpm]
Open Seawater-Hydraulic Circuit			
Pump volumetric displacement	V_{wp}	2.75	[l/rev]
Nominal pressure	p	415	[bar]
Total nominal flow	Q	4900	[lpm]
Number of pipes	N_{pipes}	1	
Pipe length	L_{pipe}	1000	[m]
Pipe diameter	D_{pipe}	20.3 (8)	[cm (inch)]
Nominal flow velocity	U	3.04	[m/s]
Equiv. nom. outlet diameter	\bar{D}_{nz}	19.5	[mm]
Nominal jet speed	v_{jet}	263	[m/s]

Table 7.2: Properties of the DOT containing the NREL 5MW reference turbine rotor

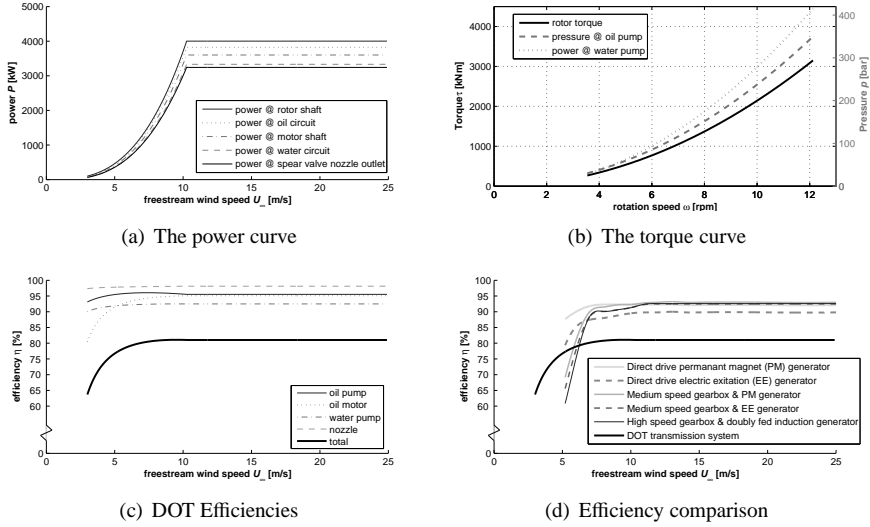


Figure 7.6: DOT power, torque and transmission efficiency curves

7.4.2 Setup of Dynamic Response Simulation

The simulation of the dynamic behavior of the 5MW DOT is done similarly to the method described in section 5.3 and figure 5.3. The main difference is the addition of the water-hydraulic circuit which incorporates the passive control method described in the chapter 6. The same method is used to model the pipeline flow dynamics. It should be noted that the modeling of these dynamics does not account for turbulent flow, which is present in the seawater line for almost the entire operational envelope.

According to [83]: *the response of the turbulence structure and strength to transient waves in pipes and the loss of flow axisymmetry in pipes due to hydrodynamic instabilities are currently not understood*. Based on simplified models published in [73] it is expected that turbulent flow will introduce slightly more damping due to friction with the pipe wall.

The blade pitching system is turned off to avoid its influence on the results. This allows the simulation to surpass the system design limits on rotation speeds, pressures and torques.

In a DOT wind farm, the distance between turbine and generator station will vary. Typically a distance of 5 to 10 times the rotor diameter is observed between turbines. With this in mind the length of the seawater pipeline is modeled here as 1km. The length of this line determines the volume of water in the system.

7.4.3 Response to Step Input and Turbulent Wind Loads

Wind Step Input

Figure 7.7 shows the response of the DOT power transmission system to a wind step input (figure 7.7(a)). Two important phenomena are observed:

1. The delay in the flow at the water pump and the flow out of the nozzle is clearly visible in figure 7.7(f). The water pump is powered by the motor, already with some delay due to the elasticity of the oil circuit. The combined delay determines the speed of the response of the rotor and drive train to wind loads. For the simulation of the system as presented in this chapter, the critical length of the seawater line is around 5km. Beyond this length the sluggish character the response could mean that in the event of a drop in wind speed, the torque from the drive train will remain high sufficiently long for the rotor to slow down to a full stop.
2. The nozzle at the end of the water circuit damps away any fluctuations in this line. However, in the oil circuit, the lack of damping by the hydraulic motor and the compressibility in the 100m lines allow for these oscillations to occur. The period of these harmonics is around 14 seconds. Although badly damped oscillations are generally undesirable, they do not appear harmful for this case where the seawater line is 1km long. The effect of the oscillations is only marginal at the rotor and non-existent at the nozzle outlet. During the experiments described in section 5.4 it was observed that in reality the pressure oscillations were damped stronger than in the simulations. In the simulation, the pipelines are assumed as rigid. In reality the elasticity of the pipelines contributes to the dissipation of pressure transients. Nevertheless, this phenomenon does require attention when performing the detailed design of a DOT.

Turbulent Wind

Figure 7.8 shows the response to turbulent wind loads. The oil circuit already smooths out the peaks in the aerodynamic torque. Note the smoothness of the changes in pressure at the spear valve and the corresponding changes in the velocity of the jet exiting the spear valve. As with the step response, oscillations are observed at the hydraulic transformer, i.e. the motor & seawater pump.

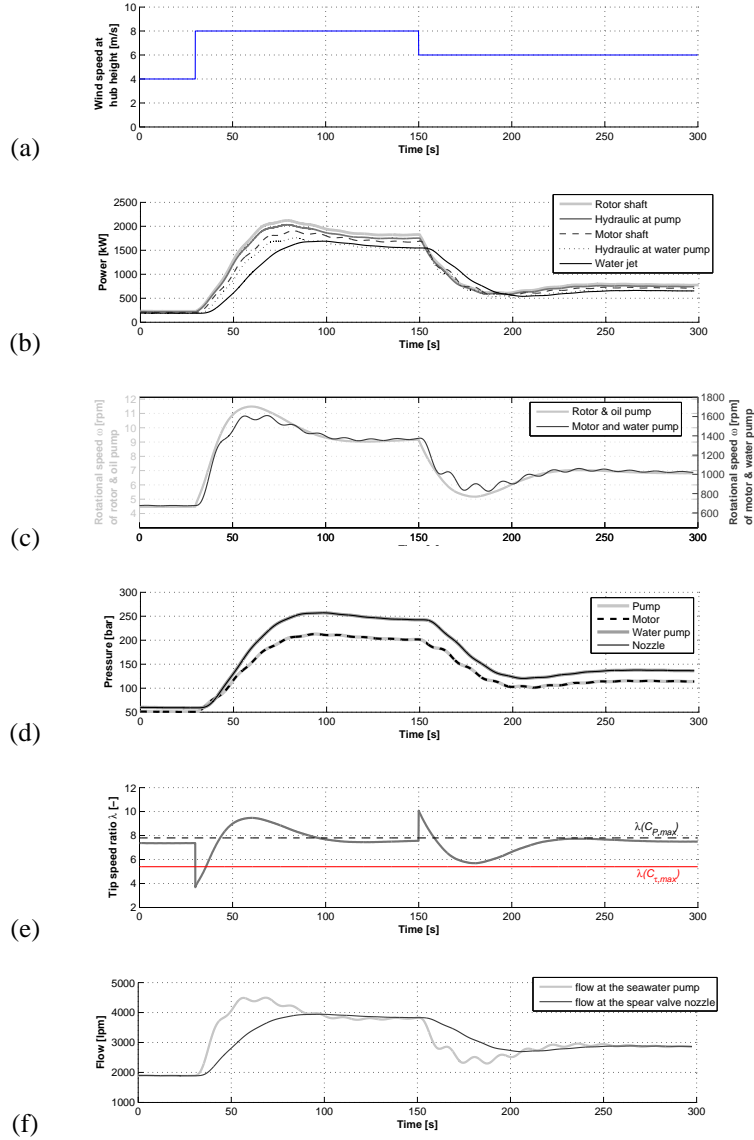


Figure 7.7: System response to a wind speed step input; the length of the seawater line is set here at 1km

7 - Preliminary Design of the DOT Fluid Power Transmission System Using the NREL 5MW Rotor

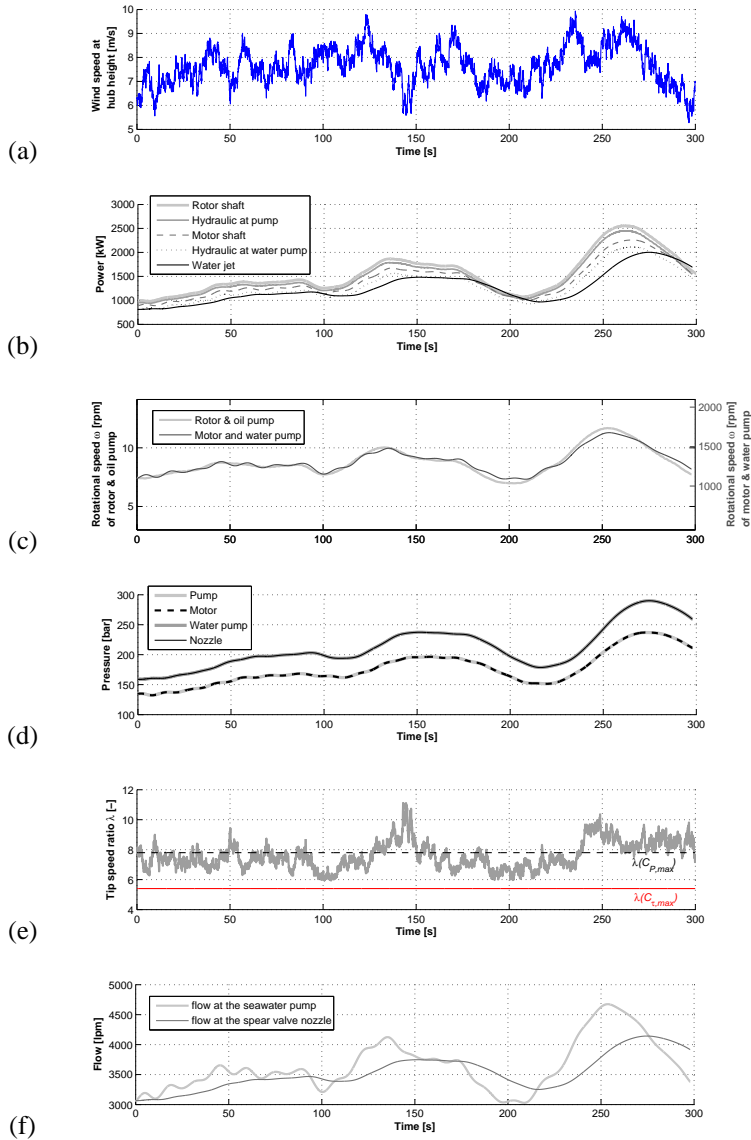


Figure 7.8: System response to turbulent wind loads

7.5 Conclusion

The design methodology presented in section 7.3.1 yields the dimensions for the main components of the DOT fluid power transmission system. As presented, the design process is straightforward, i.e. without iterations. In reality, the dimensions of the available components will not exactly match these values. When such available components have to be matched, (local) iterative design loops are required.

The estimation of the nacelle mass in section 7.3.4 yields a reduction of around 65% when compared to the nacelle mass of the reference turbine.

The nominal power output is limited due to the design constraint for the maximum speed of the blade tip: 80m/s. This constraint is based on onshore criteria for noise. Offshore these criteria don't hold any merit [1]. A higher tip speed and therefore greater nominal power output is thus possible.

The steady state response shows that for greater wind speeds than 4.5m/s, the transmission efficiency is between 75 and 81 percent. At and above rated conditions the efficiency is greater than 80%, meeting the functional requirement set in section 7.1.2. The power transmission efficiency is dependent on the properties of the main transmission components. These properties are derived from current state-of-the-art off-the-shelf components. The estimation of around 80% efficiency of the power transmission system until the Pelton turbine seems fair.

The response to dynamic input loads is well damped. The relatively large bulk modulus of seawater makes that the stiffness of the simulation response is still satisfactory for a seawater pipeline up to around 10km long, based on simulation results. This phenomenon of pipeline flow dynamics requires further research.

Conclusion

8.1 Main Conclusions

The DOT concept for power transmission is technically feasible. The design as presented in chapter 7 will significantly reduce the complexity of offshore wind energy technology. With currently available off-the-shelf components, it is possible to construct a DOT drive train prototype with up to around 1MW of nominal power output. The only way to really know how well this system performs is by building and testing it. Pumps suitable for direct coupling to multi-MW wind turbines rotors do not exist at the time of this writing. There is no technical reason for this. Current developments in the fluid power industry suggest that such pumps will be commercially available within the next few years.

8.2 Answers to Main & Key Research Questions

The current state of the art wind turbines installed offshore are overly complex systems. The move to offshore has until now not prompted a reconsideration of how the conversion from power in the wind to electricity should be done. To make offshore wind a competitive source of electricity requires more than incrementally improving and scaling-up onshore turbines.

In any industry where robust machinery is required to handle large torques, the hydrostatic solution is applied. It is therefore almost the obvious solution for wind turbines. Although the solution is not new, it has renewed potential thanks to developments in hydraulics.

The main research question of this thesis is therefore:

How can fluid power transmission be applied for large offshore wind turbine drive trains?

In figure 1.1, a schematic representation is given of the main research question, the key questions and how these are essentially approached. Through literature research, computer modeling and experimentation these questions are answered. The answer to the main research question is via the answers to the key questions.

1. *Why use fluid power technology for the drive train of an offshore wind turbine?*

Hydrostatic power transmission is beneficial for wind turbines due to the relatively low stiffness of the drive train. This allows ripples in the aerodynamic torque to be dispersed.

The application of a fluid power drive train in large offshore wind turbines is attractive because it is compact (lightweight) and provides the option of a continuous variable transmission ratio. The main construction material is steel.

2. *How can a fluid power drive train for an offshore wind turbine be configured?*

Although it is likely that the robustness of a wind turbine will improve with the switch to a hydrostatic drive train, the complexity of the system may not. In chapter 3 several concepts for hydrostatic drive trains are considered. The modularity of hydraulic components gives rise to many options. Three configurations are presented in section 3.7.1. These are the nacelle solution, the tower-base solution and the hydraulic wind farm solution. Which one is the most suitable for an offshore wind turbine depends on a variety of issues. The most unique of these configurations is that of a hydraulic wind farm, i.e. the Delft Offshore Turbine (DOT) concept. A novelty of this concept is to use sea-water as power transmission medium and use one hydro-power-like generator station for multiple turbines.

3. *How are the rotor and drive train dimensioned and modeled?*

The power performance of a wind turbine rotor is essentially a function of the tip speed ratio λ and the pitch angle θ of the wind turbine blades. In particular the presence of the turbine tower and the stochastic nature of wind introduce noise in the torque produced by the rotor.

The modeling of hydraulic pumps, motors, valves and piping is to a large extent based on empirical relations. A fluid power circuit, such as may be applied in the transmission of a wind turbine, essentially behaves as a second order system. To be able to describe a system in this way is beneficial for the simplicity of the analysis of its dynamic behavior.

4. *How are rotor and hydraulic drive train envelopes matched?*

The main challenge in coupling a hydraulic drive train to a wind turbine rotor is matching the speed and torque ranges of the aerodynamic rotor and the pump to which it is coupled. Figure 4.21 gives a simple method for dimensioning the pump on the basis of the rotor properties. The essential parameters for matching an aerodynamic rotor and a hydraulic pump are:

- the volumetric displacement, the nominal pressure and the nominal speed of the pump
- the radius, the optimal tip speed ratio and the rated wind speed of the rotor

5. *How is the response of the rotor and drive train controlled?*

The presented concept of passive control for variable speed rotors using fluid power technology works as predicted. The torque envelope of a conventional variable speed wind turbine drive train can be achieved for hydrostatic transmission through solely passive control.

The activation pressure of the relief valve effectively determines the rated wind speed. The cross-sectional area of the nozzle determines the envelope below rated wind speed.

Aerodynamic control of the rotor (for example through blade pitching) is required to force a rated wind speed and to shut down the turbine.

Experiments with a 600W setup in a wind tunnel showed that the passive torque control solution is inherently stable for all nozzles used in the experiments.

An important consideration is the overlapping of the rotor rotation frequencies with the natural frequencies of the support structure. This issue should be taken into account in the design for real-life application.

The passive control method has enormous potential for the DOT wind farm. It means that no drive train control is required. It significantly simplifies the design and regulation of the wind turbine drive train without sacrificing the aerodynamic performance of the rotor.

6. *How does the rotor and drive train system behave when subjected to dynamic wind loads?*

In general the elasticity and damping of hydraulic drive trains benefit the smoothness of the power output of the turbine. The inherent damping characteristics of the hydraulic drives are mostly associated to the leakage losses and the effective hydraulic capacitance.

The amount of oil in the system has a significant influence in the stiffness of the transmission and therefore in the pressure transients; the main reason is that the

high fluid inertia of the system is able to produce large pressure peaks (water hammer effects) whenever there are sudden variations of volumetric flow. On the other hand, the rotor mass moment of inertia has an important influence in the time response of pressure and rotational speed, leading to a slower but smoother response of the system.

In general a tower base solution with long pipelines is prone to higher pressure fluctuations with a clear effect on the controllability. The compressibility of the hydraulic fluid and the length of the high pressure line determine the hydraulic stiffness. If the stiffness becomes too low, the response becomes sluggish and large pressure overshoots occur. This effect is mitigated using pressure control, as was demonstrated by the experiments shown in section 5.4.6. Hence the idea of having a 5MW class wind turbine with the pump in the nacelle and the hydraulic motor at the base of the tower is regarded as feasible.

Low volumetric efficiency of the hydraulic transmission improves the damping of pressure fluctuations. However, its influence is minor and unlikely to be advantageous when compared to the loss in power production.

During experiments with a 1MW-class hydrostatic transmission, the system was subjected to two main types of inputload:

- (a) Simple disturbances in the form of step inputs. Although these inputs are not realistic, they clearly reveal information on the response of the system in the form of the natural frequency and damping ratio.
- (b) Simulated aerodynamic torque, resulting from wind gusts and turbulent wind loads. These experiments were conducted using input from GH Bladed which was scaled from a rotor with a 63m radius to one with a 25m radius. This conversion is an engineering trick which neglects several aerodynamic scaling effects.

Measurements were made using both static and dynamic transmission (constant and variable motor volumetric displacement).

From the conducted experiments, it is observed that torque impulses applied to the drive train are quickly dampened, leading to a smoothened electrical power output. Apart from mapping the dynamic response characteristics, the measurements were also used to validate simulation models of the test bench.

8.3 Recommendations for Future Research

A common result of any research project is that it yields more questions than answers. Here are stated what are considered to be the most pending topics for future research and development of the DOT.

Will the DOT Reduce the Cost of Energy?

The economic picture is beyond the scope of the research presented here. The expectation is that the DOT will significantly ($> 10\%$) reduce the cost of both CAPEX and OPEX. The CAPEX will to a large extent depend on how many turbines are connected to one generator station. The ability to use hydraulic lines of which the outer diameter is comparable to that of electric cables means no extra costs are expected there. The omission of the frequency converter and voltage transformer for every turbine will impact both CAPEX and OPEX. However to be able to make well-founded statements on the potential cost reduction requires an elaborate comparative study between DOT technology, “traditional” geared transmission and new direct drive technology.

“Full” Passive Control

The presented method for passive torque control of the motor can be expanded to incorporate:

1. Passive hydraulic blade pitch control. The idea is that beyond a predetermined minimum value of the pressure in the oil circuit of the drive train, the pitch system is activated in such a way that this pressure (and hence the rotor torque) determines the pitch angle of the blades.
2. Passive yaw control. The idea is to integrate the drive train circuit with a hydraulic yaw system. When allowed to rotate freely, a wind turbine rotor typically orients itself so that the rotor faces the incoming wind. As explained in [84], the required resistance to yawing is, similar to the pressure in the drive train, proportional to the squared of the wind speed. Hence at low wind speeds, the wind direction changes relatively faster and therefor lower resistance to yawing is required.

The “full” passive control would eliminate a significant number of auxiliary systems.

Oil-hydraulic Boost and Filtration System for the Open Seawater Circuit

The required boost pressure depends on the pressure difference over the seawater pump. For the DOT, this pressure difference is high when the rotation speed is also high. Regarding this relation, it should be feasible to power the centrifugal boost pump (see figure 7.2) with the same shaft as the seawater pump. An important condition for this is that the seawater pump is beneath the water intake, so that there is charge pressure even when the system is shut down.

The filtration system of the preliminary design of the DOT transmission is described in section 7.2.2. The foreseen method is to have a “suction screen” type initial filter through which the flow is sucked by a centrifugal pump. To minimize maintenance a self cleaning filter is envisioned for further filtration.

The design and implementation of the boost and filtration thus requires further attention.

Design of the DOT Generator Station

This part of the DOT power transmission concept has been left out of the preliminary design. What made this possible is that the Pelton turbine is physically decoupled from the rest of the DOT transmission system. The design of the generator station is paramount to the further detailing the DOT design.

DOT Wind Farm Control

In a DOT wind farm the connection between turbines and the hydro power station can be through individual or shared pipelines. The wind speed varies throughout a wind farm. What is the influence of pressure losses in long lines and centralized pressure control on the power performance of the individual wind turbine and the wind farm as a whole. The issue of park effects and their impact on the application of passive torque control in a DOT wind farm clearly requires further research.

Pipeline Dynamics

For short lines fluid inertia may be neglected. For long lines and wind turbine application, the rotor inertia excludes the possibility of water hammer under normal operating conditions. However, during an emergency stop, the fluid inertia could present a problem. Hence it is important to investigate and model the dynamics of (turbulent) flow through long lines.

Combining the DOT with Other Applications

Two possible additional uses of the DOT technology are for:

1. Seawater desalination, where seawater is converted to drinking water by forcing it through filtering membranes.
2. Thermal energy production in the form of cooling on an industrial scale using seawater.

Using the DOT technology, in both applications the need to convert wind energy into electricity and back is eliminated. Such add-ons to simply producing electricity could have a big impact on the economy of a DOT farm, as is argued for cooling in [85].

Bibliography

- [1] P. Jamieson. Light-Weight, High-Speed Rotors for Offshore. Technical report, Garrad Hassan & Partners Limited, European Offshore Wind, 2009.
- [2] C.J. Crabtree. Operational and Reliability Analysis of Offshore Wind Farms. In *EWEA Conference Proceedings*, April 2012.
- [3] S. Faulstich, B. Hahn, and P.J. Tavner. Wind Turbine Downtime and its Importance for Offshore Deployment. *Wind Energy*, vol. 14:p.327 – 337, 2011.
- [4] F. Spinato, P.J. Tavner, G.J.W. van Bussel, and E. Koutoulakos. Reliability of Wind Turbine Subassemblies. *IET Renewable Power Generation*, vol. 3:p.387 – 401, 2008.
- [5] S. Knight. Alpha Ventus Offshore Turbines Faced with Breakdown. *Windpower Monthly*, June 2010.
- [6] S.C. Rybak. Description of the 3MW SWT-3 Wind Turbine at San Geronio Pass, California. Technical report, The Bendix Corporation Energy, Environment and Technology Office, 1981.
- [7] H.E. Merritt. *Hydraulic Control Systems*. John Wiley & Sons Inc., 1991.
- [8] E. Trostmann. *Water Hydraulics Control Technology*. Technical University of Denmark, 1996.
- [9] Situ Biosciences LLC. Biodegradability Testing Methods. www.situbiosciences.com, November 2012.

- [10] J.S. Cundiff. *Fluid Power Circuits and Controls: Fundamentals and Applications*, volume vol. 21. CRC Press, 2001.
- [11] Hågglunds drives. www.hagglunds.com, December 2011.
- [12] Hydrowatt. www.hydrowatt.com, May 2012.
- [13] M. Schaap. Seawater Driven Piling Hammer. In *Proceedings of the Dutch Fluid Power Conference in Ede*, September 2012.
- [14] H. Lawson-Tancred. Method and Apparatus for Generating Electricity from a Fixed Pitch Wind Wheel, July 1981.
- [15] Boeing mod-2/mod-5b wind turbines. www.boeing.com, June 2012.
- [16] European Wind Energy Association. *Wind Energy - The Facts: a Guide to the Technology, Economics and Future of Wind Power*. 2009.
- [17] JERICO. Hydraulic Wind Energy Conversion. Technical report, Jacobs Energy Research, July 1981.
- [18] B.R. Höhn. Future Transmissions for Wind Turbines. *Applied Mechanics and Materials*, vol. 86:p.18–25, 2011.
- [19] B.B. Jensen, N. Mijatovic, and A.B. Abrahamsen. Development of Superconducting Wind Turbine Generators. In *EWEA Annual Conference*, Copenhagen, 4 2012.
- [20] J.A. Jensen, A.A. Furuseth, P. Chang, and K.E. Thomsen. Technological Advances in Hydraulic Drive Trains for Wind Turbines. In *EWEA Annual Event Conference Proceedings*, April 2012.
- [21] ChapDrive. www.chapdrive.com, December 2011.
- [22] Artemis Intelligent Power. www.artemisip.com, December 2011.
- [23] Sea Angel, the future of offshore wind. www.mhips.com/products/seaangel, December 2011.
- [24] J. Taylor. The Artemis Digital Displacement Transmission; a Lightweight, Network-Supporting Power-Train for Sea-Angel. *EWEA Annual Event Conference Proceedings*, April 2012.
- [25] N. Vatheuer J. Schmitz. Development of a Hydrostatic Transmission for Wind Turbines. *Proceedings of the International Fluid Power Conference 2010*, vol. 3:p.479–488, 2010.

- [26] B. Skaare, B. Hörnsten, and F.G. Nielsen. Energy Considerations for Wind Turbines with Hydraulic Transmission Systems. In *Proceedings of EWEA Offshore Conference*, Amsterdam, Netherlands, December 2011.
- [27] B. Skaare, B. Hörnsten, and F.G. Nielsen. Modeling, Simulation and Control of a Wind Turbine with a Hydraulic Transmission Systems. *Wind Energy*, October 2012.
- [28] Statoil. Hywind Project. www.statoil.com, November 2012.
- [29] N.F.B. Diepeveen and J. van der Tempel. Delft Offshore Turbines, the Future of Wind Energy. Technical report, Delft University of Technology, December 2008.
- [30] J. van der Tempel. Energy extraction system, has water pump attached to rotor, windmill for pumping water from sea, water system connected to water pump, for passing water pumped from sea, and generator connected to water system, December 2009.
- [31] Comparison of Conventional and Hydraulic Drive Train Mass and Their Influence on Support Structure Design. In *Renewable Energy Research Conference Proceedings*, June 2010.
- [32] [unknown]. The gearbox problem revisited – Danish laboratory report. *Windpower Monthly*, April 2004.
- [33] E. de Vries. Wind turbine gearboxes and the effort to improve their reliability. *Windpower Monthly*, June 2010.
- [34] European Wind Energy Association. The European Offshore Wind Industry - Key Trends and Statistics 1st Half 2012. Technical report, 2012.
- [35] A. Martin. Wind farm reliability improvement will reduce maintenance visits. *Lloyd's Register online blog*, October 2012.
- [36] G.W. van Bussel and M.B. Zaaijer. Estimation of Turbine Reliability Figures Within the DOWEC Project. Technical Report No. 10048, 2003.
- [37] E. Muljadi, C.P. Butterfield, J. Chacon, and H. Romanowitz. Power Quality Aspects in a Wind Power Plant (Preprint of Conference Paper). Technical Report NREL/CP-500-39183, NREL National Renewable Energy Laboratory, January 2006.

- [38] J. Jonkman, S. Butterfield, W. Musial, and G. Scott. Definition of a 5-MW Reference Wind Turbine for Offshore System Development. Technical Report NREL/TP-500-38060, NREL National Renewable Energy Laboratory, February 2009.
- [39] Upwind. www.upwind.eu, June 2012.
- [40] E.A. Bossanyi. Wind Turbine Control for Load Reduction. *Wind Energy*, vol. 6:p.229–244, 2003.
- [41] W.E. de Vries. Floating vs. Bottom Founded, Transition Depth for Offshore Wind Turbine Support Structures. Email to the author, October 2012.
- [42] N.D. Manring. The Discharge Flow Ripple of an Axial-Piston Swash-Plate Type Hydrostatic Pump. *Journal of Dynamic Systems, Measurement and Control*, vol. 122:p.263–268, June 2000.
- [43] A.E. Catania and A. Ferrari. Experimental Analysis, Modeling, and Control of Volumetric Radial-Piston Pumps. *Journal of Fluids Engineering*, vol. 133, August 2011.
- [44] K.K. Turekian. *Oceans*. Prentice-Hall, 1976.
- [45] Encyclopedia Britannica (online). search term “seawater”. www.britannica.com, November 2012.
- [46] National Physics Laboratory. Physical Properties of Sea Water. www.kayelaby.npl.co.uk, November 2012.
- [47] G.H. Lim, P.S.K. Chua, and Y.B. He. Modern Water Hydraulics - the New Energy Transmission Technology in Fluid Power. *Applied Energy*, vol. 76:p.239–246, September - November 2003.
- [48] M.A.K. Al-Sofi, A. M. Hassan, O.A. Hamed, A.G.I. Dalvi, M.N.M. Kither, G. M. Mustafa, and K. Bamardouf. Optimization of Hybridized Seawater Desalination Process. *Desalination*, vol. 131:p.147–156, December 2000.
- [49] D. Cerda Salzmänn. *Ampelmann, Development of the Access System for Offshore Wind Turbines*. PhD thesis, October 2010.
- [50] P. Drexler, H. Faatz, F. Feicht, H. Geis, J. Morlok, E. Wiesman, A. Krielen, N. Achten, and M. Reik. *The Hydraulic Trainer Volume 3: Planning and Design of Hydraulic Power Systems*. 2003.

- [51] C. Pencho. Layman's Handbook on How to Develop a Small Hydro Site. Technical report, European Small Hydropower, June 1998.
- [52] R.J. Barthelmie, K. Hansen, S.T. Frandsen, O. Rathmann, J.G. Schepers, W. Schlez, J. Phillips, K. Rados, A. Zervos, E.S. Politis, and P.K. Chaviaropoulos. Modelling and Measuring Flow and Wind Turbine Wakes in Large Wind Farms Offshore. *Wind Energy*.
- [53] H. Keck, G. Vulliod, and P. Joye. Commissioning and Operation Experience with the Worlds Largest Pelton Turbines Bieudron. Technical report, VATECH hydro, 2000.
- [54] J.F. Manwell, J.G. McGowan, and A.L. Rogers. *Wind Energy Explained, Theory, Design and Application*. John Wiley & Sons, England, 2002.
- [55] T. Burton and et. al. *Wind Energy Handbook*. John Wiley & Sons, second edition, 2011.
- [56] W.M.J. Schlösser. *Ein mathematisches Modell für Verdrängerpumpen und -motoren, Ölhdraulik und Pneumatik*, volume vol. 4/5. 1961.
- [57] K.E. Rydberg. *Efficiencies for variable hydraulics pumps and motors- Mathematical models and operation conditions*. Linköpings University, Department of Management and Engineering, 2009.
- [58] F.M. White. *Fluid Mechanics*. Mc Graw-Hill International, sixth edition, 2008.
- [59] A. Jarquin Laguna and N.F.B. Diepeveen. Dynamic Analysis of Fluid Power Drive Trains for Variable Speed Wind Turbines. *Proceedings of the EWEA Conference in Vienna*, February 2013.
- [60] A. Betz. Das Maximum der Theoretisch Möglichen Ausnützung des Windes durch Windmotoren. *Zeitschrift für das gesamte Turbinewesen*, vol. 26, 1920.
- [61] K.H. Bergey. The Lanchester-Betz Limit (Energy Conversion Efficiency Factor for Windmills). *Journal of Energy*, vol. 3(No. 6):p.382–384, 1979.
- [62] A. Rauh and W. Seelert. The Betz Optimum Efficiency for Windmills. *Applied Energy*, vol. 17(No.1):p.15–23, 1984.
- [63] H. Snel and J.G. Schepers. Joint Investigation of Dynamic Inflow Effects and Implementation of an Engineering Method. Technical report, April 1995.

- [64] F.D. Bianchi, H. De Battista, and R.J. Mantz. Wind Turbine Control Systems. In *Principles, Modelling and Gain Scheduling Design*, Advances in Industrial Control. Springer, 2007.
- [65] W.E. Boyce and R.C. DiPrima. *Elementary Differential Equations and Boundary Value Problems*. Wiley, second edition, 1969.
- [66] H. Murrenhoff. *Grundlagen der Fluidtechnik, Teil 1: Hydraulik*. Shaker Verlag, third edition, 2007.
- [67] W.E. Wilson. *Mathematical Models in Fluid Power Engineering, Hydraulic & Pneumatic Power*. 1967.
- [68] M. Annoni, L. Cristaldi, M. Norgia, and C. Svelto. Efficiency Measurement of Water Jet Orifices by a Novel Electro-Optical Technique. *IEEE Transactions on Instrumentation and Measurement*, vol. 57(1):p.48–54, 2008.
- [69] A.V. Akkaya. Effect of bulk modulus on performance of a hydrostatic transmission control system. *Sādhanā Academy Proceedings in Engineering Sciences*, vol. 31:p.543 – 556, October 2006.
- [70] P. Albers. *Motion Control in Offshore and Dredging*. Springer, 2010.
- [71] J. Mäkinen and H. Marjamäki. Modeling hydraulic systems as finite elements. In *The 17th IASTED International Conference on Applied Simulation and Modeling (ASM-2008)*, Corfu, Greece, June 2008.
- [72] N.F.B. Diepeveen and A. Jarquin Laguna. Dynamic Modeling of Fluid Power Transmissions for Wind Turbines. *Proceedings of the EWEA Offshore Conference in Amsterdam*, November 2011.
- [73] J. Mäkinen, R. Piche, and A. Ellman. Fluid Transmission Line Modeling Using a Variational Method. *ASME Journal of Dynamic Systems, Measurement, and Control*, vol. 122:p.153–162, 2000.
- [74] E.A. Bossanyi. *G.H. Bladed User Manual*. Glasgow, 2007.
- [75] J. Schmitz, N. Vatheuer, and H. Murrenhoff. Hydrostatic Drive Train in Wind Energy Plants. In *Proceedings of the EWEA Conference in Brussels*, March 2011.
- [76] H. Murrenhoff. *Servohydraulik - Geregelte Hydraulische Antriebe*. Shaker Verlag, 3 edition, 2008.

- [77] N. Hosman. Performance Analysis and Improvement of a Small Locally Produced Wind Turbine for Developing Countries. Master's thesis, March 2012. MSc Thesis.
- [78] J. Thake. *The Micro-Hydro Pelton Turbine Manual: Design, Manufacture and Installation for Small-Scale Hydro-Power*, 2001.
- [79] Hessels & van Rooij Engineering B.V. Design of Tower and Foundation Pile for a V80-2.0MW Wind Turbine at Location Q7-WP. Technical report, February 2005.
- [80] Germanischer Lloyd. Rules and Guidelines, Guideline for the Certification of Offshore Wind Turbines. Technical report, 2005.
- [81] R. Angehrn. Safety Engineering for the 423MW Pelton Runners at Bieudron.
- [82] E. Lepa, T. Thurnherr, and A. Faulstich. Design and Testing of a 7MW Wind Turbine Medium Voltage Electrical Drivetrain with Medium Speed Permanent Magnet Synchronous Generator. In *EWEA 2013 Annual Conference Proceedings*, February 2013.
- [83] M.S. Ghidaoui, M. Zhao, D.A. McInnis, and D.H. Axworthy.
- [84] S. Stubbier, H.C. Pedersen, and K. Markussen. Hydraulic Soft Yaw System Load Reduction and Prototype Results. *EWEA Conference Proceedings*, February 2013.
- [85] T. Sant and R.N. Farrugia. Performance Modelling of an Offshore Floating Wind Turbine-Driven Deep Sea Water Extraction System for Combined Power and Thermal Energy Production: a Case Study in a Central Mediterranean Context, June 2013.
- [86] D.J. Malcolm and A.C. Hansen. Windpact Turbine Rotor Design Study. Technical report, June 2002 (Revised April 2006).
- [87] Dutch Offshore Wind Energy Converter (dowec) project. www.ecn.nl, May 2010.
- [88] L. Fingersh, M. Hand, and A. Laxson. Wind Turbine Design Cost and Scaling Model. Technical report, December 2006.
- [89] European Wind Energy Association. Wind Energy - The Facts. www.wind-energy-the-facts.org, May 2010.

[90] Palfinger Systems. www.palfingersystems.com, May 2010.

[91] H. Piggott. *Wind Turbine Recipe Book*. 2008.



Reduction of Nacelle Mass

A.1 Introduction

It is shown here that the relatively high power density of high pressure pumps compared to mechanical gearboxes and the exclusion of additional drive train components from the nacelle leads to a significant reduction in the total nacelle mass. The NREL 5MW offshore baseline turbine [38] is used as reference turbine. The DOT is modeled as having the exact same rotor.

Data from operational offshore wind turbines and relevant hydraulic pumps are used to establish mass trends as function of the (effective) rotor diameter. The results from the NREL WindPACT [86] study on wind turbine scaling are also used to establish a mass scaling model. In all cases the mass trend is an exponential function of the (effective) rotor diameter. All consulted data is publicly available.

For this research the following assumptions & conditions were used:

- Wind turbines used for data analysis all have been installed offshore from 2002 onwards. This is done to avoid straying too far from the state of the art.
- The effect of efficiency or reliability of the drive train is assumed inconsequential. The only characteristics of influence are the mass and the rated or nominal power capacity of components.
- Additional drive train components such as cables, batteries, control unit, hoses, valves and pressure sensors are assumed not to contribute significantly to the overall nacelle mass and will not be taken into account.

- The outcome is based on a generalization of characteristics. In other words, trend lines through data are used as input.
- The rotor properties will be assumed equal for both the NREL turbine and the DOT. The control and related performance of the rotor are also assumed equal.

In the presented equations, masses are in kilograms, rotor diameter D and radius R are defined in meters.

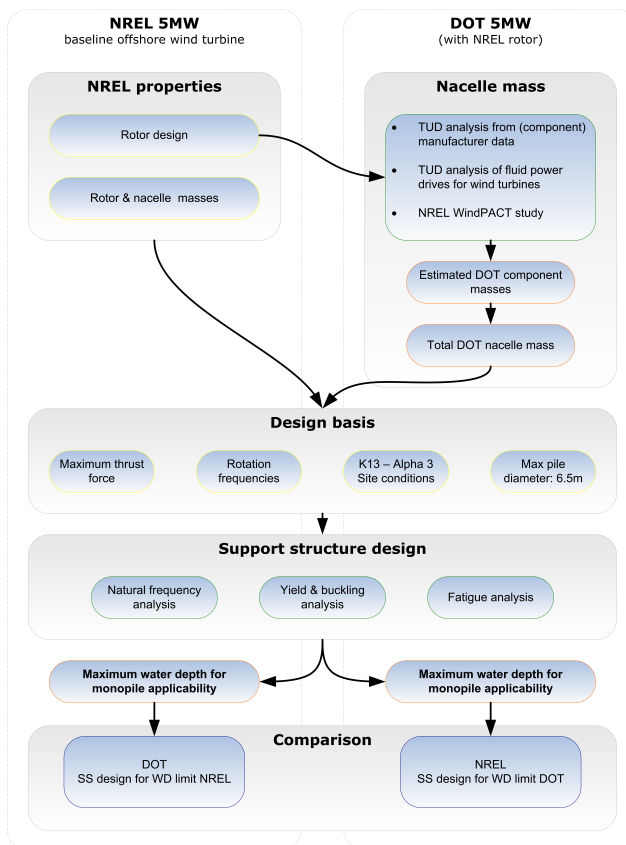


Figure A.1: Schematic of research method

A.2 Reference Turbine Characteristics

The reference turbine is the NREL 5MW offshore baseline turbine [38]. This fictitious turbine has become the standard reference turbine for many studies. The main reason for this is that all its properties are freely available. Some turbine parameters were arbitrarily selected using engineering judgment; others were selected to match those of the Repower 5MW turbine. For instance the EU-funded research project UpWind [39] also uses the NREL design. The only difference between the UpWind 5MW and the NREL 5MW turbines is that UpWind incorporates an industry standard controller developed by Garrad Hassan.

The properties assigned to the NREL turbine are aimed to represent the current state of the art for offshore wind turbines. This infers a conventional drive train with a three-stage gearbox and an asynchronous high-speed generator as the principle components. An overview of the most important reference turbine properties is given in table 3.1.

It should be noted that for the modeling of the tower top masses, the NREL did not make use of its WindPACT study (see section A.3.2 for more information). Instead, the properties of the Repower 5M prototype were taken. The arguments for this choice are given in [38]. The masses of the Repower 5M nacelle components are not publicly available. This means that the masses of the reference turbine nacelle components are unknown.

A.3 Inventory of Data and Established Relations

A.3.1 Offshore Wind Turbines Currently Installed

In terms of configuration, the wind turbines placed offshore have so far been remarkably similar. All have a three-bladed upwind rotor with pitch controlled blades. All have a similar drive train. Onshore, both geared and direct drive turbines are used. So far, only geared turbines have been installed offshore. All, with the exception of one type, have a three-stage gearbox and a high speed generator. The Areva Multibrid M5000 has a single stage gearbox with a medium speed generator.

The main differences are in the size (mass) and hence power rating of the turbines. This, along with the local environmental conditions, determines the type and size of the support structure. Other differences include the location of electric components (frequency converter, transformer) and possible additions of built-in cranes and heli-hoist-platforms. The commissioning of Horns Rev in 2002 is widely regarded as the starting point for the large scale exploitation of offshore wind. The turbines used for this research all have editions installed offshore from 2002 on. This is done to avoid

Manufacturer	Type name	Manufacturer	Type name
Areva Multibrid	M5000	BARD	VM
General Electric	GE 3.6	Repower	RE 5M
Siemens	SWT-2.3-93	Siemens	SWT-3.6-107
Vestas	V80-2.0	Vestas	V90-3.0

Table A.1: Commercial wind turbines offshore used for this research

straying too far from the current state of the art. An overview of these turbines is given in table A.1.

Trends for rotor, nacelle and total top mass relating these turbines are represented by the grey lines in figures A.2(a), A.2(b) and A.6 respectively.

A.3.2 Scaling Studies

The development of scaling models for wind turbines is complicated by the various configurations, secrecy and advances in technology. Several studies on wind turbine scaling models have been conducted in the last decade. Some well known studies are:

- *Dutch Offshore Wind Energy Converter* (1999-2003), the design of the DOWEC 6MW offshore wind turbine [87].
- *Wind Turbine Design Cost and Scaling Model* (2006) by the U.S. National Renewable Energy Laboratory (NREL) [88], which is partly based on the *Wind-PACT Turbine Rotor Design Study* (2000-2002) [86].
- The EWEA project *Wind Energy - The Facts (WindFacts)* (2007-2009) presents rotor and nacelle mass trends based solely on available data [89].
- The largest project on the modeling of turbine scaling which is currently running is the *UpWind* project (2006-2011) [39]. The 5MW reference turbine for this project is derived from the NREL 5MW baseline turbine for offshore [38].

Of these studies, the NREL model is the most important source for this paper. Whereas other studies tend to treat the rotor and nacelle as lump masses, the NREL model specifies the mass trends of the main components. The same approach is taken here, since the modeling of nacelle component masses is a necessary requirement for the mapping of the potential mass reduction of the proposed modification of drive-train technology. Equations A.2-A.7, A.12, A.14-A.16, A.18-A.20, A.28-A.31, A.33, A.34 in this report are directly copied from [88] and [86].

It is important to note that the equations given in the NREL report [88] do not match those which are used for the examples in the same report for 1500kW and

3000kW turbines. The research presented in this paper follows the expressions used in these examples.

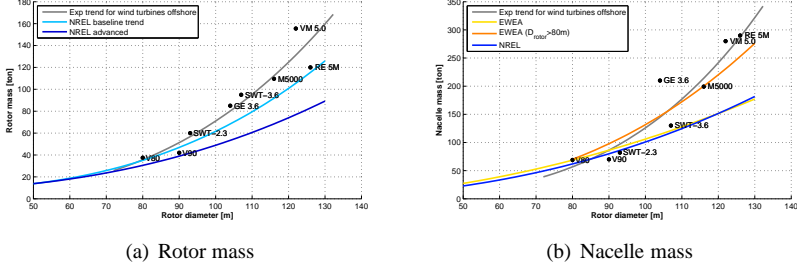


Figure A.2: Mass versus rotor diameter trend lines, established by studies in [89, 88] and from turbines listed in table A.1

A.4 Rotor Mass Modeling

As has already been established in earlier studies, the dominant parameter in wind turbine scaling is the rotor diameter D . The design strength & stiffness of the blades are determined predominantly by the maximum force on the blades, which theoretically occurs at rated wind speed v_{rated} . Mass is the product of density and volume, which are essentially determined by the shape, required strength & stiffness and the construction materials. The volume of a rotor blade is determined by its length ($\approx \frac{D_{rotor}}{2}$) and its aerodynamic shape parameters λ and c_p . The blade mass is then dependent on the same variables as the volume.

$$m_{blade} = f(c_p, \lambda, D_{rotor}, v_{rated}) \quad (A.1)$$

Here c_p is the power coefficient, λ is the tip speed ratio, D_{rotor} is the rotor diameter and v_{rated} is the rated wind speed.

The reference turbine and the DOT are modeled as having the exact same rotor. This rotor consists of three blades, attached to a hub, a system for pitching the blades and a nosecone.

From the scaling studies of the rotor mass, the NREL WindPACT [86] study provides the most detailed scaling relations. This study distinguishes between “baseline” and “advanced” rotor mass trends. Since the “baseline” trend provides the most accurate match with turbine data (see figure A.2(a)), this method is selected. The mass

trend of the rotor is thus defined by:

$$m_{Rotor} = N_{blades} \cdot m_{Blade} + m_{Hub} + m_{PitchSystem} + m_{NoseCone} \quad (A.2)$$

Here,

$$m_{Blade} = 0.1452 \cdot R^{2.9158} \quad (A.3)$$

$$m_{Hub} = 0.954 \cdot m_{Blade} + 5680.3 \quad (A.4)$$

$$m_{PitchBearing} = 0.1295 \cdot (N_{blades} \cdot m_{Blade}) + 491.31 \quad (A.5)$$

$$m_{PitchSystem} = (1.328 \cdot m_{PitchBearing}) + 555 \quad (A.6)$$

$$m_{NoseCone} = 18.5 \cdot D_{rotor} - 520.5 \quad (A.7)$$

Note that the outcome for a rotor with 126m diameter is a mass of 115,420 kg. This differs from the mass of the NREL 5MW rotor, which is 110,000kg. For the purpose of consistency, the mass of the rotor of DOT 5MW is assigned the same mass as the NREL 5MW rotor.

The bearing system and the main (low speed) shaft between the rotor and the gearbox are modeled as part of the drive train and thus as nacelle components.

A.5 Nacelle Mass Modeling

A.5.1 Introduction

The mass of the nacelle and its components depends on the design characteristics of the rotor and the configuration of the drive train. The drive train is typically defined by the components between the rotor and the electric output connection.

- The NREL reference turbine has a drive train configuration characterized by a three-stage gearbox (2 planetary, 1 helical) and a high speed generator.
- The only DOT drive train components in the nacelle are the low speed shaft and a directly driven positive displacement pump.

As is shown in section A.5.4 “Other Components”, the dimensions of the drive train also influence the dimensions of other components.

For the calculation of the mass of a number of nacelle components, the calculation of the nominal rotor torque τ_{rotor} is required. The rotor converts wind power into mechanical power. This conversion is commonly described by equation A.9. Here, ρ is

the local air density, v_{wind} is the wind speed and R is the rotor radius. The mechanical power consists of torque τ and rotational speed ω .

$$P = c_P \cdot P_{wind} \quad (A.8)$$

$$= c_P \cdot \frac{1}{2} \cdot \rho \cdot v_{wind}^3 \cdot \pi \cdot R^2 \quad (A.9)$$

$$= \tau \cdot \omega \quad (A.10)$$

The relation between τ and ω is determined by the design tip speed ratio λ .

$$\lambda = \frac{\omega \cdot R}{v_{rated}} \quad (A.11)$$

Here, for greater λ , ω will be greater and τ will be lower. For the design λ given in table 3.1 the rotational speed ω at rated conditions is 12.1 rpm. The related nominal rotor torque τ_{rotor} is then 3.95 MNm.

A.5.2 Conventional Drive Train

The mass of the low speed shaft is modeled by the WindPACT study as a function of the rotor diameter D_{rotor} .

$$m_{Shaft_{ls}} = 0.0142 \cdot D_{rotor}^{2.8879} \quad (A.12)$$

$$\tau_{Shaft_{ls}} = \tau_{rotor} \quad (A.13)$$

The bearing system which holds the low speed shaft is modeled according to WindPACT by the following expressions.

$$m_{Bearing} = \left(\frac{D_{rotor}}{75} - 0.033 \right) \cdot 0.0092 \cdot D_{rotor}^{2.5} \quad (A.14)$$

$$m_{BearingHousing} = m_{Bearing} \quad (A.15)$$

$$m_{BearingSystem} = m_{Bearing} + m_{BearingHousing} \quad (A.16)$$

The low speed shaft is coupled to the gearbox. In figure A.3, the error margin of the NREL WindPACT trend line increases rapidly for rotor diameters greater than 100m. The data points presented in this figure were taken from product folders of General Electric (GE) and Winergy AG. Equation A.17 describes the exponential data trend in figure A.3 and is hence forth used as the scaling relation for the mass of a three stage planetary & helical gearbox.

$$m_{Gearbox} = 0.0186 \cdot D_{rotor}^{3.1022} \quad (A.17)$$

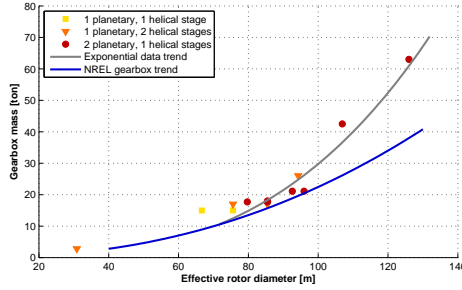


Figure A.3: Drive train component masses

The high speed shaft connects the gearbox to the generator. The gear ratio $GearRatio$ is determined by dividing the nominal generator speed (typically 1500rpm) by the nominal rotation speed of the rotor.

$$m_{Shaft_{hs}} = \frac{25 \cdot \tau_{Shaft_{hs}}}{GearRatio} \quad (A.18)$$

The mechanical brake, high speed coupling and associated components are grouped by the term $m_{BrakeCoupling}$.

$$m_{BrakeCoupling} = 0.19894 \cdot \frac{P_{rated}}{1000} - 0.01141 \quad (A.19)$$

The high speed generator is modeled according to WindPACT expression:

$$m_{Generator} = 6.47 \cdot \left(\frac{P_{rated}}{1000} \right)^{0.92237} \quad (A.20)$$

The results for the DOT and NREL turbines are given in table 7.1.

A.5.3 Fluid Power Drive Train

In the fluid power drive train, a fluid power circuit acts in similar fashion as a mechanical gearbox. The torque and rotation speed of the rotor are converted into a pressure flow by a positive displacement pump. A hydro motor converts this flow of pressurized fluid into torque and (high) speed. The gear ratio of the circuit depends on the difference in volumetric displacement of motor and pump. The Delft Offshore Turbine has a two-stage fluid power transmission, as shown in figure 3.14

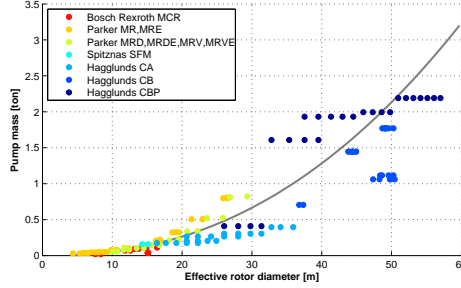


Figure A.4: Hydraulic pump mass versus effective rotor diameter

The mass of a pump is related to its performance characteristics. So far, positive displacement pumps have not been designed specifically for wind turbines. However, several types are suited for this application.

The main design challenge in matching pumps to wind turbine rotors is finding matching operational envelopes in terms of speed and torque. For an ideal pump, the power output is determined by the pressure difference Δp between inlet and outlet, the volumetric displacement V_g and the rotation speed ω . The product of the pressure difference and the volumetric displacement is the torque τ .

$$P = \Delta p \cdot V_g \cdot \omega \quad (\text{A.21})$$

$$= \tau \cdot \omega \quad (\text{A.22})$$

The maximum continuous torque τ is the starting point for the matching process.

In general, three bladed turbine rotors with a tip speed ratio of around 7 rotate significantly slower than the nominal design speed of a positive displacement pump. In many cases though, the pump is able to operate at the rotor-required nominal rotation speed. The rotor-required nominal rotation speed of the pump is hence forth referred to as the equivalent rotation speed ω_{eq} .

If ω_{eq} is higher than the rated rotation speed of the pump, then the pump is not suitable for the calculated rotor diameter (and thus rated power). The size of the rotor for which the pump may be applied is then determined by the rated operational speed of the pump. This means the rotor size decreases and rated power goes down.

If ω_{eq} is lower than the minimum speed of the pump, it may be safely assumed that the pump is not suitable for direct drive wind turbine application.

Since ω_{eq} is usually below the nominal pump speed, the power rating of the pump is reduced for this application. The power rating of the pump for wind turbine application is hence forth referred to as the effective nominal power P_{eff} .

For a pump applied to a wind turbine, the equivalent nominal rated speed ω_{eq} is calculated from the effective rotor diameter and given v_{rated} and λ . Using the reference turbine properties, the effective nominal power P_{eff} is determined. From P_{eff} the effective rotor diameter D_{eff} is derived. The following equations describe the iterative process through which this is achieved.

$$R_{eff}(i) = \sqrt{\frac{2 \cdot P_{eff}(i)}{c_P \cdot \rho \cdot \pi \cdot v_{rated}^3}} \quad (A.23)$$

$$D_{eff}(i) = 2 \cdot R_{eff}(i) \quad (A.24)$$

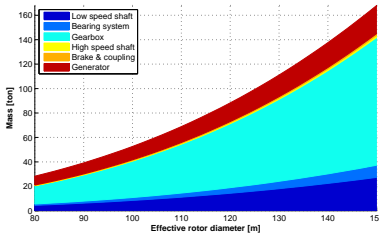
$$\omega_{eq}(i) = \frac{\lambda \cdot v_{rated}}{R_{eff}(i)} \quad (A.25)$$

$$P_{eff}(i+1) = \Delta p_{nom} \cdot V_g \cdot \omega_{eq}(i) \quad (A.26)$$

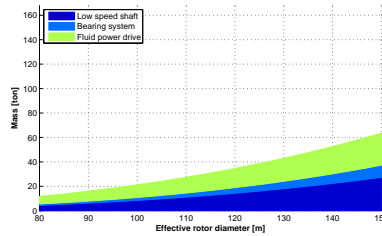
Note that expression A.23 is directly derived from equation A.9. The resulting mass trend for the positive displacement pumps with their respective effective rotor diameters is shown in figure A.4. The formula for the trendline is:

$$m_{pump} = 0.2843 \cdot D_{rotor}^{2.2809} \quad (A.27)$$

The resulting mass for the DOT pump is given in table 7.1.



(a) Three stage gearbox drive train components



(b) fluid power drive train components

Figure A.5: Breakdown of the mass of drive train components in the nacelle

Low speed positive displacement pumps with a capacity of 5MW do not yet exist. There appears to be no technical reason for this. There simply has not been sufficient demand to develop such pumps.

A.5.4 Other Components

All equations in this section are derived from the WindPACT study [86]. The bed-plate/mainframe directs the weight of and forces on the rotor to the tower/support

structure. For the reference turbine with three stage gearbox before high speed generator the mainframe mass is modeled using:

$$m_{Mainframe} = (2.233 \cdot D_{rotor})^{1.95801} \quad (A.28)$$

The pump of the DOT turbine is directly coupled to the low speed shaft. Because of this similarity with direct drive turbines, the DOT mainframe mass is modeled using:

$$m_{Mainframe} = (1.228 \cdot D_{rotor})^{1.953} \quad (A.29)$$

Platforms & railings are present inside the nacelle to facilitate maintenance and for safety. The size and amount of platforms & railings required depends on the layout of the nacelle. Hence, a compact nacelle will have fewer/smaller platforms & railings. According to NREL, their accumulative mass is related to the mainframe mass.

$$m_{PlatRail} = 0.125 \cdot m_{Mainframe} \quad (A.30)$$

The equipment in the nacelle is protected by a cover. The layout of the nacelle strongly influences the size and weight of this cover. Since the DOT has significantly less components in the nacelle, its cover is significantly smaller. For now it is assumed that the DOT nacelle cover has half the mass of the reference nacelle cover.

$$m_{NacelleCover} = 1.2819 \cdot \frac{P_{rated}}{1000} + 427.7444 \quad (A.31)$$

$$m_{NacelleCover_{DOT}} = \frac{1}{2} \cdot m_{NacelleCover} \quad (A.32)$$

The mass of the yaw system is considered to be the same for both configurations. The cooling system is only present in the nacelle of the reference turbine. The DOT cooling system is at the base of the turbine.

$$m_{YawSystem} = 1.6 \cdot (0.0009 \cdot D_{rotor}^{3.314}) \quad (A.33)$$

$$m_{Cooling} = 0.08 \cdot \frac{P_{rated}}{1000} \quad (A.34)$$

For the reference turbine the presence of a built-in crane is assumed. Having a crane in the nacelle is common in wind turbines offshore. The mass of the built-in crane is a function of maximum load F_{max} it is able to lift. This maximum load incorporates a safety factor f_s of 1.35. The formula for the trend line is established using data from [90].

$$m_{Crane} = 0.2843 \cdot F_{max}^{2.2809} \quad (A.35)$$

The heaviest component of the reference nacelle is the gearbox.

$$F_{max_{Ref}} = f_s \cdot m_{Gearbox} \cdot g \quad (A.36)$$

The heaviest component of the DOT nacelle is the hydraulic pump.

$$F_{max_{DOT}} = f_s \cdot m_{Shafts} \cdot g \quad (A.37)$$

The results for the DOT and NREL turbines are given in table 7.1.

A.5.5 The Complete Nacelle

For the reference turbine, the sum of the masses of nacelle components was smaller than the reference turbine nacelle mass. The difference is listed as “unspecified”. A breakdown of the masses which make up the total nacelle mass is given in table 7.1. To get an appreciation of the significance of these results they are compared to the turbines listed in table A.1.

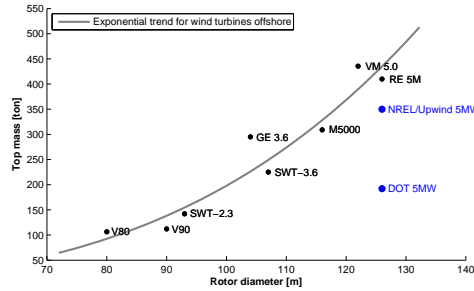


Figure A.6: Top mass trend



MicroDOT 10kW Demonstrator

This appendix is an extract of the paper “Water-Hydraulic Power Transmission for Offshore Wind Farms; Small-scale experiments with water-hydraulic power transmission” by N.F.B. Diepeveen, A. Jarquin Laguna, A.S. Kempenaar, which was presented at the Dutch Fluid Power Conference in Ede on September 13th 2012.

To demonstrate the functionality of the DOT transmission concept, a small scale (10kW) version was assembled in the water laboratory at the faculty of Civil Engineering and Geosciences of the TU Delft. The set-up includes a closedloop hydraulic circuit as well as a freshwater open loop circuit and a small Pelton turbine. The wind turbine rotor was simulated by a speed-controlled electric motor driving the oil pump. A hydraulic diagram and picture of the constructed demonstration set-up are shown in figure B.1 and figure B.2.

During the MicroDOT experiments the performance of the main components was measured for different operational conditions of the rotor (in this case simulated through an electric motor), as shown in figure B.3(a). The total efficiency of the transmission, from the oil pump up to the nozzle exit, is between 43 and 48% for rotor speeds above what corresponds to a wind speed of approximately 4.7m/s. Below this threshold, the efficiency is significantly lower, due to the reduced water pump efficiency. The nozzle efficiency is a result of the geometric properties of the tested nozzles which showed low discharge coefficients. Thus, the efficiency of the system could be improved by simply using a better geometrically shaped nozzle.

The rotor operating envelop, between 90% and 100% of the maximum rotor efficiency, is indicated by the grey area shown in figure B.3(b). The characteristic torque versus rotation speed curves of the transmission were measured for three different

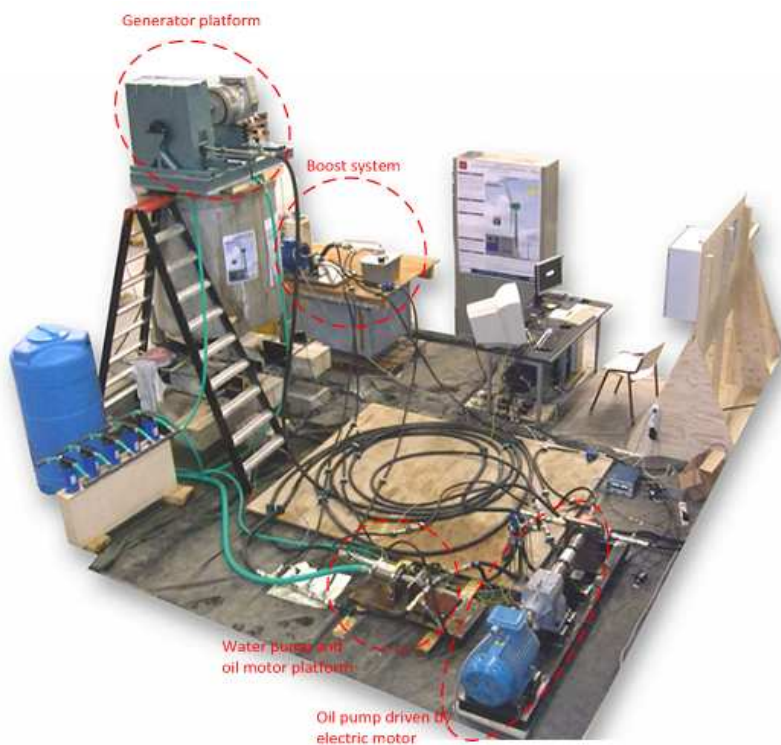


Figure B.1: Picture of the MicroDOT experimental set-up

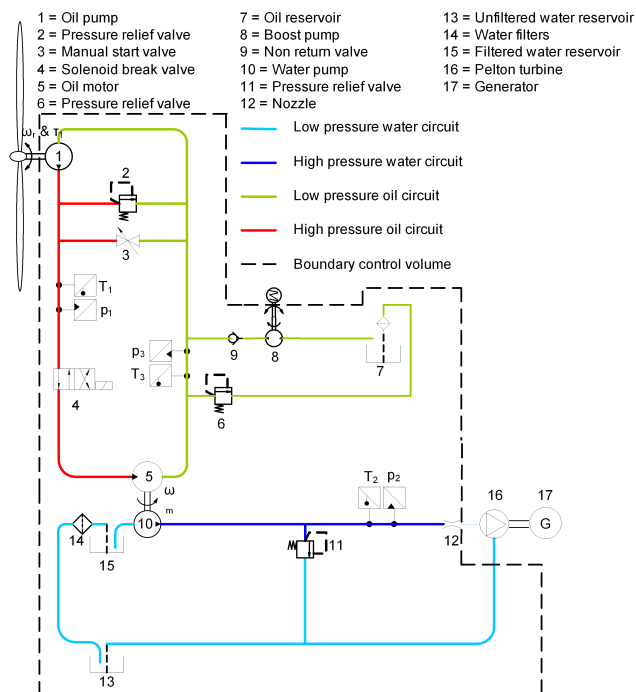
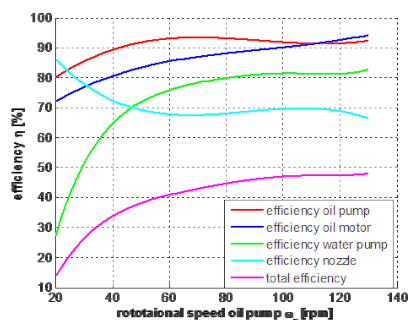


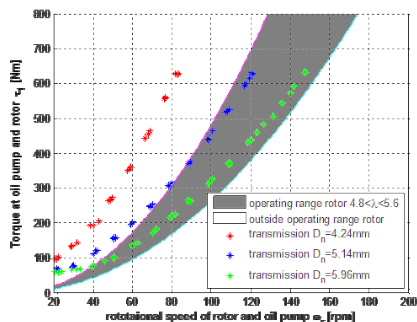
Figure B.2: Hydraulic diagram of the 10kW MicroDOT

Component	Type/properties
Rotor	Simulated by electric motor, 7.5m diameter, 10kW rated power, speed range 40-150rpm
Oil pump	Bosch Rexroth AF2M180, displacement: 180cc/rev, nominal pressure: 400bar, speed range: 0-3600rpm
High pressure oil line	Length: 10m, diameter : 0.75in
Oil motor	Bosch Rexroth AF2M16, displacement: 16cc/rev, nominal pressure: 400bar, speed range: 0-8000rpm
Water pump	Hydroton P60, displacement: 70.3cc/rev, nominal pressure: 160bar, speed range: 0-2000rpm
High pressure water line	Length: 10m, diameter: 1.0in
Nozzle Diameter:	4.24/5.14/5.96mm
Pelton Wheel	Pitch circle diameter: 0.4m, No. of buckets: 32
Electricity generator	Stamford synchronous generator PI044, rating: 8kW

Table B.1: MicroDOT demonstrator component properties



(a) Operational efficiency



(b) Torque vs. rotational speed curves matched to the rotor envelope

Figure B.3: MicroDOT performance diagrams

nozzle diameters. The curve corresponding to the 5.96mm nozzle matches the rotor envelope for almost the complete range of operation.

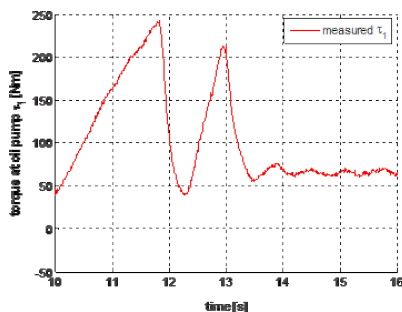


Figure B.4: Figure 12: Low efficiency of the water pump when operated at low rotational speeds due to the high start-up torque required

An important finding from the experiments with the MicroDOT set-up was the high start-up torque required to drive the water pump and therefore a high start-up torque for the wind turbine rotor was also necessary. At low rotational speeds, a minimum value of torque (and therefore oil pressure) is required to run the water pump. Figure B.4 shows how the torque is built-up to a level such that the oil pressure is enough to run the water pump. Once the water pump is rotating, the oil pressure drops causing the torque to decrease below the required minimum and the water pump

stops rotating. The pressure starts to build up again and the process is repeated. When the speed of the oil pump is slightly increased the torque at the water pump remains above the minimum torque required and normal operation of the system is realized as observed by the constant torque at the oil pump shown in the last seconds of the graph from figure B.4. This high start-up torque of the water pump will limit the operation of the turbine at low wind speeds.

Description of IFAS Experimental Setup

C.1 Description of the Main Components of the IFAS 1MW Test Bench

C.1.1 Hydraulic Drives

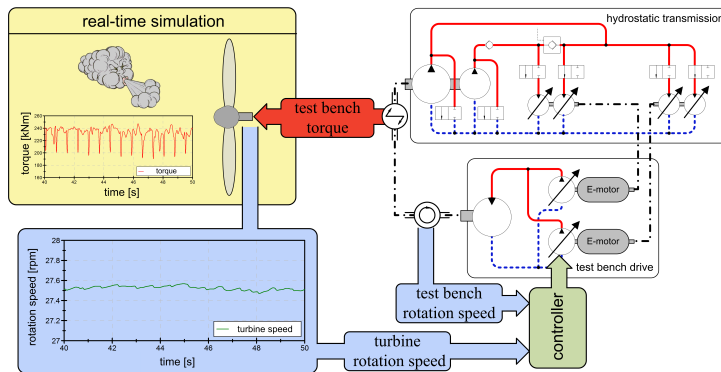


Figure C.1: Working principle of the 1MW IFAS test bench (image courtesy of J. Schmitz, IFAS)

The first step in dimensioning of the hydrostatic transmission was the selection of a wind turbine providing a torque curve over wind speed and rotation speed. Pre-

Designation	Type	V_g	p_{nom}	n_{nom}
		[cc/rev]	[bar]	[rpm]
pump 1	fixed displ.	52,800	350	80
pump 2	fixed displ.	13,200	350	85
motor 1	var. displ.	180	350	1,800
motor 2	fixed displ.	250	350	1,500
motor 3	var. displ.	355	350	1,500
motor 4	var. displ.	500	350	1,320

Table C.1: Components of the IFAS hydrostatic transmission

vious simulations have proven that by switching of single pumps and motors of a hydrostatic transmission the overall efficiency in partial load can be increased. Subsequently, different combinations of pumps and motors were analyzed leading to the transmission shown in figure 3.10.

In steady state measurements the rotation speed is controlled by the hydraulic motors of the transmission, while the test bench drive applies a specific torque controlled by altering the two axial piston pumps of the test bench drive. In order to test the transmission under realistic dynamic wind conditions, the test bench is coupled with a Real-Time Simulation as shown in figure C.2.

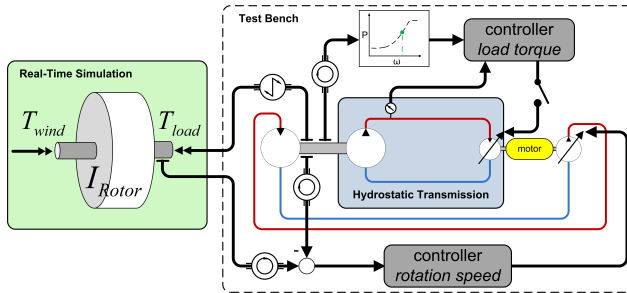


Figure C.2: Integration of the rotor inertia to the test bench

An important component is the hydraulic fluid: HPL46. Its properties are given in table C.2 of appendix C.

C.1.2 Hydraulic Fluid

An important component is the hydraulic fluid: HPL46. Its properties are given in table C.2. Note that the given values of these fluid properties hold for the reference

temperature of $313\text{K} \approx 20^\circ\text{C}$. The variations in elasticity, kinematic viscosity and

name	HPL46
ISO	VG 46 / HLP 46
reference temperature T_{ref}	313 K
density ρ	835.3 kg/m^3
elasticity E	1486.22 MPa
specific heat capacity c	2033.3 J/kgK
kinematic viscosity ν	$46.3\text{ mm}^2/\text{s}$ ($=\text{cSt}$)
thermal expansion coefficient α	0.00074 K^{-1}

Table C.2: Hydraulic fluid properties

density with respect to the fluid temperature are demonstrated in figure C.3

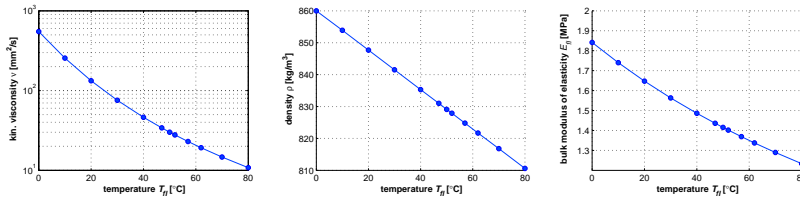


Figure C.3: Properties of hydraulic oil HPL46 as a function of temperature

C.2 Requirements & Limitations

For safety and to avoid damage to the system a number of operational limits are set.

- The simulation of the entire system should be compact enough to run in real time on a 1kHz Linux computer.
- The maximum operating pressure of the test bench is limited at 310 bar. The maximum operating pressure of the drive systems is 350 bar. A buffer of 40 bar is kept for pressure peaks due to unexpected events. Previous test have shown that the test bench operates at maximum efficiency between 200-250 bar.
- The constant speed of the generators in combination with the maximum volumetric displacement of the hydraulic motors limit the speed of the slow turning shaft. The maximum speed at full pump displacement (66,000cc) is 31 rpm.

If only the CBP840 (58,200cc) is connected, the maximum speed is around 40 rpm.

- The maximum torque for dynamic runs: the nominal pressure during dynamic tests should not exceed 220 bar. This allows room for the pressure to surge in case of a sudden torque increase. At the same time this limit brings down the maximum power to around 750kW.

When the pressure reaches 320 bar ($T_{rotor} = 300kNm$), the system shuts down.

C.3 Control Strategy for Optimal Power Production

The motors of the transmission are (dis)engaged through ball valves. Motors 1 & 4 act as one large motor with variable displacement. Motors 2 & 3 also act as one large motor, but since motor 2 has a fixed displacement and is connected to a generator operating at 1500rpm, the oil flow at startup means the minimum speed for the combined pump is around 5.6rpm. However, for steady state measurements the controls can be altered to allow the speed of the main shaft to reach 0rpm. When the pressure in the system surpasses a certain threshold, and remains there for a certain duration, motors are (dis)engaged.

The rotor of a variable speed wind turbine is typically designed so that between cut-in and just before rated wind speed, the blade pitch angle is zero and the rotor speed varies linearly with the wind speed. The relation between the linear velocity of the tip of the blade in the rotor plain to the incoming wind speed is known as the tip speed ratio λ .

$$\lambda = \frac{v_{tip}}{U} = \frac{\omega R}{U} \quad (C.1)$$

λ	tip speed ratio	[rad/s]	ω	angular velocity	[rad/s]
R	rotor radius	[m]	U	(unidirectional) wind speed	[m/s]
v_{tip}	tip speed	[m/s]			

At the optimal tip speed ratio, the rotor converts energy from the wind at maximum efficiency. The optimal rotation speed of the blades has to be adjusted by the drive train to the actual wind speed as shown in figure C.4.

For simulating start-up conditions or operation around cut-in wind speed, the pump with 80% of the total displacement can be switched off by opening a valve to low pressure, causing a local hydraulic short circuit. Due to the reduced flow rate to the motors, three of these are set to idle at this point of operation [75].

The rotation speed of the low speed shaft is controlled by varying the displacement of the hydraulic motors. Since the generators operate at grid frequency their rotation speed is constant. The swash plate motors define the flow rate and pressure in the system by changing the angle of displacement.

The pumps coupled to the low speed shaft have constant displacement, which implies a proportional correlation of flow rate and rotation speed.

Ideally, a wind turbine rotor rotates according to its optimal tip speed ratio. However, the controller needs information about the actual wind speed to define the optimal rotation speed.

There are two challenges to using wind speed measurements for control:

1. The actual wind speed is hard to measure on a real wind turbine, due to the large area covered by the blades the wind varies within this area in speed and direction. A single wind speed sensor mounted on top of the nacelle can hardly detect all these effects and deliver only approximate values.
2. The large rotor inertia makes it difficult to change the rotation speed synchronously to the fast fluctuating wind. Each short gust of wind would lead to a short acceleration of the turbine initiated by the controller. In this phase all the incoming power would be stored in the rotor inertia leading to interrupted power production. After the gust the controller would decelerate the rotor again having an increased power output for a short time. These described fast load changes are possible with the hydrostatic transmission but make the adaption of the system to the actual load more complicated. When using this control strategy, each harsh change of the braking torque involves the switching of several components. Due to a high priority on reliability such an operation of the system should be avoided where possible.

The solution is to estimate the optimal tip speed ratio and maximum power coefficient and apply them to set the desired torque speed curve. The controller of the hydrostatic transmission thus applies a braking torque on the turbine according to the actual rotation speed assuming an optimal point of operation. For this control strategy, the only control inputs are the rotational speed and either the torque, the hydraulic pressure or the swash plate angles. These can all be measured accurately.

Figure C.4 shows the torque equilibrium on the inertia of the rotor. The braking torque applied by the transmission is independent from wind speed.

$$I_{rotor} \dot{\omega} = \tau_{rotor} - \tau_{brake} \quad (C.2)$$

In case wind speed is higher than assumed, more torque than discharged by the transmission will be captured leading to an acceleration of the turbine. Figure C.4 shows

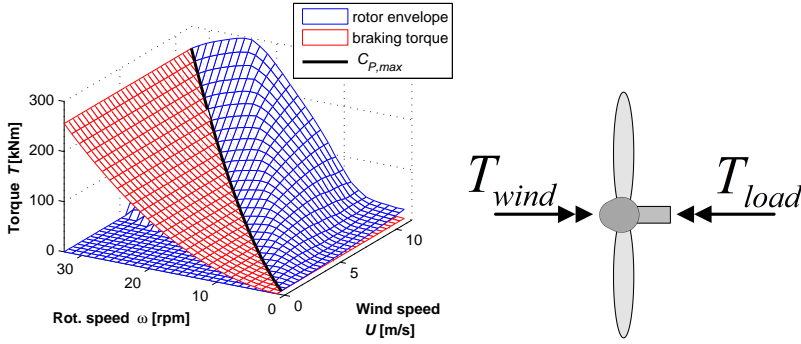


Figure C.4: Equilibrium of torque on the turbine

that valley occurs between the two surfaces in which the turbine will operate in steady state. Whenever an extreme gust occurs, the resulting rotor torque will accelerate the turbine. With the increasing rotation speed the transmission will also increase the braking torque of the drive train. Once the gust is going down, the braking torque is too high decelerating the turbine to the valley again. By varying the parameter of the torque curve deposited in the controller this valley can be adjusted to the optimal point of operation in which the overall efficiency of turbine and drive train is optimal.

Smooth switching between different transmission configurations is possible since the braking torque changes only as fast as the rotation speed does.

C.4 Hardware in the Loop

To verify simulation results of the controller on the test bench, the inertia of the turbine has to be included into the tests too. Since it is not possible to install such a huge flywheel directly on the test bench it has to be considered virtually in a real-time simulation. Figure C.2 demonstrates the coupling of the simulated inertia to the test bench and which signals are being transferred in the following test.

Initial point is a torque signal applied on the model of a flywheel in the real-time simulation. The rotation speed of the inertia is sent to the test bench drive where a rotation speed controller sets the same rotation speed on the test bench. The braking torque of the hydrostatic transmission is measured at the slow turning shaft and transmitted into the simulation to be applied on the inertia as load torque. In the following measurements all units of the hydrostatic transmission will be in operation but two different setups will be used. In the first one all motors are set to a constant displacement whereas in the second one a controller for the braking torque as shown in

section C.3 is activated.

C.5 Rotor Simulation

C.5.1 Rotor Properties

The rotor is modeled by scaling the NREL 5MW rotor [38]. Table 5.5 gives the general properties of the NREL rotor. The mass and inertia of the scalable rotor are derived according to relations for a "baseline" rotor set in [88]. The aerodynamic properties of the blade are given in table C.3. The tip speed ratio λ at peak power coefficient is 7.55 [38, p. 27].

node	length r/R	chord c/R	part length dr/R	twist angle $\theta_{twist} [^\circ]$	airfoil
1	0.0455	0.0562	0.0434	13.3080	Cylinder1
2	0.0889	0.0612	0.0434	13.3080	Cylinder2
3	0.1323	0.0661	0.0434	13.3080	Cylinder2
4	0.1865	0.0723	0.0651	13.3080	DU40-A17
5	0.2516	0.0738	0.0651	11.4800	DU35-A17
6	0.3167	0.0708	0.0651	10.1620	DU35-A17
7	0.3817	0.0674	0.0651	9.0110	DU30-A17
8	0.4468	0.0636	0.0651	7.7950	DU25-A17
9	0.5119	0.0595	0.0651	6.5440	DU25-A17
10	0.5770	0.0556	0.0651	5.3610	DU21-A17
11	0.6421	0.0517	0.0651	4.1880	DU21-A17
12	0.7071	0.0478	0.0651	3.1250	NACA64-A17
13	0.7722	0.0439	0.0651	2.3190	NACA64-A17
14	0.8373	0.0400	0.0651	1.5260	NACA64-A17
15	0.8915	0.0367	0.0434	0.8630	NACA64-A17
16	0.9349	0.0331	0.0434	0.3700	NACA64-A17
17	0.9783	0.0225	0.0434	0.1060	NACA64-A17

Table C.3: Distributed blade aerodynamic properties as function of the rotor radius R

C.5.2 Pitch Control Settings

NREL: the control of the pitch system is a function of the average wind speed and the generator speed. The control is defined for 3 regions within the operational envelope.

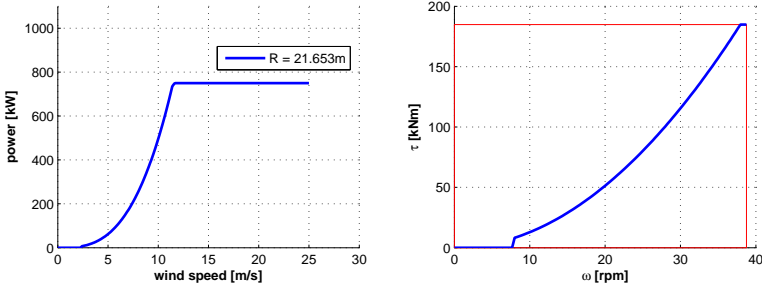


Figure C.5: $C_p - \lambda - \theta$ envelope of scaled rotor

- region 1: before cut-in
- region 1 $\frac{1}{2}$: "a start-up region, is a linear transition between regions 1 and 2"
- region 2: between cut-in and near rated
- region 2 $\frac{1}{2}$: "is a linear transition between Regions 2 and 3 with a torque slope corresponding to the slope of an induction machine"
- region 3: above rated

DOT: the control of the pitch system is a function of the rotor torque, i.e. the pressure in the system. The DOT controller works differently in 4 regions.

- region 1: under cut-in
- region 1 $\frac{1}{2}$: startup; linear speed up of rotor to design λ
- region 3: above rated torque τ : keep torque constant allow rotor speed to increase
- region 4: above rated speed ω : keep torque and rotor speed constant
- region 4 $\frac{1}{2}$: at/above cut-out: shutdown

C.5.3 Matching the Rotor Size to the Drive Train

The maximum operating torque is limited to 220kNm. For the two pumps, with a combined volume of 66,000 cc/rev ($\approx 0.0105 \text{ m}^3/\text{rad}$), this corresponds to an pressure

designation	Type	Manufacturer	series	V_g [cc/rev]	p_{nom} [bar]	n_{nom} [rpm]
motor 1 A1		same Hägglunds CBP840 in table C.1				
motor 2 A1		same Hägglunds CA210 in table C.1				
pump 1&2 A2	var. displ.	Rexroth	A4VSO	750	350	1,200
Electric power source:						
1× 200 kW motor, soft start ¹						
1× 200 kW motor, frequency converter						

Table C.4: Components of the IFAS rotor simulating drive system

difference of 209 bar. With a charge pressure of 6 bar, the nominal operating pressure is thus set to 215 bar.

$$R = \sqrt[3]{\frac{2 \cdot \tau_{nom} \cdot \lambda}{C_{P, rated} \cdot \rho \cdot v_{rated}^2 \cdot \pi}} \quad (C.3)$$

$$= 24.61 \quad (C.4)$$

$$\approx 25 \quad (C.5)$$

The power and torque curves of the rotor are given in figure C.5.



Experimental Setup for Passive Control Validation

This appendix is an elaboration of section 6.3.1.

D.1 The Open Jet Facility

The experimental validation of the passive control method was conducted at the Open Jet Facility (OJF) of the Delft University of Technology. The main features of the OJF are listed in table D.1. The hydraulic diagram in figure 6.9 identifies the essential

Type	Closed circuit
Cross section	Octagonal
Tunnel exit ($w \times h$)	$285 \times 285\text{cm}$
Maximum test section flow speed	30m/s
Turbulence level	0.23%

Table D.1: Properties of the OJF wind tunnel at the TU Delft

components of the experimental setup in the OJF. The pictures in figure D.1 show the airfoil of the blades and the configuration of the bearings, the main shaft and the connection to the rotor.

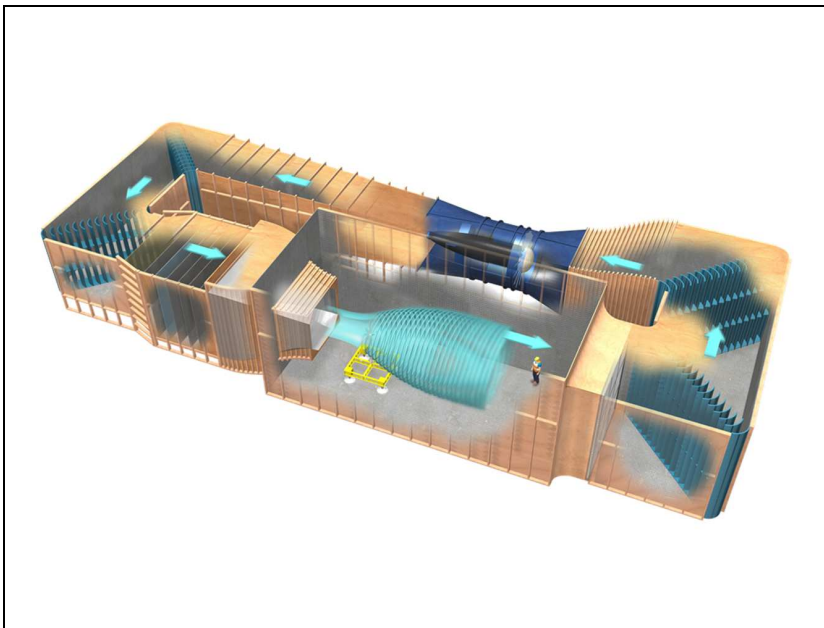


Figure D.1: Circuit layout of the Delft University Open-Jet Facility

D.2 The Aerodynamic Rotor

The rotor used for the experiments is an adaptation of Hugh Piggott [91] design, made by Nienke Hosman for her MSc Thesis project [77]. The diameter of 1.8m is around the maximum size that can be used in this wind tunnel without experiencing additional aerodynamic effects due to the limits of the tunnel exit. The wooden rotor blades are untapered and untwisted. The hub consists of two steel plates that hold the blades in place.

airfoil derived from	NACA4412	blade pitch angle θ	5°
rotor radius R	0.9m	mass m	$\approx 3.5\text{kg}$
aerodynamic chord c	75mm	mass moment of inertia I	$\approx 0.3\text{kgm}^2$

Table D.2: Properties of the aerodynamic rotor

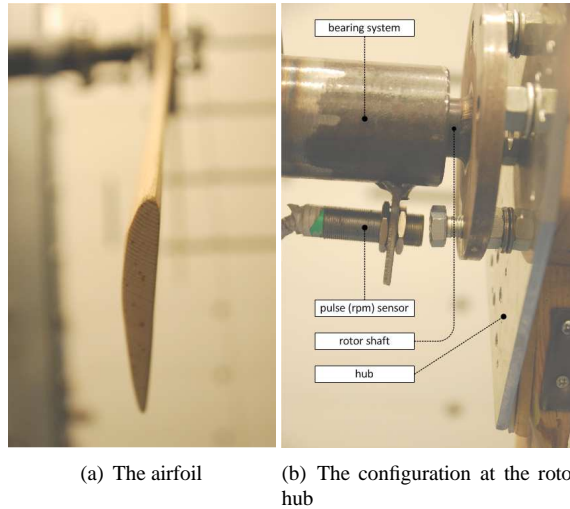


Figure D.2: Close-up images of components used in the experiments

D.3 The Water-Hydraulic Circuit

An hydraulic diagram of the water-hydraulic circuit is given in figure 6.9. The location of the water-hydraulic pump was at about 3.5m above the ground level where the mobile reservoir was placed (see figure 6.10(a)). This pump is not capable of self-priming, so a boost system was required to ensure the required 0.2 supply pressure.

The supply hose to this pump was charged from the reservoir by an electrically driven submersible pump. The pressure before the pump inlet was around 0.5bar above atmospheric pressure.

A small dose of chloride was added to the water in the reservoir to prevent salmonella growth.

D.4 Nozzles

Using the results from [77] and the pump properties from the product manual, the calculated ideal nozzle diameter is 1.32mm.

From this the braking torque of the pump is modeled. This braking torque is modeled as a function of the rotor speed ω only.

A range of nozzle diameters was assembled. Suspicions arose on the stated val-

water-hydraulic pump	manufacturer & type	Danfoss PAH12.5
	volumetric displacement	12.5cc/rev
	speed range	500 - 3000rpm
	max pressure drop	140bar
	mass	4.15kg
	filtration rating	10 micron
hoses	diameter	0.5" \approx
	length	5.0m
	max pressure	250bar

Table D.3: Properties of components of the water-hydraulic circuit

ues of the nozzle diameters when two nozzles produced very similar results. From precise laser measurements it became clear that the stated values deviated from the real values, see table D.4.

Assigned	Measured	Error	Assigned	Measured	Error
1.20	1.2357	2.98%	1.40	1.4207	1.48%
1.30	1.3188	1.45%	1.50	1.5134	0.89%
1.35	1.3539	0.29%	2.00	2.0668	3.34%

Table D.4: Assigned and real nozzle diameters

D.5 Sensors & Data Processing

The longitudinal airspeed before the rotor was determined using data from the OJF sensors for:

- air temperature
- static & dynamic air pressure at the outlet of the jet.

Functioning sensors in the hydraulic circuit were:

- a pulse sensor to estimate the rotational speed ω of the rotor and pump.
- a pressure sensor for the high pressure line (10V, 0-250bar)
- a pressure sensor for the low pressure line (10V, 0-25bar)
- a temperature sensor (10V, 0-100°C)

The shaft connecting the rotor to the pump ran through a cylinder with two sets of bearings. Within this cylinder a torque sensor was also mounted, but this sensor malfunctioned during testing.

The torque is calculated using:

$$\tau = V_p \cdot (p_{hi} - p_{lo}) \quad (D.1)$$

The power coefficient C_p is determined using:

$$C_p = \tau \cdot \omega \quad (D.2)$$

Note, the mechanical efficiency of the pump and the friction of the bearings of the rotor shaft is thus not accounted for. The braking torque at the rotor is thus likely to be larger than T , particularly at low rotational speeds where the resistance torque, due to the internal friction of water pump cylinders, becomes relatively large.

Overcoming Start-up Torque

The water-hydraulic pump used in the experiments has a minimum design speed of 500rpm. At lower speeds the internal friction of the pump increases rapidly.

Preliminary measurements had shown that the required start-up torque was around 4Nm. For the experimental setup, with the rotor blade pitch angle as shown in figure D.2(a), this corresponded to a wind speed of around 30m/s.

So, in order to be able to start up at low wind speeds, a jump start mechanism was applied in the form of a rope spun around the rotor axis. Pulling the rope would crank up the rotor. This method proved to be successful.

Expected Results on the Basis of Available Data

From pump data (table D.3) and performance modeling 6.2, together with the data from the experiments described in [77], the expected operational envelopes were determined. These are shown in figure D.3. As indicated in figure 6.4, the expected result is that the system operated at the intersection of the two surfaces that represent the operational envelopes of the rotor and the drive train.

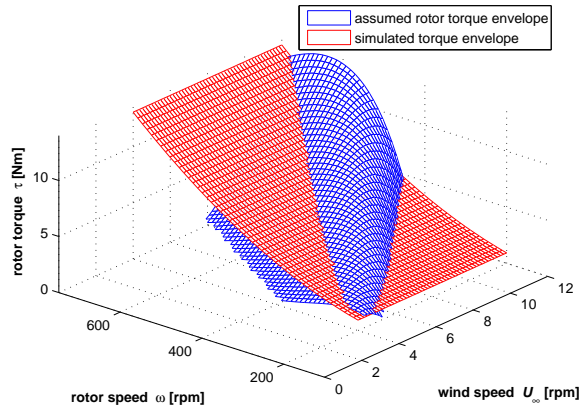


Figure D.3: Estimated operational envelope

Curriculum Vitae

Niels Frederik Boudewijn Diepeveen was born in Leiden, The Netherlands on July 9th 1979. Aged five he made his first visit to the cockpit of a Boeing 747.

As a child he lived in Brunei (1982-1986), Nigeria (1986-1991) and The UK (1991-1996). After finishing his secondary education with an International Baccalaureate diploma in 1997 he became a student at the faculty of Aerospace Engineering at the Delft University of Technology. In 2007 he graduated at the department of Control and Simulation on his M.Sc. thesis “Adaptive Flight Control Design for an Autonomous Mini-UAV”.

After working as an independent consultant he started his PhD project on the power transmission system for the Delft Offshore Turbine, a new type of wind turbine designed specifically for offshore, in 2008. The bulk of the research was carried out at the TU Delft. During his time as a PhD student he was also involved in several of the section’s commercial projects. He was the responsible instructor for the M.Sc. courses OE5662 “Offshore Wind Farm Design” and OE4653 “Marine Pipelines”.

Niels is currently employed as innovation project manager at Ampelmann Operations and remains involved in the organization, education and research at the Offshore Engineering section of the TU Delft.